Poly (*N*-isopropylacrylamide) Microgel-Based Electroresponsive Optical Devices and Anisotropic Particles

by

Wenwen Xu

A thesis submitted in partial fulfillment of the requirements for the degree of

Doctor of Philosophy

Department of Chemistry
University of Alberta

Abstract

Stimuli-responsive hydrogels, especially those with nanometer/micrometer-scale dimensions, have attracted intense research interest due to their many promising applications. Poly (*N*-isopropylacrylamide) (pNIPAm)-based hydrogel particles (nanogels and microgels) have been by far the most widely studied responsive materials, and their use in electroresponsive optical devices and as asymmetrically-modified particles are the focus of this dissertation.

According to the different focuses of the projects, this dissertation is divided into three parts.

Chapter 3, 4 and 5 focus on investigating pNIPAm microgel-based electroresponsive devices and their behavior. In Chapter 3, we demonstrate that electrical potential applied to a microgel coated electrode can induce localized solution pH changes that can be used to trigger a response from the microgel layer, and lead to the triggered release of small molecules. In Chapter 4, we show that poly (*N*-isopropylacrylamide-co-acrylic acid) (pNIPAm-co-AAc) microgels can be sandwiched between two Au layers to generate etalon devices discovered by our group. Etalons are optical devices which can present tunable color in response to different stimuli due to the light constructive/destructive interferences. The etalon was connected to a power supply and used as a working electrode, which yielded a shift in the optical properties of the devices in response to electrically-induced pH change. In Chapter 5, an external potential was directly applied to the two Au layers of the etalon device, which could

interact with the charged microgel monolayer to make the microgel layer compress or elongate.

Chapters 6 and 7 describe the generation of asymmetrically-modified pNIPAm-based microgels. Chapter 6 shows that asymmetric microgels could be synthesized through a self-assembly process to selectively coat one pole or both sides (poles) of microgels with Au nanoparticles. Chapter 7 describes that such asymmetric structures can also be obtained by selectively modifying only one side of the microgels with thiol groups.

The last part of the thesis (Appendix A and B) describes a method to form hydrogel particles with complex patterns and the generation of dissolvable supramolecular hydrogel-based wound dressings (my project conducted at Tsinghua University in China), respectively.

Preface

Chapter 4 of this thesis has been published as Wenwen Xu, Yongfeng Gao and Michael J. Serpe, "Electrochemically color tunable poly(*N*-isopropylacrylamide) microgel-based etalons", J. Mater. Chem. C, 2014, 2, 3873-3878. I was responsible for the experimental design, the data collection and the manuscript composition. Yongfeng Gao assisted in designing the pattern for display. Michael J. Serpe was the supervisory author and was involved with the experimental design and manuscript composition.

Chapter 6 of this thesis has been published as Wenwen Xu, Menglian Wei and Michael J. Serpe, "Janus microgels with tunable functionality, polarity and optical properties", Adv. Opt. Mater, 2017, 2, 2195-1071. I was responsible for the experimental design, the data collection and the manuscript composition. Menglian Wei assisted in particles' characterization. Michael J. Serpe was the supervisory author and was involved with the experimental design and manuscript composition.

Appendix A of this thesis has been published as Wenwen Xu, Yuyu Yao, John S. Klassen and Michael J. Serpe, "Magnetic field assisted programming of particle shapes and patterns", Soft Matter, 2015, 11, 7151-7158. I was responsible for the experimental design, the data collection and the manuscript composition. Yuyu Yao and John S. Klassen assisted in imaging particles. Michael J. Serpe was the supervisory author and was involved with the experimental design and manuscript composition.

Appendix B of this thesis has been published as Wenwen Xu**,** Qiao Song, Jiang-fei Xu, Michael J. Serpe, and Xi Zhang, "Supramolecular hydrogels fabricated from

supramonomer: a novel material for wound dressing", ACS Appl. Mater. Interfaces, 2017, 9, 11368-11372. Qiao Song and I were responsible for the experimental design, the data collection and the manuscript composition. We were contributing equally to this study. Jiang-fei Xu assisted in the experiment design. Xi Zhang and Michael J. Serpe were the supervisory authors and involved with the experimental design and manuscript composition.

Acknowledgement

First of all, I want to express my sincere appreciation to my supervisor Dr Michael J. Serpe for providing those wonderful PhD projects to me. Being enthusiastic, thoughtful and helpful, he is the most amazing supervisor. Mike always supports me and encourages me to try different new research ideas. Besides research, I would like to thank every opportunity Mike offered --- workshops, CIC networking events, conferences and exchange projects, to prepare me for future career. Without him, I could not achieve what I have done. To me, he is more than a research supervisor and is one of my family members who is always caring. I also would like to express my gratitude to all of the Serpe group members. I had a great time working in Serpe lab. I feel so lucky to be a Serpe group member for 5 years.

I would thank my committee members: Dr. Richard McCreery and Dr. Jillian Buriak. Thanks for the precious suggestions on my research projects. And I also would like to thank Prof. Xi Zhang to provide me a wonderful project when I was visiting Tsinghua University. I really had a great time in his group.

Last but not the least, I would like to thank my mum, dad, grandpa, grandma and boyfriend Jing for your unconditional love and support. Thanks for always being by my side and share my happiness and sorrow. The bond between us is unwavering and means a lot to me. I feel so lucky to have all of you in my life.

Table of Content

List of Figures

List of Tables

List of Abbreviations

pNIPAm: poly(*N*-isopropylacrylamide

LCST: lower critical solution temperature

UCST: upper critical solution temperature

AAc: acrylic acid

APS: ammonium persulfate

TEMED: *N, N',N'*-tetramethylethylenediamine

PVCL: poly(*N*-vinlycaprolactam)

PEO: poly(ethylene oxide)

PDEA: poly(*N,N*-diethylacrylamide)

ΔG: Gibbs free energy

ΔH: enthalpy

ΔS: entropy

VPTT: volume phase transition temperature

AAm: acrylamide

MAA: methacrylic acid

BIS: *N,N'*-methylenebisacrylamide

HEMP: 2-hydroxy-1-[4-(2-hydroxyethoxy)phenyl]-2-methyl-1-propanone

PE: polyelectrolyte

APMAH: *N*-(3-aminopropyl) methacrylamide hydrochloride

DLS: dynamic light scattering

pNIPAm-co-APMAH: poly(*N*-isopropylacrylamide-co-*N*-(3-aminopropyl) methacryl amide hydrochloride)

pNIPAm-co-AAc: poly (*N*-isopropylacrylamide-co-acrylic acid)

NPs: nanoparticles

Au NPs: gold nanoparticles

SPR: surface plasmon resonance

NIR: near infrared

QDs: quantum dots

PL: photoluminescence

ECM: extracellular matrix

CDs: cyclodextrins

Azo: azobenzene

JPs: Janus particles

EHD: electrohydrodynamic

PDMS: polydimethylsiloxane

PMs: photonic materials

PS: polystyrene

CV: crystal violet

ITO: indium tin oxide

SAMs: self-assembled monolayers

TCEP: tris(2-carboxyethyl) phosphine hydrochloride

TMP: 2,2,4-trimethylpentane

HEMA: 2-hydroxylethylmethacrylate

PEGDA: poly (ethylene glycol) diacrylate

FGG-EA: tripeptide Phe-Gly-Gly ester derivative

CB[8]: cucurbit[8]uril

Chapter 1 Introduction to Stimuli-Responsive Hydrogels

Stimuli-responsive polymers are macromolecules that can exhibit dramatic changes in response to external physical and/or chemical stimuli. They can be tailored to form free chains in solution, polymer brushes grafted on surfaces or three-dimensionally crosslinked networks. When the polymers in the crosslinked networks are hydrophilic, they form hydrogels. This Chapter discusses the general background of stimuli-responsive hydrogels with emphasis on those composed of *N*-isopropylacrylamide (NIPAm) monomers, which are the focus of this dissertation.

1.1 Stimuli-Responsive Hydrogels: from Macrogels to Microgels

Hydrogels are composed of hydrophilic polymers that are chemically and/or physically crosslinked into three-dimensional networks. They can absorb and retain water up to thousands of times their dry weight in the aqueous environment without dissolution, due to the presence of the hydrophilic moieties such as carboxyl, amide, phosphate, hydroxyl and sulfonate groups, and their crosslinked structures.[1-3] In addition, they have been shown to have porous structures allowing chemicals to be transported into/out of their matrix. Hydrogels could also be incorporated into a living system without an adverse effect, showing good biocompatibility. These properties make hydrogels ideal materials for a synthetic extracellular matrix in the field of tissue engineering, cell culture and drug delivery. [4-7]

Hydrogels can generally be made to respond to small environmental changes with a sharp transition of their swelling ratio, defined as the mass of water absorbed per gram

of a dry hydrogel. [1-3] The hydrogel's swelling process can be described by the theory of Flory and Rehner.[1] When a dry hydrogel is soaked in water, osmotic pressure can cause the water molecules to diffuse inside its matrix and this hydration process can make the polymer network expand. Since the flexible polymer chains are held together by crosslinks, the chain expansion can be counteracted by the elastic restoring force. Thus, the equilibrium swelling ratio (hydrogel's maximum degree of water absorption) is governed by the balance of these two opposing forces. That is, when the external stimuli can change a hydrogel's properties such as crosslinking density, the previous balance between chain expansion and elastic restoring force will be interrupted and the hydrogel will adapt to the new environment by altering its swelling ratio, thus exhibiting stimuli-responsivity. As shown in Figure 1-1, upon exposure to physical (temperature, light, electric field, magnetic field) and/or chemical (pH, salt concentration, biomolecules) stimuli, according to different solvation states, hydrogels can reversibly change their chain conformations, mesh sizes and refractive index,[8-13] which has allowed them to be widely utilized in sensors, switchable photonic crystals and smart surfaces.[14-18]

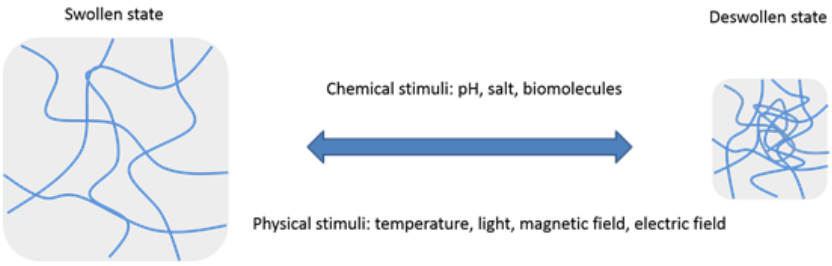

Figure 1-1 Hydrogel's solvation state changes in response to different external stimuli

Fast response is a prerequisite for stimuli-responsive hydrogels in real-world applications. Tanaka and Fillmore proposed a theory that the characteristic time (τ) for a gel's volumetric change is directly proportional to the square of the gel's size (R) but inversely proportional to the diffusion coefficient (D).[19]

$$\tau = R^2/\pi^2 D \qquad (1\text{-}1)$$

Therefore, instead of macrogels, hydrogels with submicron dimensions (microgels) have been developed to yield fast responses. Microgels, combining the advantages from colloidal particles and macrogels, have a high surface area-to-volume ratio, colloidal stability, good water absorption, proper elasticity, porous structure and fast stimuli-responsivity. Hence, they are intriguing materials that attract considerable research attention in the fields of superabsorbent materials, miniaturized devices, surface coatings and emulsion stabilizers. [20-23]

1.2 Thermoresponsive Hydrogels

Thermoresponsive hydrogels are polymers that can exhibit temperature-induced volumetric changes in a solvent. The temperature-dependent behavior, especially critical temperatures close to the physiological temperature range (30 ~ 40 ºC), have been extensively studied. Herein, thermal phase transition behaviors, especially those of pNIPAm, are of special concern in this section.

1.2.1 Mechanism for Thermoresponse

Thermoresponsive hydrogels exhibit a volume phase transition at certain temperatures. They can be divided into two main groups based on different temperature-dependent behaviors. One group deswells in a particular solvent upon heating, exhibiting a lower critical solution temperature (LCST)[24-25] while the other group presents an upper critical solution temperature (UCST) below which networks shrink.[26-27]

Hydrogels possessing a LCST generally bear both hydrophobic and hydrophilic groups. There are a plethora of examples of hydrogels with a LCST, such as poly (*N*-isopropylacrylamide) (pNIPAm), poly(*N*-vinylcaprolactam) (PVCL) and poly(*N,N*-diethylacrylamide) (PDEA).[28-32] These polymers' chemical structures are presented in Figure 1-2(a).

Of all the thermoresponsive materials, pNIPAm is the most extensively studied with a LCST around 32 ºC in water. To illustrate such temperature-dependent phase transition, pNIPAm single chain's behavior is needed to be explained first by Gibbs free energy:

$$\Delta G = \Delta H - T\Delta S \quad (1\text{-}2)$$

Where G is the Gibbs free energy for dissolution, H is the dissolution enthalpy, S is the entropy change mainly due to the interaction between water and polymer chains, T is the environmental temperature. Negative ΔG means that polymer dissolution is spontaneous and polymer solution is homogenous while positive ΔG means that polymer is insoluble in a solvent and phase separation will occur.

The temperature-induced phase transition for a single pNIPAm chain in water is shown in Figure 1-2(b). The interaction between water and pNIPAm segments plays a critical role for such a transition. At temperatures below the LCST, pNIPAm segments have two different kinds of bound water: one is the bound water around the pNIPAm amide groups and the other is the clathrate-like water with ordered structures surrounding the hydrophobic isopropyl groups and main hydrocarbon chains. [28, 33] As a result, negative ΔH and ΔS can be observed from the above hydration process. Enthalpy effect is dominant at low temperatures resulting in negative ΔG and a spontaneous polymer dissolution process. However, when temperature rises above the LCST, entropy term becomes dominant resulting in positive ΔG and an unfavorable dissolution process. As a result, the temperature-induced transition from soluble (extended coil) to insoluble (globule) state will occur.

Likewise, pNIPAm hydrogels show deswelling when the solution temperature surpasses their LCST. Such a transition temperature can also be called as a volume phase transition temperature (VPTT). At temperatures above VPTT, the transition from the preferential polymer-water interactions to favorable polymer-polymer interactions forces the hydrogels to collapse by squeezing out their retained water.

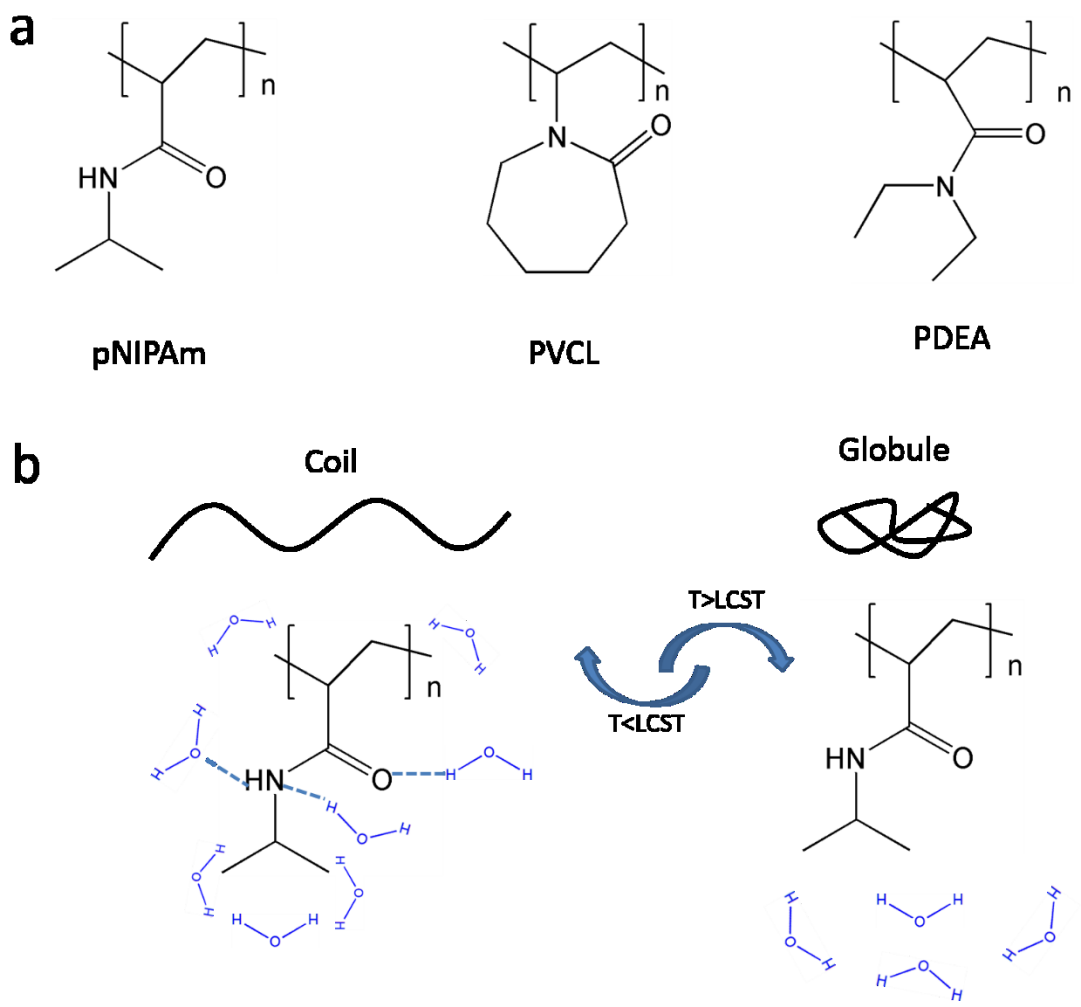

Figure 1-2 a) Chemical structures for typical polymers with a LCST; b) Schematic representation of pNIPAm's temperature-induced reversible phase transition

LCST can be influenced by several factors. For instance, the LCST will rise by adding more hydrophilic groups into the hydrogels' polymer backbone while more hydrophobic groups will cause LCST to decrease. [34-35] However, the polymer chains cannot be too hydrophobic, or else they won't be dissolved in water at all. Besides polymers' hydrophilicity, LCST is also related to co-solvent, polymers' crosslinking density, molecular weight and architectures. [36-39]

1.2.2 pNIPAm-Based Thermoresponsive Hydrogels

pNIPAm is the most extensively studied thermoresponsive polymer. Radical polymerization is generally employed to synthesize pNIPAm macrogels by mixing NIPAm monomer, initiators and crosslinkers together in an aqueous solution. *N,N'*-methylenebisacrylamide (BIS) is the most commonly used crosslinker.[40-41] As a typical initiator, ammonium persulfate (APS) can decompose under high temperature to form radicals to initiate polymerization. APS can also be used together with *N, N, N',N'*-tetramethylethylenediamine (TEMED) as a pair of redox initiators to start the reaction at room temperature.[42-43] The structures of above chemicals are presented in Figure 1-3.

Furthermore, pNIPAm hydrogels can have multiresponsivities by adding comonomers with various functional groups during polymerization. For example, AAc is the most commonly used comonomer which can render pNIPAm pH responsive and will be discussed in detail later.

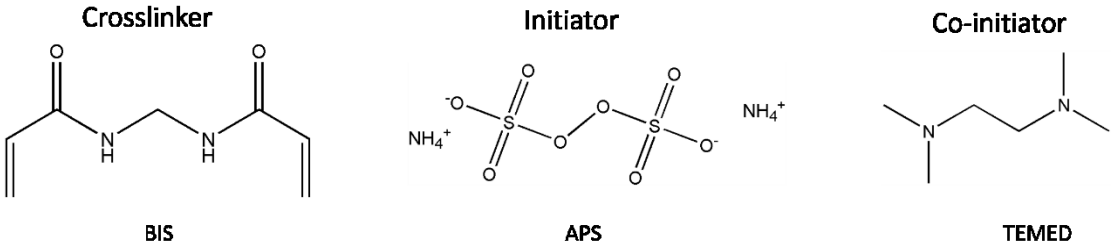

Figure 1-3 Chemical structures for BIS, APS and TEMED

Within the size range from 100 nm to 1 μm, pNIPAm microgels are colloidally stable particles benefitting from their highly charged functional groups and dangling

chains on their surfaces. [44-45] Compared to their bulky counterparts, pNIPAm microgels retain temperature responsivity and good water absorption, yet their smaller size results in much faster response. In addition, it is easy to finely tune pNIPAm microgels' morphology to make hollow and core-shell structures.[46-49] Microgels can also be deposited onto surfaces through layer-by-layer assembly approach to generate multilayers with special properties.[15, 50-51] Thus, pNIPAm microgels have attracted considerable research interests.

There are different methods developed to fabricate pNIPAm microgels,[44, 52-53] although free-radical precipitation polymerization is exclusively used in our group and will be discussed in detail next.

To synthesize pNIPAm microgels, a solution containing NIPAm, comonomers and BIS is purged with N_2 to remove O_2 and allowed to heat to a temperature which is far above pNIPAm's LCST (45 ºC ~ 70 ºC), over ~1 hour. Then a solution of APS is added to initiate polymerization. The resulting suspension is filtered to remove any large aggregates and purified via centrifugation. In addition, by adding a surfactant, sodium dodecyl sulfate (SDS), microgel's diameter can decrease since SDS helps stabilize microgels at smaller sizes. Free-radical precipitation polymerization has been shown to be advantageous since as-prepared microgels' size distribution is narrow and particles' structures can be easily tuned.[54-57] A key prerequisite for the success of this approach is that the monomer can be dissolved in water while the corresponding polymer is insoluble in water at high temperatures. As shown in Figure 1-4, at high temperatures, APS will decompose and form radicals to react with monomers and crosslinkers to

initiate polymerization. Since pNIPAm has a LCST,above a critical length, growing pNIPAm chains will collapse and form precursor particles, which serve as nuclei/precursor particles. These precursor particles which are not colloidally stable can coalesce and NIPAm monomer can also deposit onto the particles' surface. Eventually, they can further grow to form stable microgels. Since reactivity for BIS is higher than NIPAm monomer, pNIPAm microgels' structure is not homogeneous and they have higher crosslinking density at cores compared to their shells.

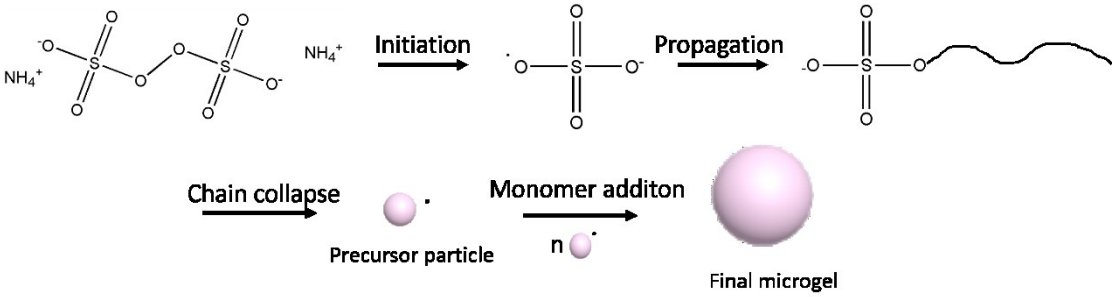

Figure 1-4 Mechanism for pNIPAm microgels' formation via free-radical precipitation polymerization method

1.3 pH-Responsive Hydrogels

pH-responsive hydrogels are polyelectrolyte (PE) gels that bear ionisable moieties in their backbones. PE gels' equilibrium swelling ratio can be significantly higher than that of corresponding neutral gels due to the Coulombic repulsion between fixed ionic groups and the additional osmotic pressure from mobile counterions in their networks. The ionic monomers, such as AAc, MAA and *N*-(3-aminopropyl) methacrylamide hydrochloride (APMAH), can be incorporated into the pNIPAm microgels to render

them pH responsive. Dynamic light scattering (DLS) data has already shown that pNIPAM-based microgels with higher AAc percentage have a larger hydrodynamic diameter. [58]

As commonly used monomers in this thesis, APMAH has a pKa of ~9 while AAc has a pKa of ~ 4.25. The structures of the monomers are shown in Figure 1-5. The pH-induced volume transition of weak PEs generally occurs in a pH range close to the pK_a of their ionizable moieties because their degree of ionization is different at different pHs. Therefore, the pNIPAm-co-APMAH microgels are positively charged at pH< 9, while the pNIPAm-co-AAc microgels are negatively charged at pH> 4.25.

As shown in Figure 1-5(b), take AAc gel as an example to explain the pH-dependent volume transition. When pH rises by adding trace NaOH and ignoring solution's ionic strength change, the additional osmotic pressure as a result of mobile sodium counterions transported into the gel network and increased electrostatic repulsion between negative charged carboxylic groups cause the whole gel network to expand. On the contrary, upon lowering pH, decreasing amount of mobile counterions and protonated carboxylic groups can make the whole gel's network collapse.

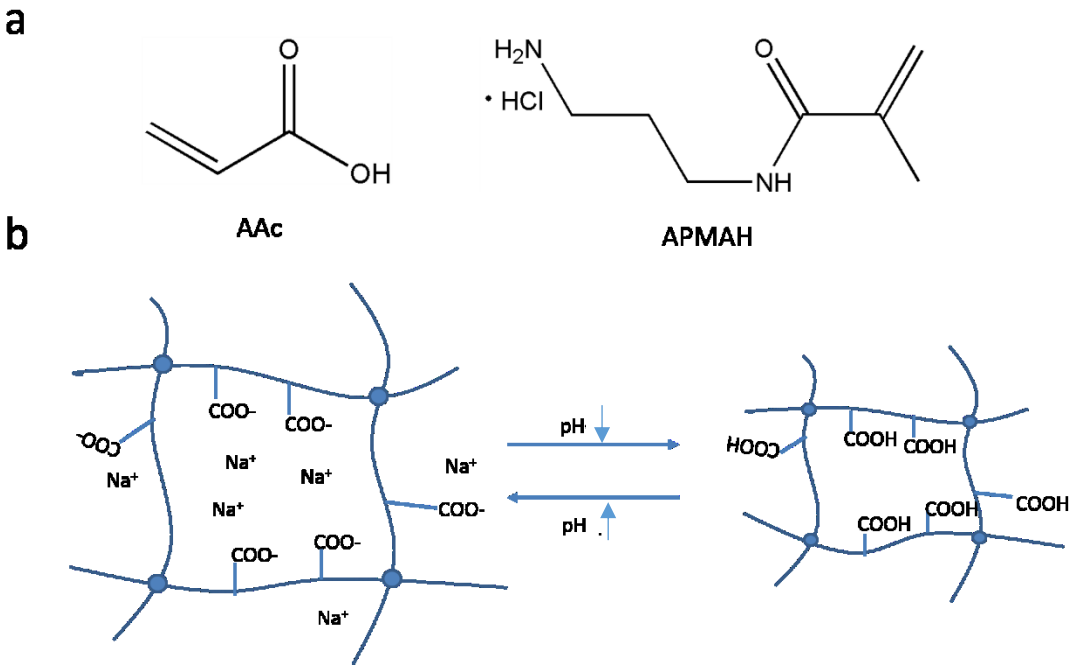

Figure 1-5 a) Chemical structures for AAc and APMAH; b) Schematic presentation of the pH-induced phase transition for AAc gel

There are several factors that influence a PE gel's pH response. For instance, the ionic strength in a solution can alter the solvation state of PE gels.[56] Consider a weak polyacid as one example. Keeping other parameter constant, when the ionic strength is low, solution's pH is the dominant factor to determine extent of swelling for PE gels. When the ionic strength is in the medium range, protons from acidic groups will exchange with mobile ions from salt resulting in increasing both the amount of ionized groups and the osmotic pressure from mobile counterions, therefore PE gels will present increased swelling behavior. At high ionic strength, Debye screening will dominate and the whole gel will deswell.[1] In addition, crosslinking density, hydrophilicity and hydrophobicity of the polymer chains could also have impacts on PE gels' pH sensitivity.[59-60]

1.4 Electroresponsive Hydrogels

Electrical signals play a central role in the movement of living creatures. For example, Venus flytraps can trap their prey by quickly closing their lobes, which is controlled by their action potentials. Inspired by mother nature, electroresponsivity has already become a hot research area, in which hydrogels are widely investigated.[61]

PE gels introduced in the previous section are also electroresponsive since water electrolysis can result in a dramatic pH change near electrodes. PE gels can be placed near one electrode to sense such pH change and thus indirectly respond to electric field. Generally speaking, for anionic gels at the anode where H^+ is produced, negatively charged groups will be protonated resulting in network collapse while for cationic gels at the cathode where OH^- is generated, positively charged groups will be deprotonated and these gels will shrink.[61] Another mechanism for the hydrogels' electroresponsiveness is that electric field can induce a stress gradient within the gel's network, resulting in anisotropic deswelling. Tanaka et al. fixed a partially hydrolysed polyacrylamide hydrogels to one of the electrodes.[62] Experimental results shows that the mobile hydronium ions inside the gel's network migrate to the cathode while the negative charged immobilized carboxylate groups are attracted to the anode. The attractions between mobile/immobilized groups and two electrodes can generate a stress gradient along the gel's axis, resulting in anisotropic deformation.

In this dissertation, the above two mechanisms are employed to make the etalon

device discovered by our group respond to external electric field, which could have potential applications in display as well as sensors.

1.5 Hybrid Hydrogels

Hydrogels could be hybridized with various nanoparticles (NPs) (quantum dots, Au NPs, Ag NPs, magnetic NPs), generating novel optical, catalytic and magnetic properties.[63, 64] There are several approaches to hybridize hydrogels with different NPs. In one approach, NPs can be synthesized first. Hybridized hydrogels can be obtained by dispersing NPs into the pre-gel solution, which will subsequently undergo polymerization or by soaking hydrogels in an aqueous solution containing NPs.[65-67] In another case, NPs can be synthesized in situ within hydrogels' three-dimensional networks.[41, 68-69] Polymer chains can also be grafted onto NPs' surface first to form the nucleation center for subsequent microgel growth.[70]

Au NPs are the most commonly studied nanomaterials to be incorporated in hydrogels. They can either be immobilized in hydrogels' networks or be coated with thin gel layers. Au NPs are well-known for their surface plasmon resonance (SPR), thus possessing highly enhanced visible/near infrared (NIR) light absorption. Their strongly absorbed light can then be quickly converted to heat resulting in photothermal phenomena. Thus, Au NPs are often selected to be covalently/noncovalently embedded in pNIPAm's network to make photothermally responsive hydrogels. These Au NPs can convert light energy to heat, upon exposure to proper light, resulting in pNIPAm's shrinking.[71-74] Additionally, the temperature-dependent solvation state from pNIPAm

can have influences on optical properties of such hybrid system.[75-76] Previous literatures show that above LCST, change in environmental refractive index and distance between Au NPs can result in relatively strong plasmon coupling between the Au NPs thus red shift of UV-Vis absorbance peak.

Quantum dots (QDs) are semiconductor nanocrystals which attract considerable research attention in the biomedical field. QDs are easy to aggregate in aqueous solution and have considerate cytotoxicity. Hydrogels can stabilize QDs and decrease their cytotoxicity by incorporating them inside the polymeric networks. At the same time, these hybrid hydrogels would obtain new properties from QDs. In one example, Bai's group immobilized CdTe nanocrystals inside the pNIPAm hydrogel. The resultant hybrid gel's photoluminescence (PL) density and peak position will reversibly shift in a temperature cycle.[77]

1.6 Other Stimuli-Responsive Hydrogels

Hydrogels can have cellular/biochemical responsivities by incorporating biomolecules in their networks. In one example, the interaction between antigen-antibody pairs within the polymer matrix can form the reversible crosslinkers of an antigen-responsive hydrogel.[78-79] Upon exposure to free antigens, the competitive binding between free antigens and immobilized antigens can break the crosslinking points and hence make the whole gel swell. Another intriguing example of biomolecule responsive hydrogels is degradable hydrogel scaffolds. In tissue engineering, it is desirable to have the hydrogel scaffolds' degradation rate in sync with tissue

regeneration speed. To achieve this goal, a hydrogel crosslinked with oligopeptides is synthesized and degradable only under certain cell-secreted enzymes that can cleave its peptide crosslinkers.[80]

Hydrogels containing light-sensitive moieties (usually photochromic molecules) show interesting photo-responsive property.[81-82] Among various photoreactive molecules, azobenzene (Azo) derivatives have been the most extensively studied and are therefore often incorporated into hydrogels' networks. In one typical strategy, the mixture of a host polymer containing cyclodextrins (CDs) and a guest polymer containing Azo can form a supramolecular hydrogel crosslinked by the complex of CDs-Azo which is a light responsive host–guest pair. Upon UV irradiation, Azo moieties undergo cis-trans isomerization, thus the host-guest interaction can be disrupted and such a hydrogel is degradable. Finally, hydrogels could be made to have different solvation states when exposed to various organic solvents which makes them a perfect candidate for solvent sensors. [65, 83]

In this dissertation, we mainly utilized the stimuli-responsivities of the hydrogels to realize applications in electroresponsive devices and Janus particles, which will be detailed in Chapter 2.

Chapter 2 Applications for Stimuli-Responsive Hydrogels

This Chapter describes four major existing applications of stimuli-responsive hydrogel-based materials: Janus particles, photonic materials, drug delivery carriers and sensors, which are also topics investigated in this dissertation.

2.1 Janus Particles

Named after the two-faced Roman God Janus, micro and nanoparticles modified with two chemically/physically distinct regions are referred to as Janus particles (JPs). Since their first mention by De Gennes in his Nobel Prize lecture in 1991, JPs have been synthesized by a variety of novel approaches over the years and used for a diverse range of applications. e.g., as electronic paper (e-paper). Specifically, first generation e-paper utilized JPs that were coated on one side with white titanium oxide, and black polyethylene on the other. The different coatings resulted in optical and electronic anisotropy, which could be used to display black and white images that depended on the potential applied to the particles embedded in a transparent silicone film.[84-85] In another interesting demonstration, Crespi and coworkers showed that Janus nanorods with Pt and Au segments could be generated, and act as micro/nanomotors. This was due to the ability of the Pt portion of the nanorod to catalytically decompose hydrogen peroxide to generate oxygen bubbles, which propels them.[86]

Since numerous approaches have been developed to synthesize a tremendous diversity of JPs, for simplicity, here we restrict our discussion to polymer-based JP fabrication, which are summarized in Figure 2-1.[87] The simplest and the most

traditional approach is toposelective modification. As presented in Figure 2-1(a), a monolayer of particles can be deposited onto a solid substrate which serves as a mask and only one hemisphere of the particle is exposed and can be modified by further chemical/physical treatment, such as metal vapor deposition and fluorescent labeling.[88-89] The specially designed microfluidic device is also a popular method to break particles' symmetry.[85, 90] The geometry of a typical microfluidic channel is sketched in Figure 2-1(b). Two separate UV-curable streams flow through the two central channels 1 and 2, coalesce at the end of the central channels and later break up into droplets with two distinct phases that can be stabilized by surfactants from the side channel 3 and solidified eventually under UV light. Finally, Figure 2-1(c) shows the process for electrohydrodynamic (EHD) co-jetting technique. Two or more polymer solutions are pumped simultaneously in capillary needles.[91] The multicompartmental droplets are formed at the outlet region of the needles, which can be ejected under a high electric field and collected from the counter electrode. Unlike the previous microfluidic technique where only spherical JPs are synthesized, Janus cylinders and fibers can be obtained by tuning jetting conditions such as concentration of the polymers, viscosity of the solutions, the external electric field and flow rates.[92]

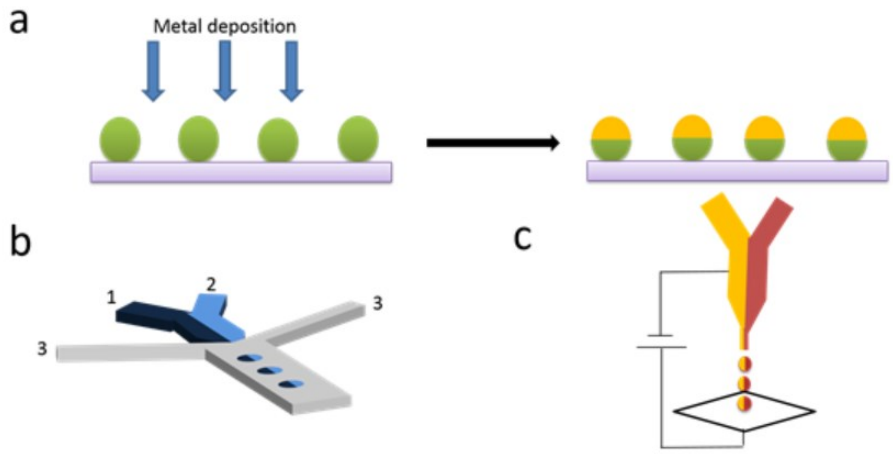

Figure 2-1 Three common approaches to generate polymeric JPs: a) Toposelective modification; b) The geometry of microchannels to generate JPs, channel 1 and 2 contain different monomer solutions and channel 3 contains an aqueous surfactant solution which can stabilize resultant droplet; c) The design of EHD co-jetting technique to produce JPs

In the above examples, the resulting particles normally have one side of the particle that is distinct from the other. Although, there are specific approaches that yield particles that have multiple distinct regions spatially isolated on a particle surface. A number of approaches have been used to generate particles with complex and isolated surface chemistries, with sequential masking/unmasking approaches being among the most widely used and easiest to implement. Granick and coworkers reported a two-step μ-contact printing method to synthesize trivalent colloidal particles — these particles can be modified from both sides while the central region of the particle is left unmodified, resulting in particles with three distinct regions (trivalent).[93] To accomplish this, different silane "inks" were transferred onto two different

polydimethylsiloxane (PDMS) stamps by spin coating. One PDMS stamp was brought into contact with one side of a layer of silica particles that were previously deposited on a flat substrate. With applied pressure, the silica particles adhered to the first PDMS stamp, which allowed them to be lifted off the flat substrate. Then, a second PDMS stamp containing another silane ink was brought into contact with the exposed, unmodified side of the silica particles, which allowed the ink to transfer to that side of the particle. Sonication allowed the modified particles to be released from the surface and isolated. In another example, Mowald's group developed an approach to generate particles with multiple distinct regions spatially isolated on a particle surface.[94-95] This was accomplished using surface-adsorbed colloidal spheres as masks when evaporating layers of Au followed by reactive ion etching steps to yield microparticles with Au "dots" spatially arranged on particles similar to sp, sp^2, sp^3 molecular orbitals. These Au-modified regions of the resultant particles can be modified and treated as binding sites to form complex clusters, and offer a new route to creating complex assemblies with novel physiochemical properties. In yet another example, Huskens' group coated a monolayer of silica particles with a sacrificial layer of poly (methyl methacrylate) (PMMA). Then, the PMMA layer was partially removed by O_2 plasma, exposing some portion of the silica particles, which depended on the time of plasma exposure. Only the exposed portion of the particles could then be chemically modified. Later, the sacrificial layer could be dissolved and the unmodified part of the released particles can be further functionalized with another chemistry.[96]

Finally, in this dissertation, we showed that complex anisotropic particles could be

generated using iron oxide microparticles suspended in a pre-gel droplet. The magnetic particles could be induced to assemble into complex patterns, which could be locked into place by polymerizing the pre-gel solution. The advantage of the approach is that the number, direction and distance between the magnetic microparticle features could be tuned by manipulation of the external magnetic field that directs the organization of the microparticles.[97]

2.2 Photonic Materials

Photonic materials (PMs), consisting of at least two periodically arranged materials with different dielectric constants, can exhibit color by interacting with light propagating through its structure. Specifically, light interacting with ordered elements in PMs leads to constructive and destructive interference of light waves propagating through it, yielding color.[98-99] There are many examples of PMs existing in nature. Butterfly wings, beetle shells, peacock feathers and opal gemstones all show vivid colors because their ordered microstructures can interact with light. This kind of material is inherently bright under strong light illumination, and is not subject to photobleaching making it is more durable than pigments/chromophores and an ideal candidate for applications in optical sensors and colored e-paper.[100]

PMs can have a periodic variation of the refractive index in one, two or three dimensions (1D, 2D, 3D), which can prohibit propagation of certain wavelengths in 1D, 2D and 3D, thus serving as optical filters. 1D PMs consist of multilayers with different refractive indices and exhibit periodicity only in one direction, which have the simplest

structure and are widely studied.[101] pNIPAm microgel-based etalon devices discovered and investigated by our group are also belong to 1D PMs which will be discussed in great detail in next section. 2D PMs possess periodicity in two directions and traditionally have a structure of parallel arrays of dielectric rods in air which can form triangular and square lattices.[102-103] 3D PMs have periodic spatial variations in three directions and they can be fabricated from closely-packed monodispersed nano/microspheres.[104-105]

PMs capable of changing their optical properties in response to external stimuli have a lot of applications in displays, barcode technologies, inks, photovoltaic devices, high efficiency reflectors and sensors.[106] In one interesting application, a stimuli-responsive PM can be made to only show the useful information under a specific stimulus such as a solvent, which can be used as an anti-fraud material.[107] Similarly, if stimuli-responsive PMs can give out different optical signals upon exposed to different concentration of analyte, they can be used as chemical/biological sensors.[108-109]

2.2.1 Basic Concept of 1 D PMs

The key to successful preparation of 1D PMs is to deposit multilayers with alternatively high and low refractive index (n_H and n_L) onto a substrate. Spin-coating and self-assembly methods are traditionally employed to prepare 1D PMs which are also known as Bragg stacks.

The schematic depiction of a Bragg stack is illustrated in Figure 2-2. When incident

light impinges on a Bragg stack, at each boundary between the layers, multiple light reflection and transmission will happen, giving rise to constructive/destructive interferences of specific wavelengths. When the stack's periodicity is on the order of the wavelength(s) from visible light, they can display brilliant colors. In addition, Figure 2-2 also shows that increasing the number of layers can increase Bragg stacks' reflectivity.

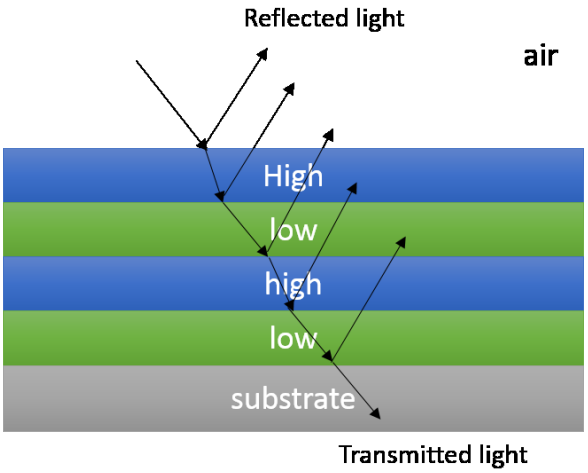

Figure 2-2 A Bragg stack's multilayer structure and light can be reflected or transmitted through its ordered structure

Assuming that all of the multilayers' thicknesses are perfectly uniform, the central wavelength, λ_{max}in the reflectance band can be determined according to the following equations:

$$m\lambda_{max} = 2(d_H + d_L)\sqrt{n_{eff}^2 - sin\theta^2} \qquad (2\text{-}1)$$

$$n_{eff=}{}^{(n_H d_H + n_L d_L)}\Big/_{(d_H + d_L)} \qquad (2\text{-}2)$$

$$W = \frac{4}{\pi}\lambda_{max}\left|\frac{n_H - n_L}{n_H + n_L}\right| \qquad (2\text{-}3)$$

Where m is the diffraction order, n_H, n_L and n_{eff} are high, low and effective refractive index of the alternative layers respectively; θ is the angle of incident light with respect to the normal of the Bragg stack's surface; d_H and d_L are the thickness of the corresponding layers and *W* is the band width.

If the incident light is perpendicular to the stack's surface, θ is 0, and equation 2-1 can be converted into:

$$m\lambda_{max} = 2(n_H d_H + n_L d_L) \qquad (2\text{-}4)$$

From these equations, we can draw the conclusion that the color exhibited by a Bragg stack is related to the refractive index, thicknesses and number of alternating layers. Specifically, if the thicknesses and/or the refractive index of the multilayers decreases, we will observe a blue shift of the Bragg peak. Additionally, the refractive index contrast (n_H-n_L) determines the bandwidth of the reflectance spectral and increasing contrast between the multilayers increases both the reflectivity and the bandwidth. Large refractive index contrast is often the prerequisite of PM's real world applications which can effectively decrease the amount of multilayers needed to achieve the desirable reflectivity. For example, PMs can be composed of SiO_2/TiO_2 bilayers, since they are transparent and have high refractive index contrast (n_{SiO2}=1.24 and n_{TiO2}=1.74). In summary, by varying the parameters in above equations, PMs can have tunable optical properties, which will be discussed in detail in next section.

2.2.2 Polymer-Based PMs

Stimuli-responsive PMs can dynamically change their spectra position in response to different stimuli by tuning their refractive index and/or thickness of the multilayers. As stated in Chapter 1, stimuli-responsive polymers can change their volume by reversible expansion/shrinking in response to small changes in their environment. Furthermore, they are low-cost, robust and can be easily modified. Polystyrene (PS), poly(methyl methacrylate) (PMMA) and polyethylene terephthalate (PET) are all typical polymers used for PMs. Polymer as an active part could also be coupled with inert inorganic materials to fabricate hybridized PMs.

There are different strategies to synthesize polymer-based PMs, besides layer-by-layer deposition method mentioned in the previous section. Monodisperse polymeric microspheres can self-assemble into closely-packed crystals to form 3D PMs. Gravity, centrifugation, pressure or filtration are all common driving forces to form the close-packed structure.[110] Furthermore, these crystals can be utilized as removable templates to make inverse opal structure because their interstitial spaces are available for further monomer infiltration or modification.[111-112] Ordered patterns generated from lithography and self-assembly of block copolymers are also popular methods to fabricate polymeric PMs.[113-114]

2.2.3 Etalon Device

Our group has previously fabricated and characterized 1D PMs using pNIPAm-based optical devices, known as etalon. A etalon device has a three-layer structure by sandwiching the pNIPAm-based microgels between two reflective metal layers (Au). Specifically, the etalon device's fabrication process is shown in Figure 2-3. 2 nm Cr as an adhesive layer and 15 nm Au layer were evaporated onto a pre-cleaned glass slide sequentially. Next, the as prepared Au coated slide was annealed at 250 ºC for 3 h and then cooled down to room temperature prior to use. A single layer of pNIPAm-based microgels could be painted on such a Au-coated glass substrate following‘paint-on’ protocol published previously. [115] In brief, a 40 μL aliquot of concentrated pNIPAm microgel solution was trasferred by a micropipitte onto the annealed Au surface and the pipitte tip was used to spread the microgel solution to each edge of the slide until the whole slide is covered with microgels. Then the resultant slide was allowed to dry completely on a hot plate at 35 ºC for 2 h. Later, the slide was washed copiously with DI water to remove the microgels that are not bound directly to the Au surface and soaked into DI water overnight at 30 ºC on a hot plate. After overnight incubation, the slide was washed again by DI water, and dried with N_2 gas. In such a process, drying of the highly concentrated microgel solution is critical to form closed-packed microgel monolayer. The interaction between microgel layer and Au layer is so strong that there is no observation of microgel layer migrating on the Au surface during soaking process. Another 2 nm Cr/ 15 nm Au overlayer was deposited onto the microgel layer by thermal evaporation.

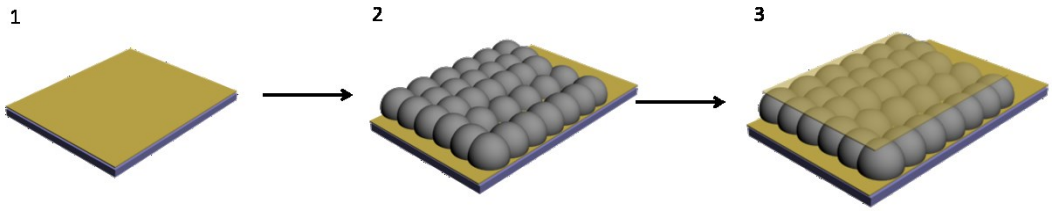

Figure 2-3 The etalon device‘s fabrication process: 1) A thin Cr/Au layer was deposited on a glass slide; 2) The pNIPAm microgels were painted onto the annealed Au layer; 3) Another Cr/Au layer was deposited on top of the microgel layer

Such a device displays vivid colors, which are dynamically tunable over a large range of visible wavelengths. As presented in Figure 2-4(a), the devices operate by light impinging on the etalon, entering the microgel-based cavity and resonating between the two semi-transparent Au layers. This behavior leads to constructive and destructive interference, which leads to color. This is a direct result of interference, where specific light wavelengths are reflected, while others are transmitted.[116] The specific reflected wavelengths lead to multipeaks in a reflectance spectrum, where the peak position(s) can be predicted by Equation:

$$m\lambda = 2nd\cos(\beta) \qquad (2\text{-}5)$$

Where λ is the wavelength maximum of a peak with a given peak order m, n is the refractive index of the dielectric (microgel) layer, d is the distance between the Au layers and β is the angle of incidence. Under most situations, the incident light is normal to the etalon surface and the effect of refractive index is negligible compared to the change induced by the change in d. Generally speaking, as shown in Figure 2-4(b), for a given m, microgel swelling leads to an increase in d, which yields a red shift in the

position of a given reflectance peak. Likewise, microgel collapse leads to a blue shift. Therefore, pNIIPAm is the active component of a etalon device which can sense pH,[117] glucose,[118] temperature,[119] and macromolecules[120] after modification and convert these stimuli into optical signals. Compared to other stimuli, electric signal is easy to apply, program and shows the tremendous value to power sensors, screens and robots. In this dissertation, we expand the application of the etalon devices by exploring their color change in response to external electric fields. The aim of this research is to find out the possible mechanisms for electrically color-tunable devices which could show potentials to be incorporated in electronic circuits to make displays and sensors.

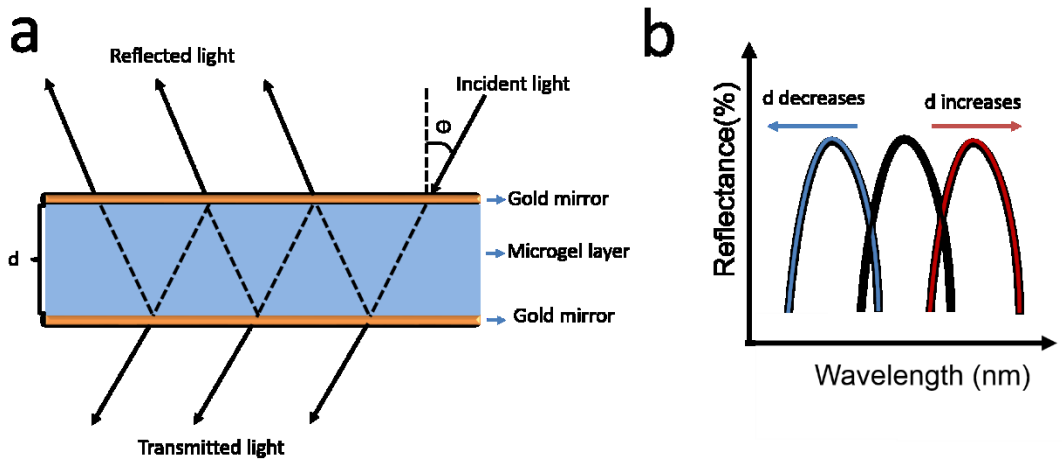

Figure 2-4 a) The interaction between incident light and the etalon device leading to light interference, b) The distance between two Au layers decreases resulting in a blue shift while a red shift will be observed for a larger distance

2.3 Controlled Drug Delivery

Drug delivery devices capable of controlling the release of loading and releasing therapeutic small molecule ("drugs") to a system can have major positive implications on human health care and disease treatment. Because of the potential impact, this research area has been receiving a considerable amount of attention over the past number of years.[121-123] In order to have practical applications, the drug delivery devices need to be capable of releasing precise amounts of drug (dosage) over many cycles. The devices should also be non-toxic/biocompatible and allow for easy triggering of drug release. In previous studies, various materials have been for intelligent drug delivery devices, such as graphene based scaffolds[124-126], magnetic nanoparticles[127-128], liposomes[129] and hydrogels[130].

For this application, hydrogels are of particular importance, and show a considerable amount of promise.[4, 123, 131] Generally speaking, since hydrogels are soft materials, they are better tolerated by the body, and lead to a low amount of inflammation and irritation.[132-133] To realize controlled drug release from hydrogels, their chemistry can be modified in such a way to allow them to respond to temperature, light, magnetic field and electricity. For example, pNIPAm hydrogels are widely used for temperature-triggered drug release. Generally speaking, at low temperature, a pNIPAm hydrogel can swell and drug is easy to diffuse out of the hydrogel network resulting in on-state. On the contrary, when temperature rises above LCST, the

pNIPAm hydrogel collapses and forms a dense, compacted, less permeable surface, turning off drug release. Hydrogels can also be designed to biodegrade, thereby disintegrating after they are exhausted of their drug payload.[134-135] It is also possible to modify hydrogels' properties by hybridizing them with metal NPs[136], carbon nanotubes[137-138] and QDs[139] to realize different controlled drug release.

Among various stimuli, electric stimuli is believed to be an efficient approach to realize drug controlled release because it is easy to precisely control the magnitude, frequency of applied voltage/current and miniature power supply. Electro-powered drug delivery products have already been commercialized such as iontophoresis device from IOMED Inc. which can deliver drug through skin by a low level current.[140]

Therefore developing hydrogel-based drug delivery systems controlled by electric field will be promising approach to enhance the medical treatment. The electroresponsive moieties of hydrogels are generally from the ionisable groups in their networks, which will also render them pH-responsive. There are different mechanisms for hydrogels to release drugs triggered by electric field. For example, when there is an electric field applied on the negatively charged hydrogel, free cations will move to the cathode while polyion will remain immobilized and be attracted to anode. Thus osmotic pressure difference will be generated and become the driving force to trigger drug release. Electric field can make certain gels' network degrade resulting in drug release. For example, Kwon et al. found out that polyethyloxazoline and PMMA can form a complex through hydrogen bonding and trap drugs inside its network. This hydrogen bonding can only be stable at pH<5. When pH rises above 5 due to water electrolysis,

hydrogen bonding is destroyed. Such a complex will decompose and release the drug. [61]

2.4 Hydrogel Sensors

A sensor is a device, which can detect and respond the changes from environment. Generally speaking, a sensor has a receptor, which can interact with analytes to generate specific stimuli; a transducer that can convert above specific stimuli to readable signal and a data process system. Hydrogels are widely used both as receptors and transducers in sensors, which can sense environmental trivial changes and convert them into a magnified readable output (normally optical or electrical signal).

Consider hydrogels as optical transducers as an example. Turbidity of a hydrogel is highly related to hydrogel's solvation state. In the fully expanded state, hydrogels are transparent and have a high transmission, while transmission will decrease when the hydrogels shrink. Analytes can have a large influence on the hydrogel's swelling ratio which can be converted into the transmission change and measured by UV-Vis. For example, carboxylic groups from hydrogels' backbone can form complex with certain cations (Ca^{2+}, Cu^{2+}), resulting in hydrogels' shrinking. By correlating analyte concentration with transmission, metal ion sensors can be obtained. [141]

Chapter 3 Electro-Triggered Small Molecule Release from A Poly (*N*-isopropylacrylamide-co-acrylic acid) Microgel layer

This Chapter describes electrically (electro)-stimulated small molecule release from a pNIPAm-based microgel monolayer. As detailed in Section 1.4, electroresponsive hydrogels can be made from PE gels with ionizable groups in their networks which are also pH-responsive. Electric fields can alter the solution's pH via water electrolysis which will modulate the PE gels' extent of ionization and can be used to trigger drug release. According to different charged groups, these PE gels can be divided into three broad categories: polyanions, polycations and polyampholytes, while polyanions (pNIPAm-co-AAc) are the most intensively studied which are also the focus in this Chapter.

3.1 Introduction

As mentioned in the previous Chapters, pNIPAm microgels are extensively studied in our group which are thermoresponsive with a LCST around 32 ºC in water.[142-143] Generally speaking, when the temperature increases above the LCST, the favorable interactions between the polymer and water are weakened (swollen state) while polymer-polymer interactions start to play a dominant role (deswollen state), resulting in a volume phase transition. Through free radical precipitation polymerization, pNIPAm microgels can be easily synthesized. Furthermore, by incorporating different functional monomers during polymerization, pNIPAm-based microgels can be multiresponsive. Specifically, in this work, AAc was chosen to render pNIPAm

microgels pH responsive. AAc groups have a pK_a ~4.25. That is, when the solution's pH is below AAc's pK_a, most of the AAc groups will be neutralized while the majority of AAc groups can be deprotonated and negatively charged at pH > 4.25. Therefore, poly pNIPAm-co-AAc microgels can act as a reservoir and trap positively charged molecules at high pH via electrostatic interactions while release these molecules when they are neutral at low pH. Such pH-dependent behavior can be used for controlled drug release mentioned in section 2.3.

In this Chapter, a monolithic pNIPAm-co-AAc microgel layer was deposited on one Au electrode following a 'paint on' protocol detailed in the experimental section of this Chapter, and loaded with a positively charged dye, tris (4-(dimethylamino)phenyl) methylium chloride (crystal violet, CV). Next, the as-prepared slide was treated as an anode and assembled in an electrochemical cell. It has been proven that the application of a suitable potential between two electrodes in water leads to water electrolysis (reduction potential for water is 1.23V at pH 7), which results in a decreasing pH near the anode. Hence, the ionization degree of AAc groups can be totally controlled by the external potential, which can disrupt the strong electrostatic interactions mentioned previously and realize controlled small molecule release. In the meanwhile, it could also be possible that electrophoresis effect also contributed to the CV release..Since CV is a positively charged small molecule, it is possible that CV could migrate toward the cathode, accelerating the release process.

3.2 Experimental Section

Materials: N-isopropylacrylamide (NIPAm) was purchased from TCI (Portland, Oregon) and purified by recrystallization from hexanes (ACS reagent grade, EMD, Gibbstown, NJ) prior to use. *N,N'*-methylenebisacrylamide (BIS) (99%), acrylic acid (AAc) (99%) , ammonium persulfate (APS) (98%) were obtained from Aldrich (St. Louis, MO) and were used as received. Deionized (DI) water with a resistivity of 18.2 MΩ·cm was used. Microscope glass slides were and obtained from Fisher Scientific (Ottawa, Ontario) and cut into pieces (25 × 25 mm).

Microgel Synthesis: Microgels were synthesized by free radical precipitation polymierzation. In one typical experiment, NIPAm (10.52 mmol) and BIS (0.702 mmol) were dissolved in 99 mL deionized water first, which was later filtered through a 0.2 μm filter. We filtered the monomer solution at this step because impurities inside the solution can have influence on the nucleation process resulting in inhomogeneous particles. Then the filtered solution was transferred to a 3-necked round bottom flask equipped with a reflux condenser, N_2 inlet, and thermometer. The solution was purged with N_2, stirred at 450 rmp and heated to 70 °C for about 1 hour. AAc (2.81 mmol) was added to the heated reaction solution in one aliquot. The addition of 1 mL APS (0.2 mmol) then initiated polymerization. The reaction was allowed to proceed at 70 °C for 4 hours under a nitrogen atmosphere. The reaction solution was allowed to cool overnight, and then it was filtered through glass wool to remove any large aggregates. The resulting microgel solution was placed in centrifuge tubes and then purified via

centrifugation at ~8300 relative centrifugal force (rcf) to form precipitation at the bottom of the centrifuge tubes, followed by removal of the supernatant and resuspension with deionized water; this process was repeated 6 times.

Fabrication of Au electrodes: Au coated coverslips were generated by thermally evaporating 2 nm Cr followed by 50 nm of Au onto a 25 × 25 mm pre-cleaned glass slide. (Torr International Inc., thermal evaporation system, Model THEUPG, New Windsor, NY).

'Paint on' protocol to deposit a microgel layer and CV loading procedure: Before the microgel monolayer's deposition, 2 × 25 mm PDSM film was used as mask to cover one side of the Au coated glass slide where is used to connect to external power supply. A 40 μL aliquot of concentrated microgels (obtained via centrifugation of a microgel solution) was added to the substrate and then spread by a micropipet tip at 30 ºC until the whole slide was covered with microgels. The microgel solution was allowed to dry completely on the substrate for 2 h at 35 ºC on a hot plate. After that, the glass slide was rinsed copiously with DI water to remove excess microgels which were not directly attached to the Au surface. The glass slide was then placed into DI water again and incubated overnight on a hot plate at 30 ºC. Following this step, the substrates were then rinsed with DI water, dried with N_2, and then soaked into 10 mL 0.04 mg/mL CV solution at pH 6.5 overnight. After overnight, CV loaded glass slides were thoroughly washed with DI water and then soaked into pH=6.5 solution for 2 hours to remove the excess CV.

Electrochemical cell assembly: The electrochemical cell was constructed as depicted in Figure 3-1. The two electrodes (one 50 nm Au glass slide and one CV loaded slide) were placed inside a cubic glass cell with 3cm × 3cm × 3cm dimension and 2 mm wall thickness. The distance between each slides is 2.4 cm.

Next, 20 mL pH=6.5 2 mM solution were added into the glass cell. And the two electrodes were connected to the external power supply. Paraffin film was used to seal the cell to prevent water evaporation and the solution was stirred at 60 rmp. 1 mL solution was transferred by a digital pipite into a quartz cuvette to monitor the absorption change during the whole process. After taken UV-Vis spectra, the solution were redumped into glass cell.

UV-Vis spectra were obtained using an Agilent 8453 UV−Vis spectrophotometer. pH was measured with a Jenco model 6173 pH meter (San Diego, CA).

3.3 Results and Discussion

Devices used for electro-stimulated drug release were fabricated as shown in Figure 3-1. To prepare the Au electrode, 2 nm Cr was deposited on glass (as an 'adhesive' layer) followed by the deposition of 50 nm Au. Following a 'paint-on' protocol mentioned in the experimental section of this Chapter, [115] we painted a densely packed pNIPAm-co-AAc microgel monolayer on top of an Au electrode. In order to connect to an external power supply conveniently, we left one side (0.5 mm × 2.5cm) of the slide unpainted. Once the microgel layer was deposited on the Au-coated

glass slide, the whole slide was incubated in a CV solution with a pH of 6.5 overnight to load CV. [144-145] We also observed there is no color change for the bare Au slides soaked into CV solution. Only the color of the microgel-coated slide became dark purple after incubation, demonstrating the successfulness of CV loading. To remove any excess CV, the CV-loaded slide was washed under copious DI water and then soaked into pH=6.5 solution for 2 h before continuing any experiment. Then two electrodes, the CV-loaded slide as an anode and the bare Au electrode as a cathode, were inserted into a homemade glass cell. An aqueous solution (20 mL, pH=6.5) was added into the glass cell and one piece of paraffin film sealed the cell to prevent water evaporation. Two leads from a power supply were clipped to the two electrodes to provide DC voltages.

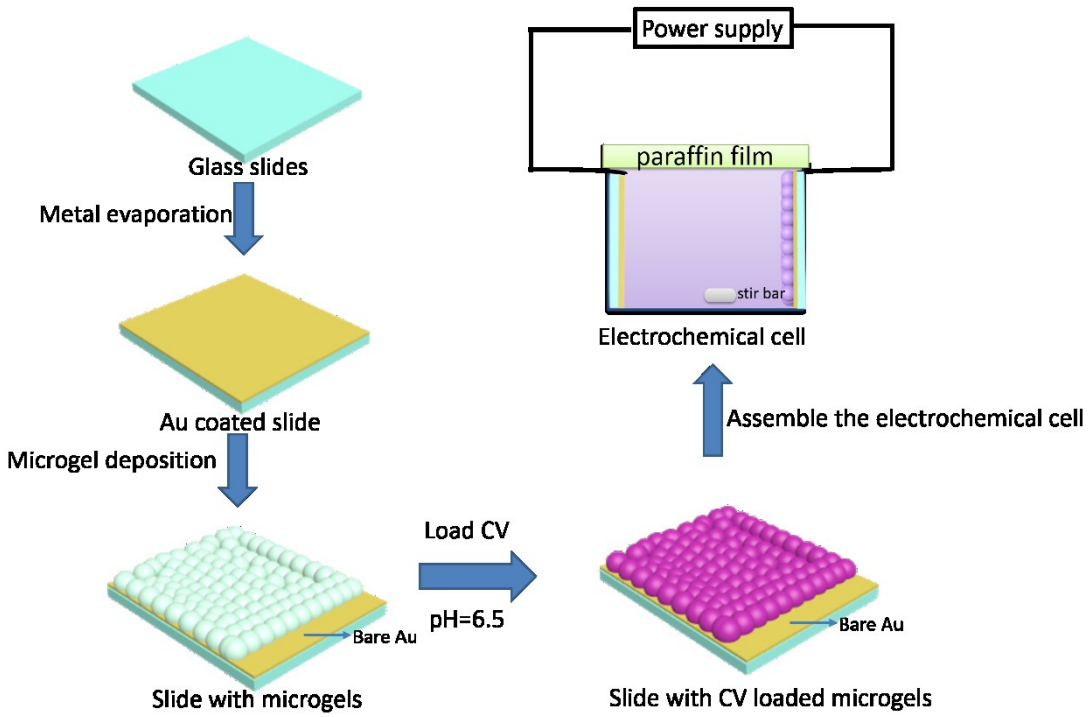

Figure 3-1 Schematic of the fabrication of the microgel coated electrode and the construction of the electrochemical cell

Figure 3-2(a) shows the chemical structure of CV, a model drug used in this work. It is a hydrophilic, positive charged small molecule. Furthermore, CV can easily dissolve in water, exhibiting a purple-violet color. Its typical UV-Vis spectrum is shown in Figure 3-2(b) and in this work, the amount of CV release was quantified by monitoring the change of the absorbance maximum at 590 nm over time.

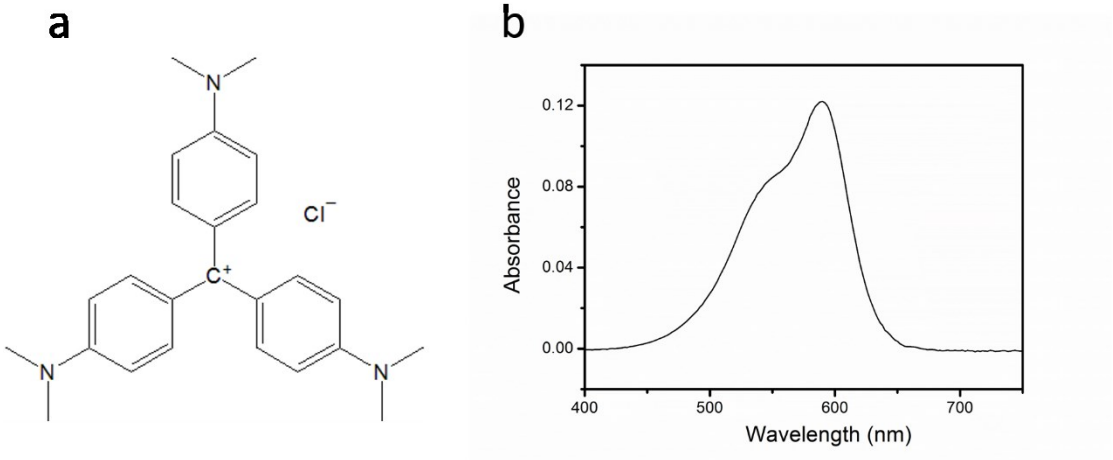

Figure 3-2 a) The chemical structure of CV; b) The UV-Vis spectrum of a CV solution

The CV loading and release mechanism is shown schematically in Figure 3-3. The strong electrostatic interactions between positively charged CV and negatively charged pNIPAm-co-AAc microgel at pH 6.5 can trap CV into the microgels' networks. However, upon exposure to a proper anodic potential, water electrolysis makes the pH near the anode drop dramatically, which neutralizes AAc groups and weakens CV-microgel interactions. [146] As a result, pNIPAm-co-AAc microgels collapse and expel CV from their networks.

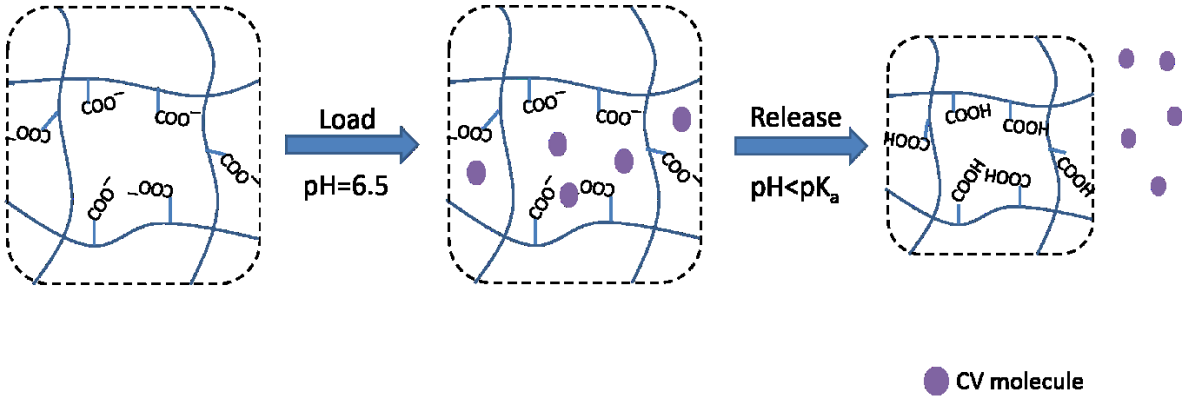

Figure 3-3 CV's loading and release mechanism

As stated above, we assume that the water electrolysis can decrease pH near the anode which can modulate the CV-microgels' electrostatic interaction and trigger CV release. To prove this hypothesis, we measured the pH value in the vicinity of the anode upon exposure to different external electric potentials. To accomplish this, two naked Au electrodes were connected to a DC power supply. A miniature pH electrode was placed near the anode at a distance of ~ 2 mm to monitor the pH change. Water electrolysis potential is ~1.23 V in a neutral solution [147] and the potentials we used here were all more than 1.23 V to ensure water electrolysis. However, the potential should not be too large as this can lead to the Au layer peeling off the glass slide and bubble generation. To establish a stable drug delivery device, we kept the voltage ≤ 4 V throughout the whole experiment. In such a way, there is no Au detachment, and the bubble generation is minimized and cannot be observed directly by naked eyes.

The result for electrochemically-induced pH changes near the anode is shown in Figure 3-4. The application of different voltages to the electrochemical cell was large

enough to yield water electrolysis, leading to a subsequent pH decrease near the anode. In detail, increasing the magnitude of the applied potential (from 2 V to 4 V) will accelerate the water electrolysis rate and result in a larger drop of pH value near the anode over a range of ~ 5.2 to ~ 3.2. Upon removal of the applied potential, the pH quickly changed back to the original bulk solution's pH around 6.5.

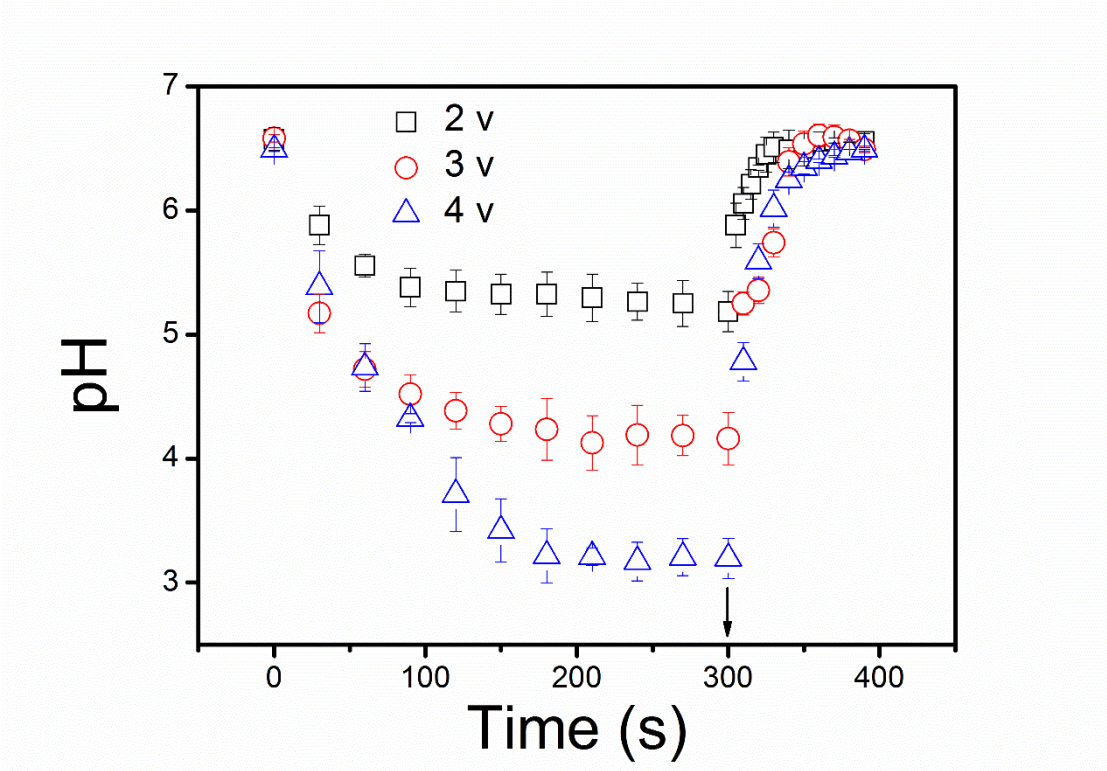

Figure 3-4 Potentials higher than the water electrolysis potential were applied across the cell and the pH near anode was monitored by a miniature pH electrode. After 300s (as the arrow points out), these potentials were removed

As detailed above, the solution's pH change is totally controlled by the external potential, which could modulate the interaction between CV molecules and microgels,

thus realizing controlled release. To demonstrate our assumption, we applied different pulsed voltages to trigger the CV release. Specifically, in one cycle, we applied the external potential on for 1 min and then removed it for 5 min. The whole on-off process was repeated four times. As detailed in the experimental section, we monitored the CV solution's absorbance change at 590 nm every one minute to determine the amount of CV release. As shown in Figure 3-5, in the controlled experiment, when there was no potential applied, no obvious CV release was observed. Absorbance only increased when the voltage was applied. Thus, the pulsed CV release profile was in sync with the frequency of applied potential. In addition, increasing the external potential resulted in a higher CV release rate. For example, in Figure 3-5, when the external voltage was applied under the same amount of time, the UV-Vis absorbance was higher under larger voltage. Such a phenonenon can be explained from the above pH measurement results. That is, the higher the potential can make the pH near anode lower. As detailed previously, electroresponsivity of the device stems from the negatively charged carboxylic groups of pNIPAm-co-AAc microgels. Lower pH means more negatively charged group will be neutralized and more CV will be released from the microgel layer, thus resulting in a higher release rate under larger voltage. In addition, upon potential removal, pH quickly changes back to 6.5, carboxylic groups become negative charged and CV was held up again in the polymer network through electrostatic attraction, thus turning off CV release.

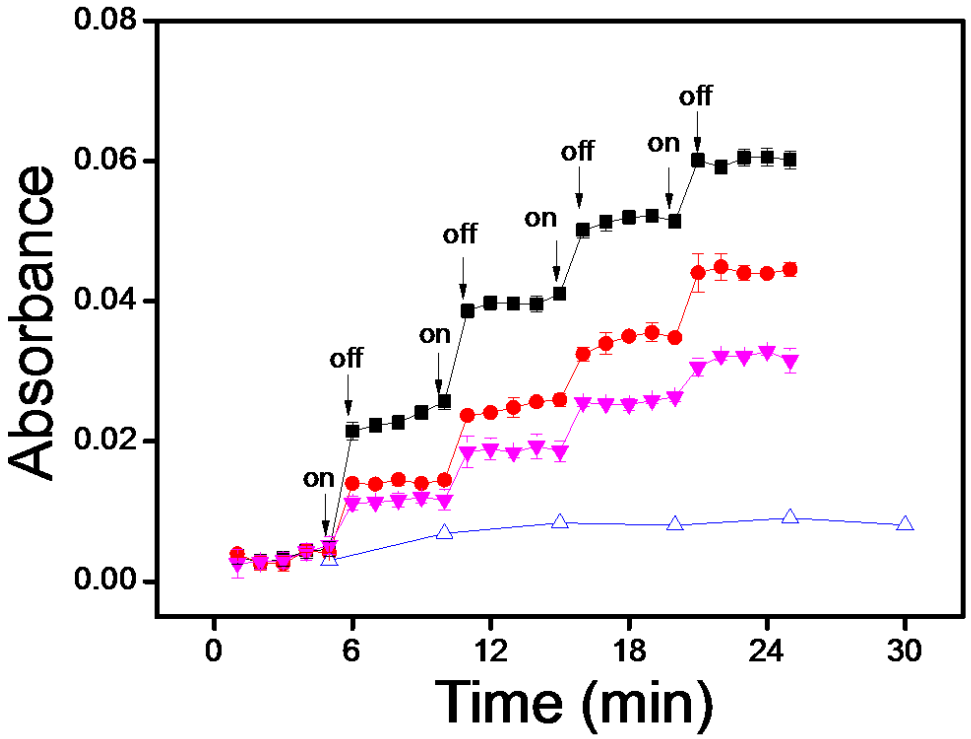

Figure 3-5 CV release profile for pulsed voltages with different magnitude. For controlled experiment, when there is no applied voltage, minimal CV release is observed. For this plot, square is 4 V, circle is 3 V, solid triangle is 2 V, hollow triangle is the control experiment

By a close examination of the CV release profile, Figure 3-6(a) shows the cumulative absorbance at 2 V/ 3V was directly proportional to the cycle number. That is, the absorbance increased linearly with the cycle numbers and these release profiles were in zero-order. However, for higher voltage (4 V), the curve was only straight initially and its slope representing the CV release rate decreased as the cycle number increased. The reason might be that the CV loaded inside the microgel monolayers was eventually depleted and it is harder for CV to transport out of the microgels in lower

concentration. To better compare the release rates under different voltages, assuming that there is enough CV inside microgels' networks, the initial slope from 4 V and slopes from 2 V and 3 V in Figure 3-6(a) were plotted against their corresponding voltages. As shown in Figure 3-6(b), the release rate increased linearly as the external voltages increased.

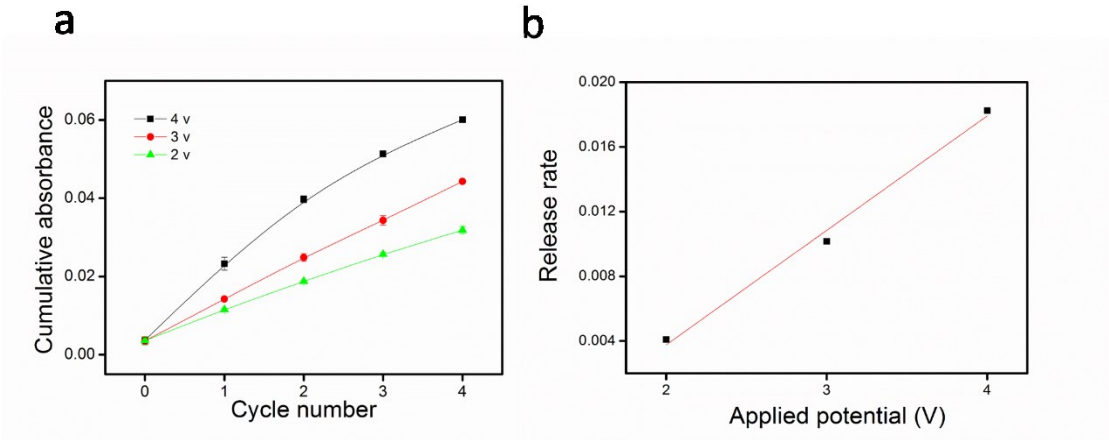

Figure 3-6 a) The relationship between cumulative absorbance and cycle numbers under different voltages; b) The relationship between release rates and the different external voltages. The red line represents the best fit curve to the data plotted under linear regression analysis

One of the major advantages for electro-triggered drug delivery is that the external potential is very easy to be programmed and different drug release profiles can be generated under the same device. Next, we want to prove that we can alter the release profile by simply tuning external potentials. In Figure 3-7, to release the same amount of CV (the absorbance reached around 0.08), continuous or pulsed voltages were used. For continuous release profiles, the external voltages were applied all the time. The

results showed that decreasing continuous voltages (from 4 V to 2 V) leaded to a longer time (from 7 min to 16 min) to release the same amount of CV. We also chosed a pulsatile pattern to control CV release. As shown in the hollow triangle curve from Figure 3-7, we did the on-off switching under 4 V, compared to continuous 4 V, pulsatile 4 V needed 33 min to reach the similar aborbance, which demonstrated that the external electric field can control the CV release precisely by varying the magnitude and frequency of the applied voltage. It is worth to mention that at 4th cycle, we observed slightly decreasing in absorbance when voltage was off. Back flow of the drug from environment to hydrogel is also reported previously.[61] The reason might be that the gel's reswelling process could re-absorb the surrounding liquid containing CV.

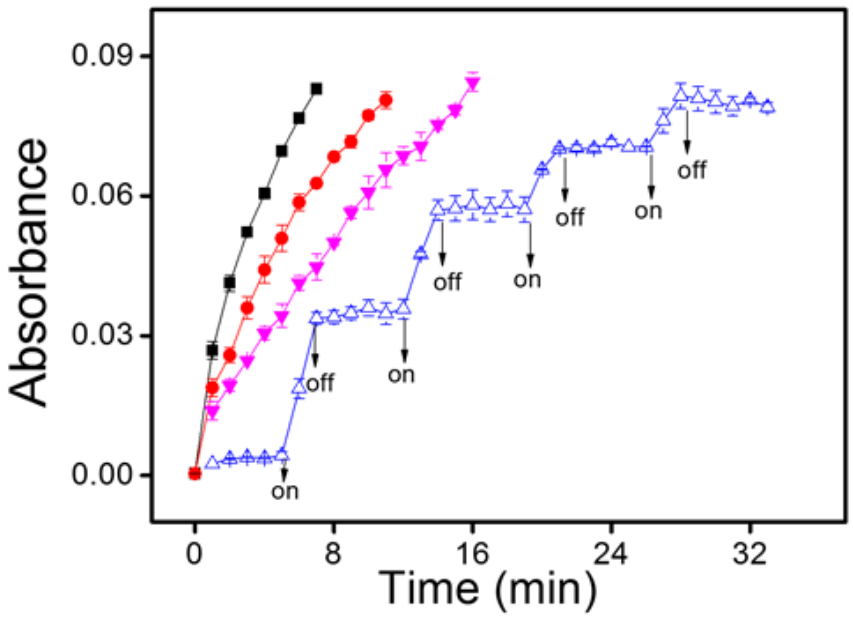

Figure 3-7 To release same amount of CV, continuous/ pulsed potential supply strategies were used. For this plot, Square is 4 V, circle is 3 V, solid triangle is 2 V, hollow triangle is pulsed 4 V

Finally, we showed that the microgels deposited on the electrodes could be used to load and release small molecules multiple times. To demonstrate, after the CV release was complete, we resoaked the microgel-coated Au electrode in a CV solution overnight and assembled the same electrochemical cell to conduct the experiment. Figure 3-8 shows that the same microgel deposited electrode had a similar release profile when reused for five times under 4 V.

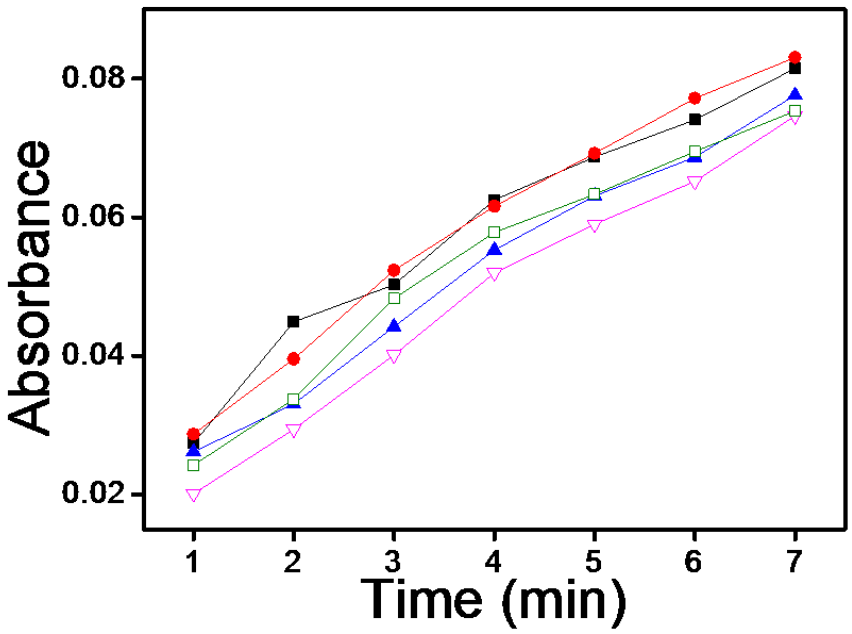

Figure 3-8 Reusage of the microgel coated Au electrode. Solid circle is the first run; solid square is the second run, solid triangle is third run; hollow triangle is fourth run and hollow square is the fifth run

3.4 Conclusion

In this Chapter, we demonstrated that a monolithic layer of pNIPAm-co-AAc microgel as a reservoir to load and release a model drug, CV. pNIPAm-co-AAc microgel deposited Au electrode was used as an anode throughoutall experiments. The pH dropped near the anode upon the application of proper potentials, which neutralized carboxylic group and triggered CV release. Upon the potential removal, pH near the anode went back to 6.5, which made carboxylic group charged again, hence CV release was turned off. We demonstrated that CV release profiles were influenced by the magnitude, duration and interval of the applied anodic potential. Furthermore, we proved that our device could be reused multiple times by showing similar release profiles after reloading CV. This study may find application in on demand drug release in real time.

Chapter 4 Electrochemically Color Tunable pNIPAm Microgel-Based Etalons[1]

In this Chapter, we show that by deposition of another Au layer on top of a microgel monolayer (as in Chapter 3), optical devices (etalons) could be generated that respond by changing color in response to an applied electric field. Specifically, we demonstrated that the optical properties of the etalon could be manipulated upon the application of an appropriate electric potential between the etalon and a counter electrode, both in an electrolyte solution. The dramatic optical property changes coupled with the reversibility of the device's color makes this system potentially useful for display device applications.

4.1 Introduction

Display devices that utilize light emission to produce high quality images have enormous utility, but do not produce high fidelity images when used in certain environments, e.g., bright sunlight. In contrast, electronic paper (e-paper) utilizes reflected light from an external light source to generate an image. The effect leads to a display that is more like "real" paper, allowing it to be used more effectively in bright environments. However, up to now, commercialized e-paper devices are available in black-and-white, while it is still difficult to develop and commercialize multicolor e-paper.

PMs, as detailed in section 2.2, can exhibit color by affecting light propagating through its ordered structure. [106, 148-149] Specifically, light interacting with ordered

[1] This Chapter has been adapted from a previously published paper. Wenwen Xu, Yongfeng Gao and Michael J. Serpe, J. Mater. Chem. C, 2014, 2, 3873-3878.

elements in a material leads to constructive and destructive interference of light waves propagating through it, yielding color. This kind of material is inherently bright under strong light illumination, and is not subject to photobleaching making it is more durable than pigments/chromophores and an ideal candidate for colored e-paper. [100, 150-155]

Along these lines, Ozin and coworkers reported that iron based metallopolymer films display voltage-dependent color due to a redox reaction.[100] The Kang group fabricated polystyrene-block-poly(2-vinyl pyridine) (PS-b-P2VP) block copolymer based photonic gel where recorded information can be maintained for longer than 96 h.[153] The Yin group embedded silica-coated Fe_3O_4 colloids into poly(ethylene glycol) diacrylate (PEGDA) films to make rewritable photonic paper.[154] All of the above materials are capable of maintaining their recorded information (e.g., color, image) without the use of an external power supply. Hence, lower power consumption is one of the major advantages of e-paper displays, compared to light emitting diode (LED) and liquid crystal display (LCD) technologies. Therefore this relatively new area is worth much more research attention.

Our group has previously fabricated and characterized etalon devices using pNIPAm-based microgels sandwiched between two semi-transparent metal layers.[116, 156] Such a device (referred to as an etalon) displays vivid colors, which are dynamically tunable over a large range of visible wavelengths. The devices operate by light impinging on the etalon entering the microgel-based cavity and resonating between the two Au layers. This behavior leads to constructive and destructive interference, which

leads to color. This is a direct result of interference, where specific light wavelengths are reflected, while others are transmitted. The specific reflected wavelengths lead to peaks in a reflectance spectrum, where the peak position(s) can be predicted by Equation (4-1):

$$m\lambda = 2nd \cos(\beta) \qquad (4\text{-}1)$$

Where λ is the wavelength maximum of a peak with a given peak order m, n is the refractive index of the dielectric (microgel) layer, d is the distance between the Au layers and β is the angle of incidence. Under most situations, the incident light is normal to etalon surface and the effect of refractive index is negligible compared to the change induced by the change in d. Therefore, generally speaking, for a given m, microgel swelling leads to an increase in d, which yields a red shift in the position of a given reflectance peak. Likewise, microgel collapse leads to a blue shift.

Since discovering these devices, they have been used to sense pH,[117] glucose,[118] temperature,[119] and macromolecules.[120] Here, we expand the utility of these devices by showing that their color can be made tunable to electric fields for possible e-paper display applications.

4.2 Experimental Section

Materials: N-isopropylacrylamide (NIPAm) was purchased from TCI (Portland, Oregon) and purified by recrystallization from hexanes (ACS reagent grade, EMD, Gibbstown, NJ) prior to use. *N,N'*-methylenebisacrylamide (BIS) (99%), acrylic acid

(AAc) (99%), ammonium persufate (APS) (98+%) and lithium acetate (99%) were obtained from Aldrich (St. Louis, MO) and were used as received. Deionized (DI) water with a resistivity of 18.2 MΩ·cm was used. Cr/Au annealing was done in a Thermolyne muffle furnace from ThermoFisher Scientific (Ottawa, Ontario). Fisher's finest glass coverslips were 25 × 25 mm and obtained from Fisher Scientific (Ottawa, Ontario). Indium tin oxide (ITO) coated glass slide were 25 × 25 × 1.1 mm with a resistivity of 30-60 Ω from Delta technologies. Cr was 99.999% and obtained from ESPI as flakes (Ashland, OR), while Au was 99.99% and obtained from MRCS Canada (Edmonton, AB). Spacers with thickness: 2.5 mm were purchased from Life Technologies (Eugene, OR) and cut into suitable sizes for the particular experiment. Polydimethylsiloxane (PDMS) was purchased from Dow Corning Corporation (Midland, MI).

Instruments: Reflectance spectra were collected by a Red Tide USB650 spectrometer, using a reflectance probe connected to a LS-1 tungsten light source (Ocean Optics, Dunedin). The spectra were collected over a wavelength range of 400–1000 nm and analyzed by Ocean Optics Spectra Suite Spectroscopy software. pH was measured with a Jenco model 6173 pH meter (San Diego, CA)

Preparation of electrochemical color tunable devices: Microgels and etalons were fabricated as previously described.[116] The electrochemical cell was constructed as depicted in Figure 4-2(a). The two electrodes (etalon and ITO glass slide) were separated using a spacer and clamped together. Electrolyte solution was then injected into the gap between the two slides. Finally, two leads from a power supply were

clipped to the two electrodes.

Patterned etalon fabrication: PDMS elastomer was molded and cured in a Petri dish. The PDMS base was first mixed with curing agent at a ratio of 10:1 in volume. The PDMS mixture was then poured into the Petri dish, which formed a thin layer, and allowed to cure overnight at 70 ºC. Finally, the PDMS layer was mechanically peeled off from the Petri dish and cut into a shape of maple leaf (12 mm × 15 mm). The prepared PDMS maple leaf pattern was used as follows. First, the PDMS mask was used to cover the Au, while pNIPAm microgels (non-pH responsive) microgels were painted on the uncovered portions of the substrate. The PDMS mask was removed and pNIPAm-*co*-AAc microgels were painted on the patterned area. Then following the normal etalon fabrication process described above to yield the patterned device -- a maple leaf structure composed of pNIPAm-*co*-AAc microgels surrounded by non-pH responsive microgels.

4.3 Results and Discussion

To render etalon devices electroresponsive, we treated the etalon as one electrode in an electrochemical cell. It has been proven in Chapter 3 that a suitable potential between two electrodes in water leads to water electrolysis (reduction potential for water is 1.23V at pH 7[157]), which leads to a pH change near both the anode and the cathode. Similarly, to make our devices electrochemically active, we fabricated etalons

from pH responsive pNIPAm-co-AAc microgels. These microgels, and etalons, respond to pH by swelling at high pH. This swelling is a result of the majority of AAc groups becoming negatively charged at high pH, leading to electrostatic repulsion and osmotic pressure effects. At low pHs, the AAc groups are protonated, and the microgels deswell back to their initial diameter. We have shown that the solvation state modulation as a function of pH leads to an etalon color change and a shift in the position of the peaks in the reflectance spectra.[158] As such, we hypothesize that the pH change of the solution in response to water electrolysis should lead to a color change, and a shift in the peak positions.

For this investigation, pNIPAm-*co*-AAc microgel-based etalons were fabricated and displayed characteristic multipeak reflectance spectra. A schematic of the device structure and a representative reflectance spectrum is shown in Figure 4-1.

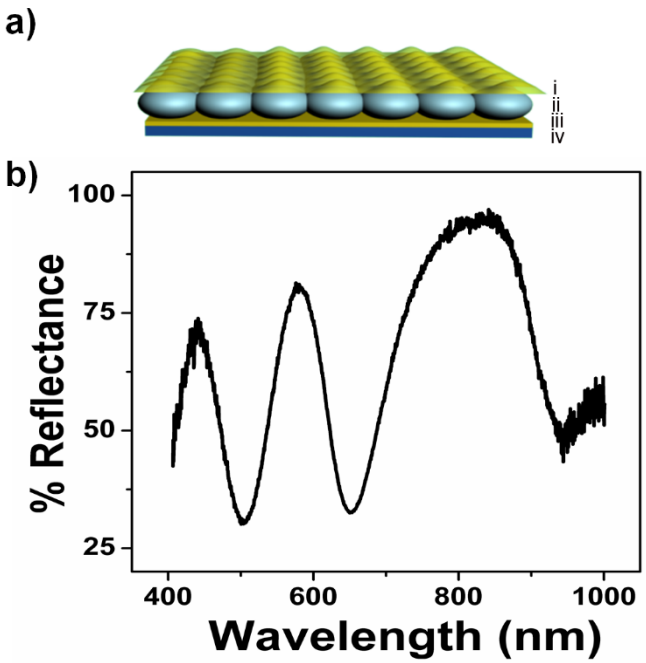

Figure 4-1 a) Microgel-based etalons were fabricated by (ii) sandwiching a microgel layer between (i, iii) two 15 nm Au layers (2 nm Cr used as an adhesion layer) (iv) all supported on a glass microscope slide. b) A representative reflectance spectrum for an etalon with no voltage applied. Reproduced with permission from ref. 157, Copyright 2014, Royal Society of Chemistry

For all experiments here, the position of the peak centered at ~574 nm was monitored. As depicted in Figure 4-2 (a), the etalons were connected to a power supply and used as the working electrode, while an indium tin oxide (ITO) glass slide functioned as a counter electrode. An insulator separated the two electrodes and a selected electrolyte was introduced into the space between the ITO slide and etalon. We found the selection of the electrolyte solution to be critical. First, the electrolyte solution should swell the microgels in the etalon; still allowing them to respond to the electrochemically-induced pH changes. Second, ITO glass has been shown to react with water electrolysis products, leading to a decrease in its conductivity and transparency.[159-160] For our experiments we found that a solution of 0.1 M $LiOOCCH_3$ in a mixture of water and ethanol (1:9 by volume, respectively) yielded all of the desired properties. As mentioned above, application of a DC voltage with the appropriate magnitude to electrodes in water leads to electrolysis, which results in a change in the solution's pH.[161] In this case, when an appropriate negative potential was applied to the etalon, water reduction occurred, leading to hydrogen gas generation and an increase in the water pH in the vicinity of etalon. On the contrary, when the etalon was

held at positive potential, oxygen gas will be produced, resulting in a decrease in the water pH near the etalon. In all of the experiments, voltages were carefully controlled so that the gas generation is minimized and does not damage the optical properties of our device. This process is depicted schematically in Figure 4-2 (b). Thus, pNIPAm-*co*-AAc microgel-based etalons should change their optical properties (color) when the respective potentials are applied to the etalon.

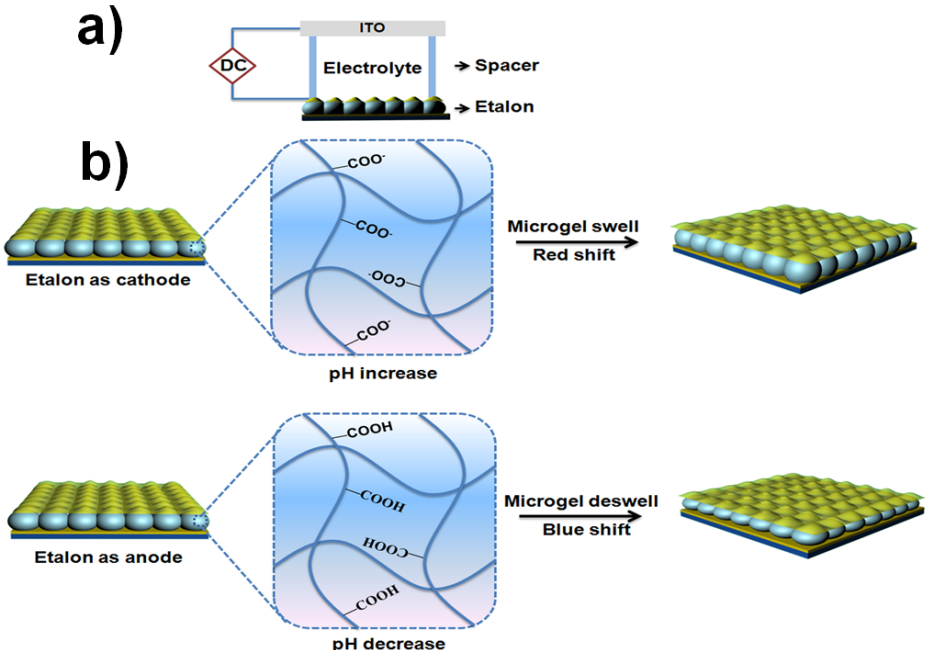

Figure 4-2 a) Schematic of the etalon-based electrochemical cell and b) Schematic representation of the responsivity of the etalon when it behaves as a cathode and anode.

Reproduced with permission from ref. 157, Copyright 2014, Royal Society of Chemistry

To investigate this, we exposed the etalons to an aqueous solution with a pH of 9.4 and varied the voltage applied to the etalon. Specifically, the etalon was initially held at a more negative voltage and scanned to a more positive voltage while the pH near the etalon was monitored using a miniature pH electrode. In addition, the reflectance spectrum was monitored as the voltage was varied. The results are shown in Figure 4-3 and show that the application of different voltages to the etalon was enough to yield water electrolysis and a concomitant change in the solution pH. Specifically, application of increasingly positive voltages to the etalon leads to a decrease in the solution pH, which leads to protonation of the microgel's AAc groups and a concomitant blue shift of the monitored reflectance peak. On the other hand, when increasingly negative potentials are applied to the etalon, the solution pH increases, leading to deprotonation of the microgel's AAc groups and a concomitant red shift of the monitored reflectance peak. It is worth pointing out here that we were only able to vary the solution pH in the range of ~9-13 electrochemically. Over this pH range, we don't expect AAc to be significantly protonated/deprotonated since the pK_a for AAc is ~4.25. While this is the case, we believe that even at this high pH, there is enough change in the protonation state of the microgels to yield the appropriate amount of relative deswelling/swelling required to give a significant blue/red shift of the reflectance peaks. There have been literature reports supporting this behavior; AAc-

based gels swelling at pHs well beyond their pK_a.[161] The another reason for the AAc-based gel responding at high pH might be that AAc could have different dissociation constant in ethanol/water mixture compared to pure water. While the etalon is capable of responding to solution pH changes well above AAc's pK_a, it should be capable of significantly more response if the pH of the solution could be further decreased to below AAc's pK_a. To investigate this, we maintained the etalon's potential at 2 V while varying the pH of the solution by the addition of a dilute solution of HCl to the etalon while monitoring the position of the monitored reflectance peaks. As can be seen in the shaded region of Figure 4-3, the device is capable of significant response as the pH of the solution is varied near AAc's pK_a.

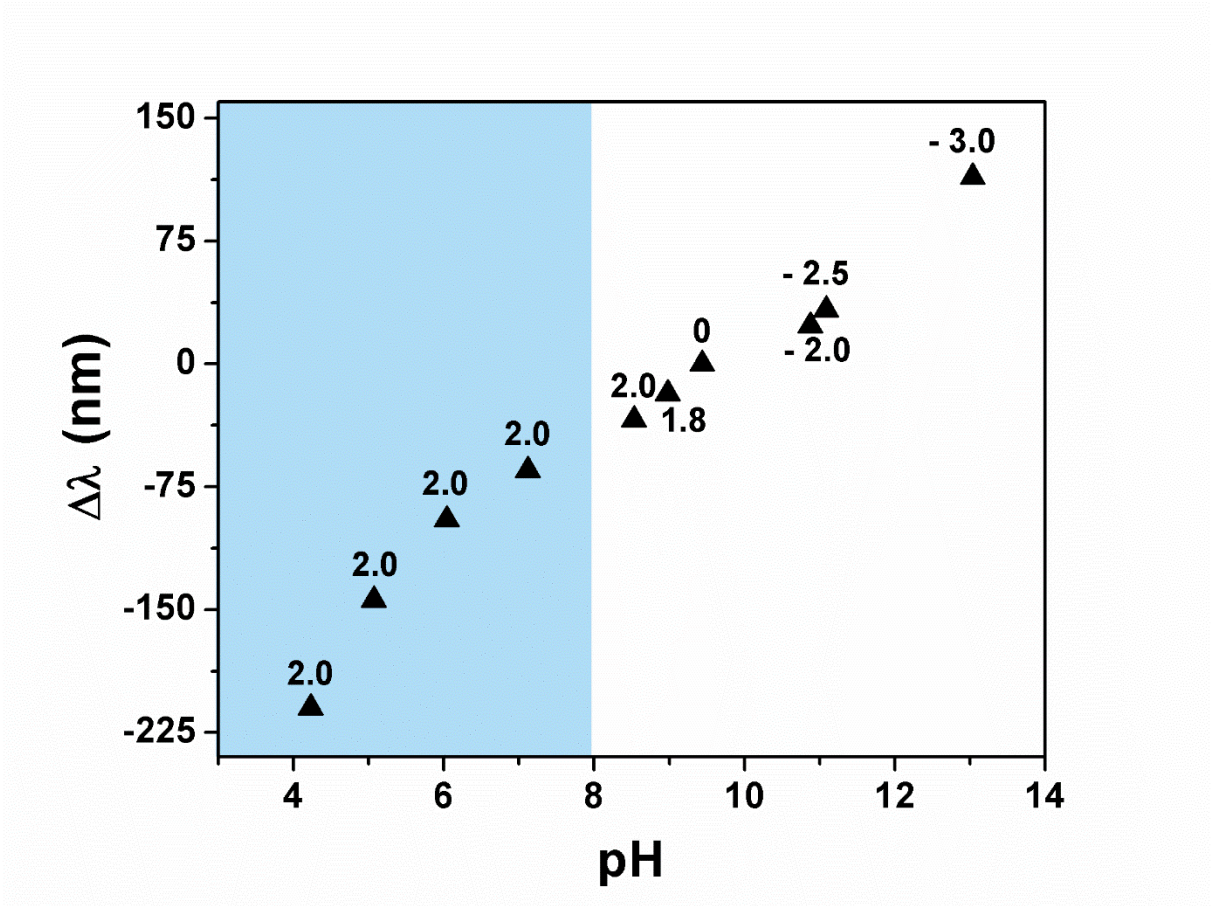

Figure 4-3 Etalon wavelength shift as a function of pH induced by the applied voltage (indicated as numbers by the individual data points). The wavelength shift ($\Delta\lambda$) is $\lambda_{pH} - \lambda_{0V}$, where λ_{pH} is the position of the peak when a given voltage is applied that yields a specific solution pH and λ_{0V} is the initial position of the peak when there is no voltage applied. (Shaded region) The solution pH in this range was varied by adding dilute HCl to the device while maintaining the etalon at 2 V. The solution pH was monitored at ~ 0.5 mm away from the etalon surface using a miniature pH electrode. Reproduced with permission from ref. 157, Copyright 2014, Royal Society of Chemistry

To further support this hypothesis, we monitored the etalon's optical response to changes in solution pH in the range of 9 to 13, in the absence of an applied electric field.

The results, which are shown in the Figure 4-4, show that the etalon is able to respond to solution pH changes in this range.

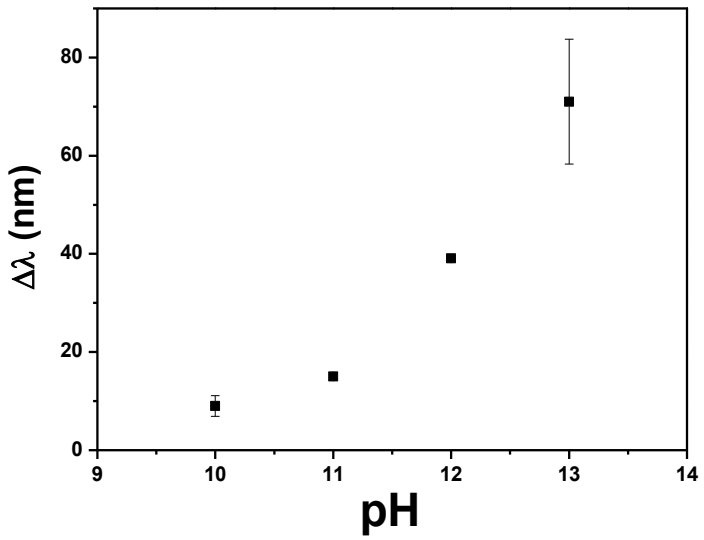

Figure 4-4 Etalon's optical response in different pH environment, $\Delta\lambda$ is λ_m - $\lambda_{original}$, where λ_m is the position of the peak at a given pH (m) and $\lambda_{original}$ is the initial position of the peak when the pH=9. Each data point is the average of 3 experiments, with the error bars as the standard deviation. Reproduced with permission from ref. 157, Copyright 2014, Royal Society of Chemistry

It is worth pointing out though that the etalon's response to pH alone is not as pronounced as its response to pH change induced by the applied potential. While it is not completely understood why this is the case,[62, 162-163] we believe that the electrode's electrostatic interactions with the counterion Li^+ results in electrodiffusion phenomena, yielding the enhanced response. Specifically, when a negative voltage is applied to the etalon, the Li^+ will move to the etalon due to electrophoretic migration and facilitate

the ionization of the microgels AAc groups. This yields more Coulombic repulsion and osmotic swelling of the polymer layer, and a greater optical response.

Finally, we point out that there is no response to pH changes for pNIPAm microgel-based etalons, i.e., etalons composed of microgels with no AAc. We add here that since pNIPAm is thermoresponsive, the solution temperature was monitored throughout this process, and no significant temperature change was observed. Therefore, we attribute the changes of the etalon's optical properties to the both the solution pH changes and the apparent sensitivity of the microgel solvation state to the applied electric field.

We also investigated the kinetics of the etalon's spectral response to the application of a potential and how the response kinetics varied with the magnituge of the applied potential. In this part of experiment, we assembled the cell and waited for the optical spectra to stabilize with no voltage applied. After the spectra were stable, we applied various voltages to the etalon. Figure 4-5 shows that the rate of the monitored reflectance peak shift depended dramatically on the applied voltage. Specifically, when the applied potential is relatively low (-2.0 and -2.5 V) the monitored reflectance peak shifts slowly with time, while it is significantly faster at -3.0 V. We hypothesize that this is a result of the increased rate of water electrolysis at -3.0 V, which is capable of changing the solution pH in a shorter time period. It is important to point out that the etalons are stable after 30 minutes.

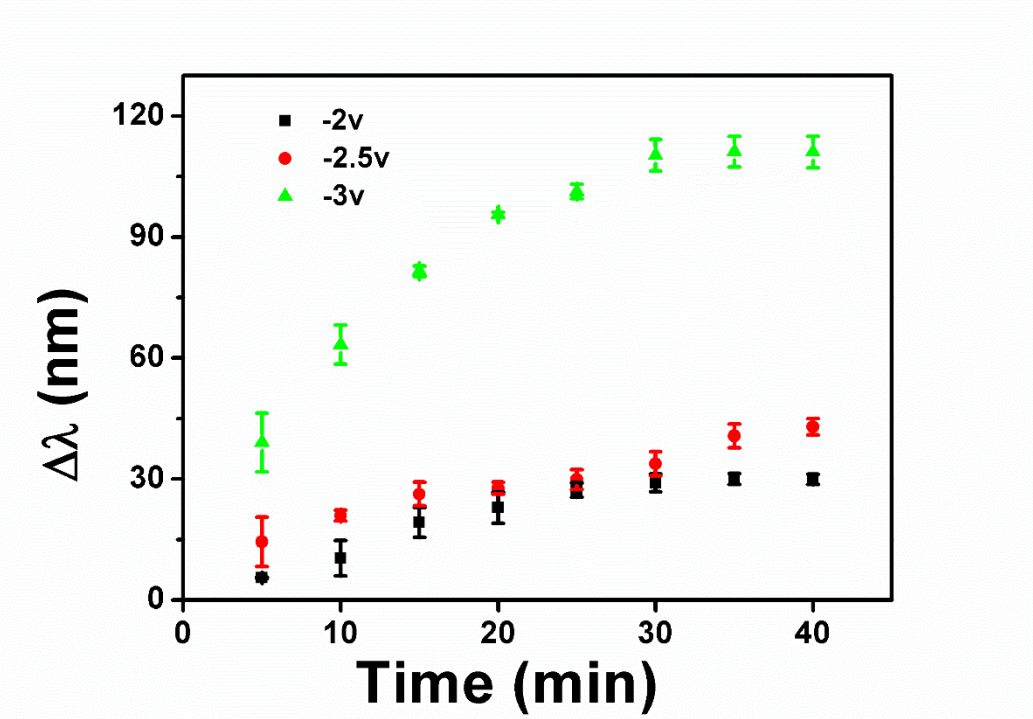

Figure 4-5 Change in the reflectance peak position (Δλ) as a function of time for various applied potentials. Here, Δλ is $\lambda_t - \lambda_{original}$, where λ_t is the position of the peak at a given time after applying a given potential and $\lambda_{original}$ is the initial position of the peak. Each data point is the average of 3 experiments, with the error bars as the standard deviation. Reproduced with permission from ref. 157, Copyright 2014, Royal Society of Chemistry

The reversibility of the etalon's response to the voltage induced solution pH changes was also investigated. Initially, we determined if the device's optical properties were stable after the application of a specific voltage to the etalon, followed by the removal of the applied voltage. We found that the reflectance peak shifts 70 nm back toward its initial position after application and removal of -3 V followed by overnight

incubation. We point out though that the etalon's optical properties could not return to their initial state by simply waiting, even though the solution pH returned to its initial value, see Figure 4-6 and Figure 4-7.

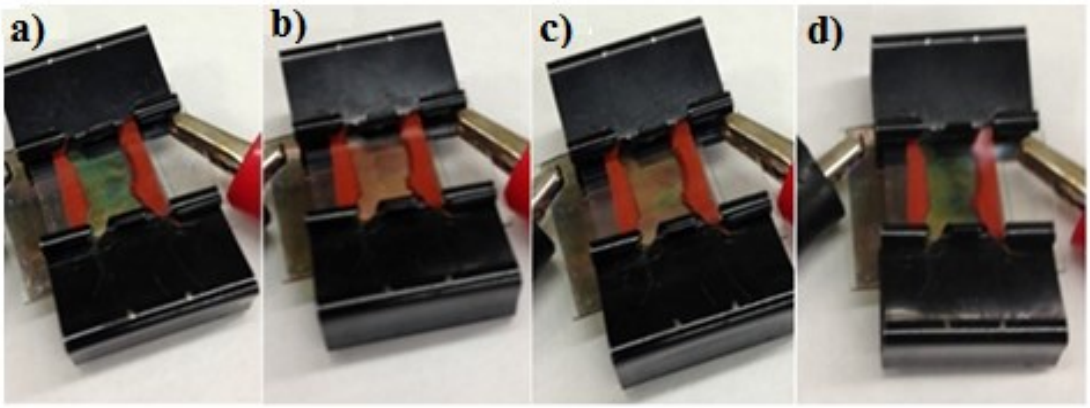

Figure 4-6 Photographs of an etalon at: a) 0 V, b) – 3 V, c) after five days at 0 V after the -3 V in (b), and d) 2 V. Reproduced with permission from ref. 157, Copyright 2014, Royal Society of Chemistry

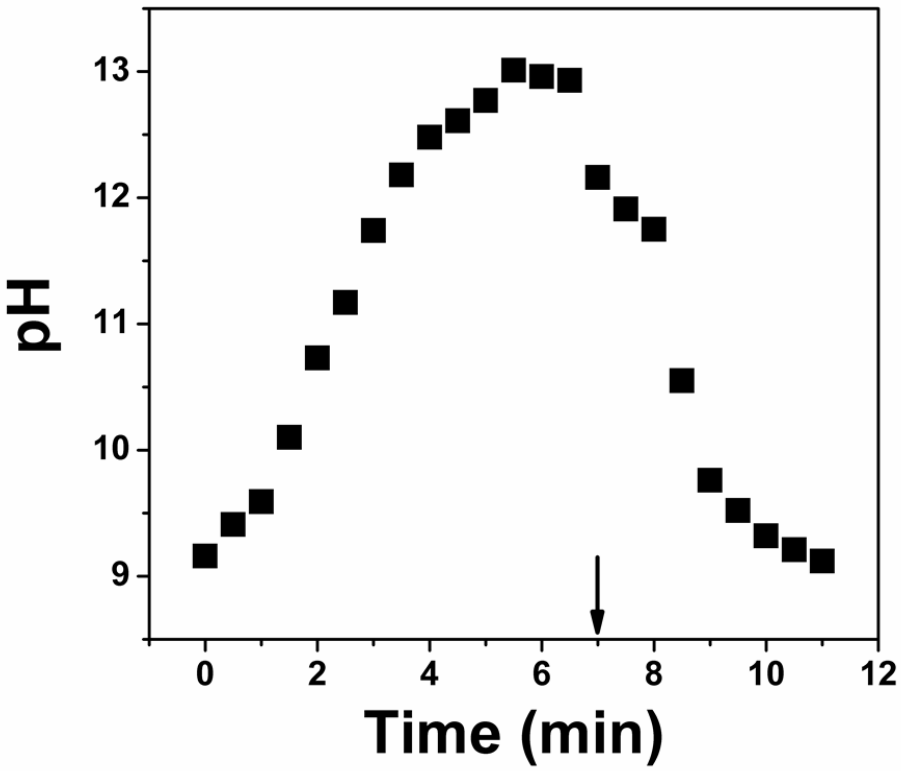

Figure 4-7 -3V is applied across the cell. After 7 min (as the arrow points out), the potential is removed. Reproduced with permission from ref. 157, Copyright 2014, Royal Society of Chemistry

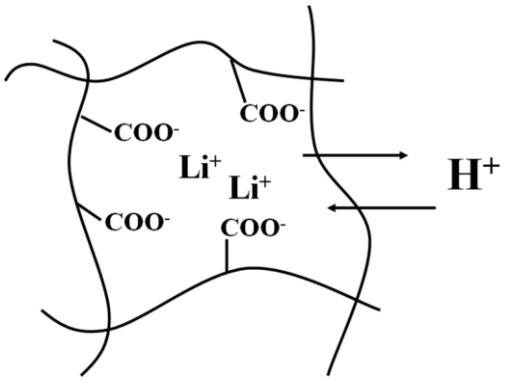

Figure 4-8 Proposed mechanism for color stability. The presence of Li ions makes the protonation of the deprotonated AAc groups difficult, hence the device's color is stable.

Reproduced with permission from ref. 157, Copyright 2014, Royal Society of Chemistry

We attribute this to ion-induced hysteresis (shown in Figure 4-8) that has been previously observed by our group and others. According to our group's previous inviestigation, it is possible that H^+ has to overcome the cation-carboxylate binding energy in order to protonate carboxylic groups, which could trigger the hysteresis in a pH cycle.[164-165] In this case, we investigated if the etalon could be made reversible by applying the opposite polarity on the etalon. That is, immediately after the application of a negative voltage to the etalon, a positive voltage was applied, while monitoring the etalon's optical properties. The results are shown in Figure 4-9, which reveal that the etalon is capable of reversible red/blue shifts in response to systematic voltage variations from negative to positive voltages.

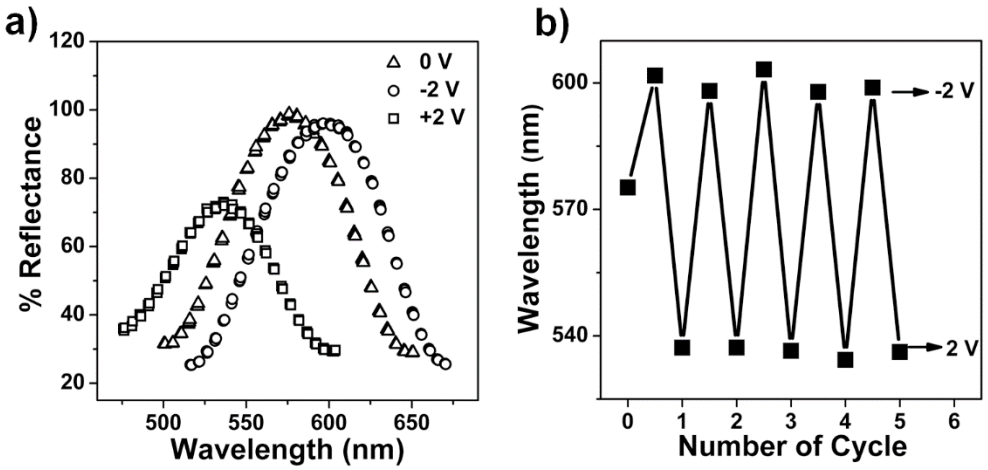

Figure 4-9 a) Reflectance spectra collected from an etalon after the application of the indicated voltages. b) Final peak positions after application of the indicated potentials

to the etalon over many cycles. Reproduced with permission from ref. 157, Copyright 2014, Royal Society of Chemistry

The kinetics of the reversibility are shown in Tables 4-1 and 4-2, which reveal that the reversibility was faster when the applied voltage to trigger the reversibility increased. This is most likely due to the faster solution pH changes at the larger applied potential. We again attribute the reversibility to both pH change from water electrolysis and electrokinetic process. That is, when a positive voltage is applied to etalon, Li^+ will move away from the etalon, making AAc protonation more efficient. We also point out that since a voltage of <1.8 V cannot hydrolyze water, and a voltage >3 V dissolves the Au layer, we must work in a narrow voltage range.

Voltage (V)	Time (min)	Total shift (nm)	Rate (nm/min)
-2	3.8 ± 0.3	61 ± 1	16
-2.5	5.1 ± 0.8	77 ± 3	15
-3	12 ± 4	140 ± 10	12

Table 4-1 Reversibility of the etalon's reflectance peak after application of 2 V followed by application of the indicated potentials. Total shift is $\lambda_{\text{negative voltage}} - \lambda_{\text{positive voltage}}$, time is the time required to achieve the total shift and rate is average total shift/average time. Each value is the average of 3 experiments, with the error bars as the standard deviation. Reproduced with permission from ref. 157, Copyright 2014, Royal Society of Chemistry

Voltage (V)	Time (min)	Total shift (nm)	Rate (nm/min)
-2	9 ± 2	49 ± 6	5
-2.5	12 ± 1	68 ± 7	5.7
-3	16 ± 2	110 ± 10	6.9

Table 4-2 Reversibility of the etalon's reflectance peak after application of 1.8 V followed by application of the indicated potentials. Total shift is $\lambda_{\text{negative voltage}} - \lambda_{\text{positive voltage}}$, time is the time required to achieve the total shift and rate is average total shift/average time. Each value is the average of 3 experiments, with the error bars as the standard deviation. Reproduced with permission from ref. 157, Copyright 2014, Royal Society of Chemistry

Finally, we wanted to show that the change in the device's spectral properties could translate into visual color changes. To demonstrate this, we fabricated a patterned etalon, where the patterned portion of the etalon was constructed from pH responsive microgels while the rest of the device was constructed from non-pH responsive microgels. Therefore, when a potential is applied to the device, it should only change color in the patterned region. As shown in Figure 4-10, when an appropriate voltage is applied to the system, the patterned region changes color, while the background remains largely unchanged. The patterned region is capable of reverting to its initial color upon the application of the opposite potential. We acknowledge that the maple leaf pattern is not completely uniform, which may be a result of the nonuniformity of the painting protocol, e.g., some non-pH responsive microgel may be painted at the edges of the

pattern. This, combined with the slight imperfections in the etalon itself, could lead to the observed imperfections. We point out here that the device's color is stable for many hours upon removal of the initial "color changing" voltage. We attribute the color stability to previously studied ion-dependent hysteresis.[158]

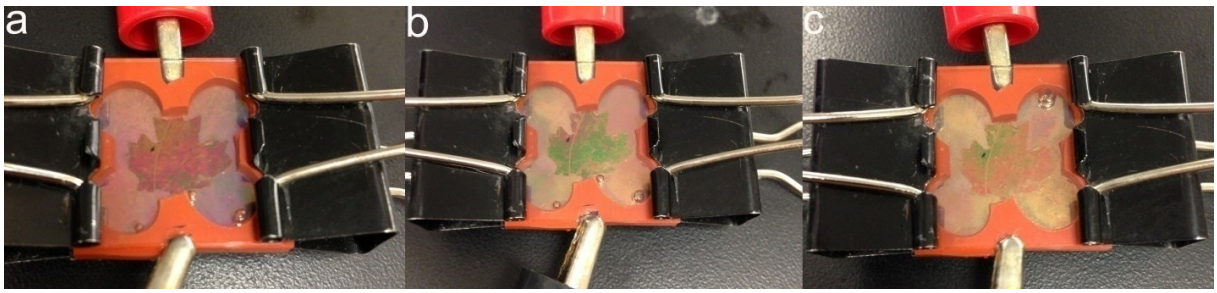

Figure 4-10 Photographs of a patterned etalon in an electrochemical cell at: a) 0 V, b) 2 V, and c) -2 V. Reproduced with permission from ref. 157, Copyright 2014, Royal Society of Chemistry

4.4 Conclusion

In conclusion, we demonstrated that microgel-based etalons could be made to respond to the application of an electric field by incorporating pH responsive microgels into their structure. Water electrolysis at the etalon surface upon the application of a suitable potential to the device is able to change the pH of the surrounding solution enough to make the microgels change size, changing the etalon's color as a result. The observed spectral shifts and color changes were attributed to both the etalon's sensitivity to pH and the applied potential itself. We showed that the color change is stable for many hours, until an appropriate potential is applied to make the solution pH revert to its initial value, combined with the potential-induced effect. The device color switching

kinetics were also probed, and showed significant color changes on the minute time scale. While we would like to make the response of the devices faster, we are confident that this is a step forward for photonics-based display technologies.

Chapter 5 Electrically Actuated pNIPAm Microgel-Based Etalons

Chapter 3 and 4 shows that pNIPAm-based microgels can be made to respond to electrically-induced pH changes which can potentially be used for controlled/triggered drug delivery and display devices. However, there are drawbacks for the previous investigations. For example, the response speed in Chapter 4 is slow and the device needs almost half an hour to reach equilibrium. In the meanwhile, the reusability of the device is limited since ITO glass tend to react with water electrolysis products and lose its conductivity. In order to overcome the above problems, this Chapter further proposed that instead of just relying on the pH change, pNIPAm-based microgels can have electroresponsivity stemming from the charge-charge interactions between the two Au electrodes and the charged microgel layer. We showed in this Chapter that the reponse speed is much faster and by avoiding ITO glass, our device can be used at a larger voltage range in water.

5.1 Introduction

As detailed in Chapter 1, hydrogels are hydrophilic polymer-based networks that are capable of swelling with water to many times their dry volume. Generally, they are mechanically robust, high water absorbent and transparent, which makes them perfect materials for actuation study.[4, 166-167] For example, hydrogels can absorb ionic liquids and behave as conductors. Compared to tradition rigid metal conductors, hydrogel conductors are soft, which can allow them to be used as stretchable electronics.[168] An ionic gel can be incorporated into an electrochemical cell and water electrolysis can be

used to change the environmental pH, which can affect the gel's solvation state resulting in gel bending.[169] By imposing a polyanionic gel on top of an Au electrode, the Hayward group demonstrated that the flat gel surface can be actuated to form crease/crater patterns at the anode under low voltage.[170]

While macroscopic hydrogel's actuation has been intensively investigated, micro/nanogel's actuation has not been thoroughly studied. In this Chapter, we investigate pNIPAm microgel layer's electrically-stimulated actuation. There are several reasons for us to be interested in pNIPAm microgels. First, pNIPAm is a typical thermoresponsive material, which has a LCST around 32 ºC.[171] Short circuits can generate large amount of heat which can stimulate the pNIPAm polymer's temperature response. Secondly, pNIPAm-based microgels are soft and deformable; according to previous AFM data, 1 nN can deform the pNIPAm microgels on the order of 100 nm.[15] Hence, it is possible to elongate and compress pNIPAm microgels under a moderate electric field. Last but not the least, pNIPAm microgel properties can be easily tuned as desired. By varying crosslinking density, we can obtain pNIPAm microgels with different stiffnesses. Via addition of different functional comonomers during polymerization, we can synthesize pNIPAm-based microgels with different functionalities.[172-174] For example, AAc is commonly employed during pNIPAm microgels' synthesis which can make the negatively charged microgels when pH > 4.25. In another example, through copolymerizing of NIPAm with APMAH, the resultant microgels have positive charged primary amine groups at pH < 9. All the pH responsivities of microgels and the chemical structures of these comonomers are

detailed in section 1.2.

In this Chapter, we continued to explore etalon devices' response to electric fields (electroresponsivity). The work in this Chapter is distinct from the previous Chapter due to the etalon being connected to both leads of an external power supply. In addition, to simplify our data interpretation, we use DI water as the solvent as opposed to solutions with pH adjusted containing various ions. This was primarily to allow us to rule out the possibility of external ions influencing the behavior of our systems. Since we use rigid glass slides as substrates, the confined microgel layer has only one free end and can only move in one direction. We demonstrate that there are two mechanisms capable of actuating the microgel layer in an external electric field. First, in short circuit, significant amount of heat will be generated. The Au electrode can be treated as a heater and the whole device's temperature will rise above pNIPAm's LCST which can lead to the microgel layer's deswelling. Secondly, in non-short circuit, potential will be applied across the microgel film through the two Au electrodes. In this case, no significant temperature change is observed as monitored by digital thermometer. Since pNIPAm is dielectric and non-conductive, the whole device can be treated as a capacitor and opposite charges are accumulated onto each Au plates. We showed that in non-short circuit, microgel layer's actuation is highly related to its stiffness, sign and density of charge, polarity and magnitude of the applied potential. This work shed light on the hydrogel's actuation in micron range.

5.2 Experiment Section

Materials: N-isopropylacrylamide (NIPAm) was purchased from TCI (Portland,

Oregon) and purified by recrystallization from hexanes (ACS reagent grade, EMD, Gibbstown, NJ) prior to use. *N,N'*-methylenebisacrylamide (BIS) (99%), acrylic acid (AAc) (99%) , ammonium persufate (APS) (98+%), *N*-(3-aminopropyl) methacrylamide hydrochloride (>98%) (APMAH) was purchased from Polysciences (Warrington, PA). Deionized (DI) water with a resistivity of 18.2 MΩ·cm was used. Microscope glass slides were and obtained from Fisher Scientific (Ottawa, Ontario) and cut into pieces (25 × 25 mm). Cr was 99.999% and obtained from ESPI as flakes (Ashland, OR), while Au was 99.99% and obtained from MRCS Canada (Edmonton, AB).

Microgel Synthesis: pNIPAm-co-10% AAc microgels were synthesized following previously described protocols.[116] In detail, to synthesize pNIPAm-co-10% AAc microgel, a 3-neck flask was fitted with a reflux condenser, nitrogen inlet, and thermometer, and charged with a solution of NIPAm (11.9 mmol) and BIS (0.703 mmol) in 99 mL DI water, previously filtered through a 0.2 μm filter. The solution was purged with N_2 and allowed to heat to 70 °C, over ~1 hour. AAc (1.43 mmol) was added to the heated reaction mixture in one aliquot. The reaction was then initiated with a solution of APS (0.2 mmol) in 1 mL of deionized water. The reaction was and allowed to proceed at 70 °C for 4 hours under a blanket of nitrogen. The resulting suspension was allowed to cool overnight, and then it was filtered through a Whatman #1 paper filter to remove any large aggregates. The microgel solution was then distributed into centrifuge tubes and purified via centrifugation at ~8300 rcf, followed by removal of the supernatant

and resuspension with DI water, 6x.

pNIPAm-co-APMAH microgels were composed of NIPAm (90%), BIS (5%), APMAH (5%); pNIPAm-co-5 % AAc microgels were synthesized by NIPAm (90%), BIS (5%), AAc (5%); pNIPAm-co-20 % AAc microgels were made from NIPAm (75%), BIS (5%), AAc (20%); 1% BIS microgels were composed of NIPAm (89%), BIS (1%), and AAc (10%); 10% BIS microgels were NIPAm (80%), BIS (10%) and AAc (10%). And all were synthesized in a similar approach.

Instruments: Reflectance spectra were collected by a Red Tide USB650 spectrometer, using a reflectance probe connected to a LS-1 tungsten light source (Ocean Optics, Dunedin). The spectra were collected over a wavelength range of 400–1000 nm and analyzed by Ocean Optics Spectra Suite Spectroscopy software.

5.3 Results and Discussion

Figure 5-1(a) schematically shows the process used to generate the sandwiched structure devices. The detailed fabrication steps are described in Chapter 4.[116] Figure 5-1 (b) depicts how we connected the devices to the external power supply. In the short circuit strategy, we directly connected both leads of the power supply to the bottom Au layer. In the non-short circuit configuration, one lead from the power supply was connected to the top Au layer while another one was connected to the bottom Au layer. In the following discussions, we split our discussion into two aspects according to the different connection approaches.

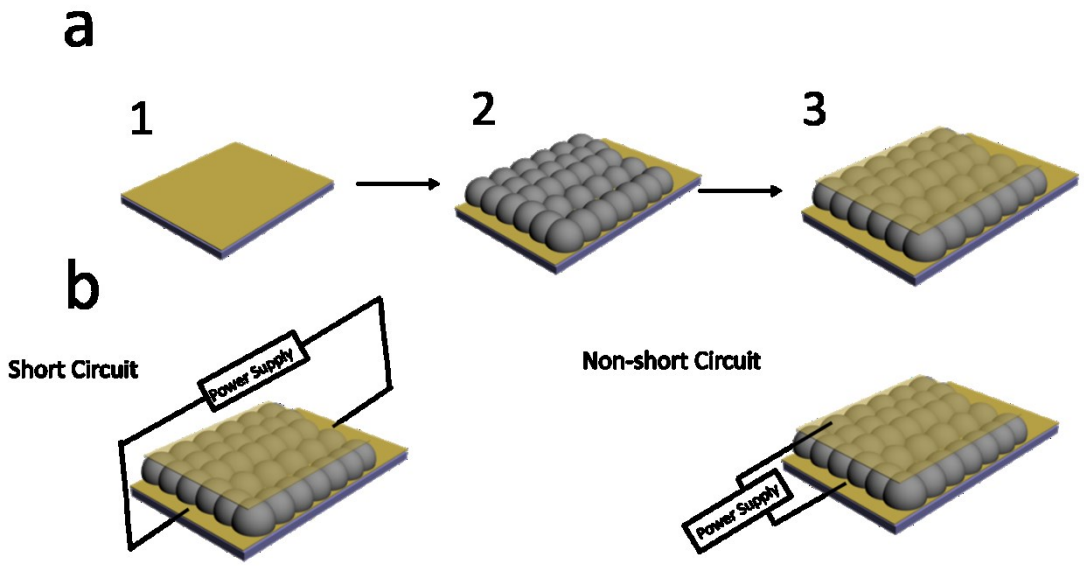

Figure 5-1 a) Process to make the sandwiched structure on top of the glass slide b) Two different strategies to connect to external power supply

As mentioned previously, the sandwiched Au-microgel-Au structure can form a one-dimensional PM exhibiting color due to the constructive/destructive light interference when incident light enters the microgel cavity and resonates between two Au layers. Figure 5-2 shows the typically optical spectrum for our device in this work. In this Chapter, we kept monitoring the peak at ~525 nm. The relationship between the reflected wavelength peak and microgel layer's thickness can be summarized by equation 5-1:

$$m\lambda = 2nd\cos(\beta) \quad (5\text{-}1)$$

Where λ is the wavelength maximum of a peak with a given peak order m, n is the refractive index of the dielectric (microgel) layer, d is the thickness of microgel layers and β is the angle of incidence. Under most situations, the incident light is normal to etalon surface and the effect of refractive index is negligible compared to the change

induced by the change in d. Therefore, generally speaking, for a given m, microgel's elongation leads to an increase in d, which yields a red shift in the position of a given reflectance peak. Likewise, microgel's compression leads to a blue shift. Therefore, we can monitor the microgel layer's actuation indirectly through optical wavelength shift. We define that

$$\Delta\lambda = \lambda_{\text{final}} - \lambda_{\text{initial}} \qquad (5\text{-}2)$$

Therefore, if $\Delta\lambda$ is negative, it means blue shift, the microgel layer is compressed; on the contrary, if $\Delta\lambda$ is positive, it means red shift and the microgel layer is expanded.

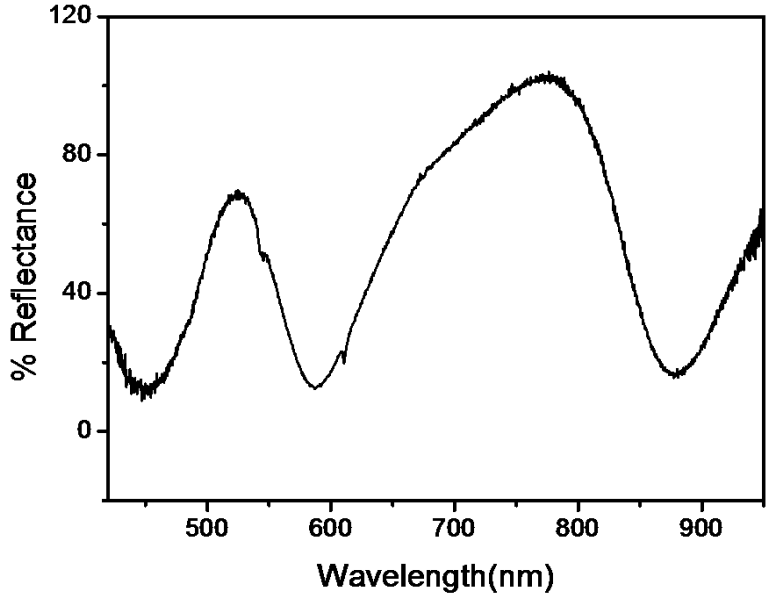

Figure 5-2 A representative reflectance spectrum for an etalon with no voltage applied

In the case of short circuit, the large current in the circuit was measured and generated significant amount of heat, which heated up the electrode. We attached a sensor wire from a digital thermometer on the back of the glass slide and the

temperature change was monitored during the whole experiment. Figure 5-3 shows that larger current could generate higher temperature on Au electrodes. When the current in the circuits increased from 0.1 A- to 0.3 A, the corresponding temperature was elevated from 25 ºC to 50 ºC, which could be higher than microgel's LCST~ 32 ºC. Once turning off the power supply, the electrode cooled down to room temperature gradually, which demonstrated the external power supply was the only heating source.

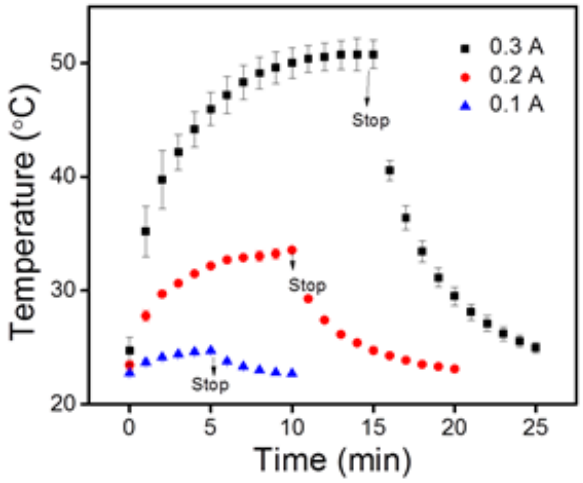

Figure 5-3 For short circuit, temperature goes up and after stopping applying external voltage, temperature goes down

Figure 5-4 shows the results from a series of short circuit experiments. We first started to conduct the experiments with the pure pNIPAm microgel layer. When there is no functional comonomer addition, the pNIPAm microgels are still slightly negatively charged originating from the negatively charged initiator APS used during polymerization, which could be ignored due to the different behavior of the pNIPAm microgel layer and the pNIPAm-co-AAc microgel layer from the following

experimental results. In this Chapter, we will treat the pNIPAm microgels as neutral gels.

For the neutral microgel layer, as shown in Figure 5-4(a), at 0.1 A, the Au electrode's highest temperature was about 25 ºC, which was much lower than pNIPAm's LCST, thus no obvious peak shift was observed. However, when the current increased to 0.3 A, temperature rose above LCST and we could observe large blue peak shift ($\Delta\lambda<0$) over 300 nm. Thus circuits under higher current will result in larger blue shift of the spectra due to the higher temperature. It should be noted that the direction of the peak shift (blue shift) does not depend on the direction of current flow.

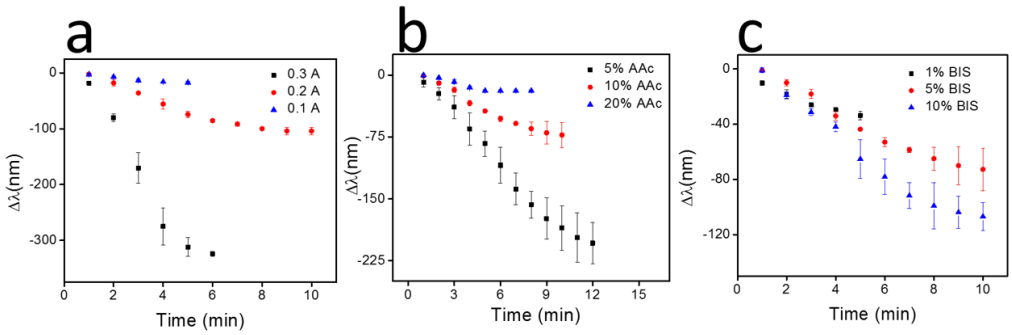

Figure 5-4 In short circuit, a) Pure PNIPAm microgel layer's behavior under different current; b) At 0.3 A, microgel layer with different AAc percentage's behavior c) At 0.3 A, microgel layer with different BIS percentage's behavior

We also investigated how the microgels' chemical compositions influence the electroresponsivity of the corresponding devices. As can be seen in Figure 5-4(b), microgels with different AAc percentage were tested. Keeping other parameters constant, larger AAc percentage resulted in smaller blue shift. This is because DI water

has pH around 5.5 at which the carboxylic groups are negatively charged. The stronger electrostatic repulsion from higher amount of negative charged AAc groups prevents microgels' shrinking, resulting in smaller peak shift.

Figure 5-4(c) shows that while keeping current and AAc percentage constant, increasing the microgels' crosslinker (BIS) percentage from 1% to 10% can yield larger blue shift from around 34 nm to 107 nm even though higher BIS percentage can make the resultant microgels stiffer. We attribute this behavior to the pNIPAM microgels' deformation on surface.[175-178] pNIPAm microgels are colloidal soft spheres therefore a strong flattening of microgels on the surface is reported by several other groups. For example, Hellweg's group measured the pNIPAm-co-AAc microgels' dimension both in bulk solution and adsorbed on the surfaces. They found out while the microgels' hydrodynamic diameter was around 600 nm in bulk solution; once deposited on a silicon surface, their average height was only around 60 nm – 100 nm which is much smaller compare to particles' lateral dimension on the scale of 500 nm. And higher BIS percentage can result in increasing the microgels' average height which can make the flattening less pronounced.[175] In addition, it has been suggested that microgel's shrinking mainly happened perpendicular to the surface instead of in lateral direction. As presented in Table 5-1, we measured the thickness of etalon by ellipsometry. Similar to previous study, increasing BIS percentage from 1% to 10%, the thickness of the etalon device increases from 66.1 ± 0.7 nm to 137.1 ± 0.7 nm. Since we use the same Cr/Au bilayer to prepare all of the etalon devices, the variation of devices' thickness is only from microgel layer and the stiffer the microgel is, the larger the average height.

Even though larger crosslinker percentage can make the microgel stiffer, softer microgels will experience much more pronounced flattening on surface which will make the in plane deswelling more difficult and smaller blue shift.

	20%AAc 5%Bis	10%AAc 5%Bis	5%AAc 5%Bis	10%AAc 10%Bis	10%AAc 1%Bis
Thickness(nm)	119.2±1.8	79.2±0.7	70.2±1.5	137.1±0.7	66.1±0.7
+top, threshold (V)	0.15±0.02	0.12±0.01	0.08±0.01	0.13±0.02	0.03±0.01
Voltage/meter（+top)	1.3×10^6	1.5×10^6	1.1×10^6	9.5×10^5	4.5×10^5
-top Threshold (V)	0.67±0.09	0.54±0.06	0.26±0.03	0.96±0.1	0.11±0.02
Voltage/meter(-top)	5.6×10^6	6.8×10^6	3.7×10^6	7.0×10^6	1.7×10^6

Table 5-1 Threshold voltages in non-short circuit and the thicknesses for different microgel layers

Next, we moved on to the more complex situation and investigate the behavior of microgel layer in the non-short circuit condition. As detailed previously, we connected both of the Au layers of the device to the circuit. The microgel layer is non-conductive and minimal current is observed in this case, therefore it is non-short circuit. The temperature of the electrodes was monitored as well and didn't change for these non-short circuit experiments. We define that when the positive lead of the power supply is connected to the top Au layer, the potential is positive. On the contrary, if the negative lead of the power supply is connected to the top Au layer, the potential is negative.

As shown in Figure 5-5 Table(a), neutral pNIPAm microgel layer didn't show an obvious peak shift trend in both non-short circuit cases. However, for the negative charged pNIPAm-co-AAc microgel layer, the positive potential results in a red shift,

which we correlate with an elongation of the microgel layer and the negative potential results in a blue shift which we correlate with a compression of the the microgel layer. Furthermore, the positively charged pNIPAm-co-APMAH microgel layer shows the opposite peak shift behavior under the same external potential.

a

Microgel Functionality	No charge	5% AAc	5% APMAH
Non-short circuit (-v)	N/A	Blue shift	Red shift
Non-short circuit (+v)	N/A	Red shift	Blue shift

b

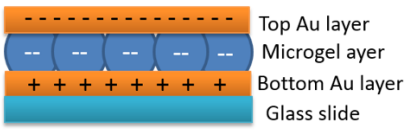

c

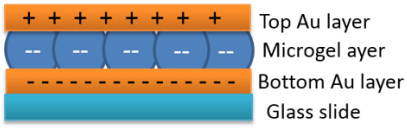

Figure 5-5 a) Peak shift direction for different charged microgel layer under different polarities of external potential; b) Negative voltage is applied to AAc microgel layer c) Positive voltage is applied to AAc microgel layer

Next, we moved on to investigated the threshold actuation voltage, which is important for the following reasons. First, in order to explain the actuation mechanism under non-short circuit conditions, the threshold voltage is needed to be determined to illustrate whether or not the microgel layer's actuation is related to water electrolysis. It is well known that under voltages high enough >1.23 V, water electrolysis will alter pH near the Au electrode, which can have influence on charged microgels' solvation state. Secondly, low threshold actuation voltage is desired for many applications.[179-180]

The threshold actuation voltage is defined as the peak shift at least 10 nm within 5 min. As can be seen in Table 5-1, all of the pNIPAm-co-AAc microgels' threshold

voltages are listed. All the microgel layers show low threshold actuation voltages, which are all lower than 1 V. Therefore, the electrically-induced pH change mentioned in the previous chapters is not the only reason for such microgel layers' actuation. It is also worthwhile to pay attention that for the same pNIPAm-co-AAc microgel layer, the threshold positive actuation voltages are always smaller than threshold negative actuation voltages. It is probably because the strong electrostatic repulsion between AAc groups can counteract the compression force.

Summarizing the above experimental results, we proposed that the mechanism behind the microgel layers' actuation in the non-short circuit is due to the interaction between the charged microgel layer and the two Au electrodes. Under the non-short circuit, the microgel layer works as a dielectric material separating the two conductive Au electrodes to form a capacitor. When a voltage is applied, opposite charges will accumulate on Au plates. Take the pNIPAm-co-AAc microgel layer under the negative potential as one example. Below the water electrolysis potential, shown in Figure 5-5(b), the top negative charged Au electrode repels the negatively charged pNIPAm-co-AAc microgel layer while the bottom positive side attracts the pNIPAm-co-AAc microgel layer, resulting in microgel layer's compression, yielding a blue peak shift. Above water electrolysis potential, the pH of the solution near the Au electrode will change due to water reduction at the top negative electrode to form hydroxide ion while oxidized at the bottom positive electrode to generate hydronium ion. Compared to the non-water electrolysis case, more negative charged groups will be generated near the top negative electrode and repulsion will become more severe while carboxylic group

will be neutralized near the bottom electrode, accelerating the compression process. On the contrary, shown in Figure 5-5(c), when positive potential is applied, top positive Au plate will attract the negatively charged microgel layer while the negative bottom Au plate will repel the microgel layer resulting in microgel's elongation and red shift in optical spectra. In a similar way, water electrolysis will also accelerate microgel elongation process.

The above mechanism can fully explain the experimental data. The influence of the negative voltage on the representative AAc microgel layer's actuation is investigated and presented in Figure 5-6(a). For the same microgel layer (5% AAc, 10% BIS), increasing negative voltages from -0.5 V to -1 V can result in stronger interactions between the charged Au electrode and the microgel layer which leads to larger compression, thus a larger blue shift. In the meanwhile, if the voltage is increased to -3 V, a larger and quicker blue shift is observed. This is because above the water electrolysis voltage, the pH changes near the electrode can accelerate the whole compression process. Keeping other parameters constant, if we only vary the AAc percentage of the microgels, from 5 % to 20 % in Figure 5-6(b), we will observe the larger and faster blue peak shift from ~ 42 nm to ~ 118 nm which is oppose results compared to the short-circuit case. It is because that higher AAc percentage in this case can generate stronger interactions with the two Au plates. We also tested the microgels' actuation under different BIS percentage. As shown in Figure 5-6(c), decreasing the BIS percentage from 10 % to 1 % led to a significant increase of the peak shift and shift rate. Unlike the short circuit approach, in which the microgel's flattening on surfaces

can prevent in plane microgel shrinking, stiffer microgel layer in non-short circuit can make compression process more difficult, resulting in smaller peak shift.

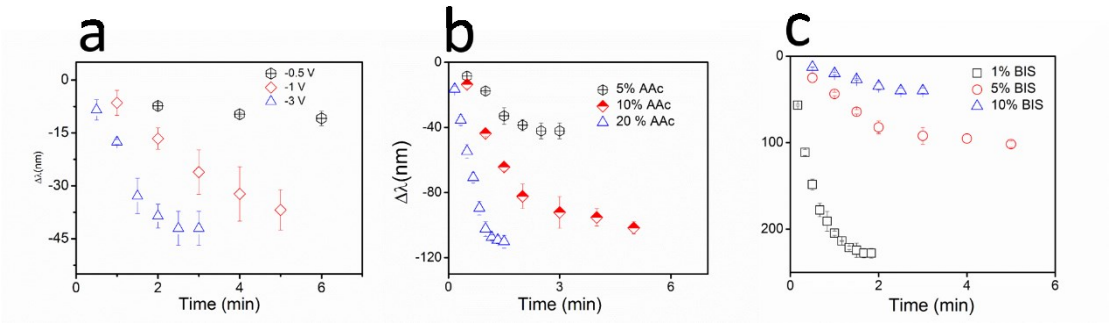

Figure 5-6 a) 5% AAc microgel layer's response for different voltage; b) At -3v, microgel layer with different AAc percentage's optical response c) At -3v, microgel layer with different BIS percentage's response

5.4 Conclusion

Here, we investigated pNIPAm microgel's actuation upon exposure to different external voltages. We showed two different mechanisms for microgel layer's actuation. In the case of the short circuit, large amount of heat will be generated which can increase the electrodes' temperature above pNIPAm's LCST leading to microgel layer's compression. For non-short circuit, no obvious temperature change is observed. Opposite charges are accumulated onto each gold plates, and interaction of the charge on each electrodes and microgel layer can result in elongation and compression of the microgel layer. Microgel layer's electrical actuation is highly related to magnitude and polarity of the applied potential, microgel layer's stiffness and sign and density of

microgel layer's charge. This work might find applications in structural display and miniature actuation.

Chapter 6 Janus Microgels with Tunable Functionality, Polarity and Optical Properties[2]

This dissertation's second part consists of Chapter 6 and 7, where the fabrication approaches of asymmetric pNIPAm-based microgels were studied. In Chapter 6, a facile self-assembly method is presented to prepare pNIPAm-based microgels modified anisotropically with Au NPs to yield Janus microgels. Transmission electron microscopy (TEM) is used to confirm that microgels are selectively coated on one or both sides with Au NPs. This approach is able to generate microgels with the same (monopolar) or different (bipolar) charge on either side of the microgel surface. The optical properties of the Au NPs adsorbed to the microgel surface are also characterized as a function of temperature and pH. We found that the plasmon absorption of the Au NPs depends on each, which could be explained by the microgel's solvation state dictating the distance between the Au NPs. The surface adsorption behavior of the monopolar and bipolar microgels is also investigated, and we demonstrate that the bipolar microgels exhibit enhanced surface adsorption compared to the monopolar microgels. Finally, we show that the Janus microgel assembly could be controlled by modifying the Au NPs of at least two different sets of Janus microgels with complementary DNA sequences. The work here could find utility for generating surface adsorbed materials with controllable optical properties, sensors, and for studying fundamental behavior of self-assembling materials.

[2] This Chapter has been adapted from the previously published paper. Wenwen Xu, Menglian Wei and Michael J. Serpe, Adv. Opt. Mater, 2017, 2, 2195-1071.

6.1 Introduction

Au NPs have been utilized in a variety of applications such as for biological imaging, sensing, and cancer therapy due to their unique optical properties resulting from localized surface plasmon resonance (LSPR).[181] Furthermore, Au NPs have also been used as Janus particle precursors, which have been shown to have tunable optical properties and sensing applications.[182-183] In many examples, the Au NPs have been adhered to spatially isolated regions of particle surfaces, to generate Janus particles. However, due to their high monodispersity and easy surface modification, most of the investigations used polystyrene or silica as core particles and the Au NPs were selectively adhered to one side of the core particles.[184-185] These traditional core particles are generally non-responsive and do not have the ability to modulate their properties (and the Au NP optical properties) in a dynamic and reversible fashion; if this was possible, new applications could be accessible. While there have been efforts to generate such responsive Janus particles, assembly of Au NPs on responsive polymer-based particle cores is much more complex, and not as well understood.

In this Chapter, we developed a self-assembly method to selectively coat one pole or both sides (poles) of pNIPAm-based microgels with Au NPs. Briefly, pNIPAm-based materials are among the most widely studied stimuli (temperature) responsive polymers to date. pNIPAm-based microgels are well known to be water swollen (and large in diameter) at $T < 32$ °C, while they are deswollen (relatively small in diameter) at $T > 32$ °C; the transition is fully reversible over many cycles. As part of this investigation we synthesized two different sets of pNIPAm-based microgels —

pNIPAm-co-APMAH microgels and pNIPAm-co-AAc microgels.[18] The structures of the monomers are shown in Chapter 1.2. APMAH has a pK_a around 9 while AAc has a pK_a around 4.25. Therefore, the pNIPAm-co-APMAH microgels are positively charged at pH<9, while the pNIPAm-co-AAc microgels are negatively charged at pH>4.25. It is important to note that most of the Au NPs, unless specifically mentioned, used in this investigation were capped with citrate. Therefore, microgels with different charges isolated on their surface could be generated with pNIPAm-co-APMAH microgels at pH<9 because one side of the microgels will be positively charged, while the Au NPs will be negatively charged. These microgels are referred to here as being "bipolar", as they are zwitterionic, with the charges isolated from one another on the microgel surface. Similarly, "monopolar" microgels could be generated with pNIPAm-co-AAc microgels at pH>4.25 because both sides of the microgels will be negatively charged. We go on to show that bipolar microgels adhere to surfaces in a manner that is dramatically different than monopolar microgels. Finally, we demonstrate that the anisotropic structure can be used for ordered DNA guided assembly.

6.2 Experimental Section

Materials: N-isopropylacrylamide (NIPAm) was purchased from TCI (Portland, Oregon) and purified by recrystallization from hexanes (ACS reagent grade, EMD, Gibbstown, NJ) prior to use. *N,N'*-methylenebisacrylamide (BIS) (99%), acrylic acid (AAc) (99%) , ammonium persulfate (APS) (98+%), hydrogen peroxide and sulfuric acid (99.999%) were obtained from Aldrich (St. Louis, MO) and were used as received.

N-(3-aminopropyl) methacrylamide hydrochloride (>98%) was purchased from Polysciences (Warrington, PA). Deionized (DI) water with a resistivity of 18.2 MΩ·cm was used. All of Au NPs used in the Chapter were purchased from Nanocomposix (San Diego, CA) and concentration is 0.05 mg/mL. Microscope glass slides were and obtained from Fisher Scientific (Ottawa, Ontario) and cut into pieces (25 × 25 mm). All DNA was purchased from Integrated DNA Technologies (Coralville, IA). Tris(2-carboxyethyl) phosphine hydrochloride (TCEP•HCl) and 1-Ethyl-3-[3-dimethylaminopropyl] carbodiimide hydrochloride (EDC) were purchased from Thermo Fisher Scientific (Rockford, IL).

Microgel Synthesis: Microgels were synthesized following previously described protocols. Briefly, a 3-necked round bottom flask was fitted with a reflux condenser, nitrogen inlet, and thermometer, and charged with a solution of NIPAm (11.9 mmol) and BIS (0.703 mmol) in 99 mL deionized water, previously filtered through a 0.2 μm filter. The solution was purged with N_2 and allowed to heat to 70 °C, over ~1 hour. AAc (1.43 mmol) was added to the heated reaction mixture in one aliquot. The reaction was then initiated with a solution of APS (0.2 mmol) in 1 mL of deionized water. The reaction was allowed to proceed at 70 °C for 4 hours under a blanket of nitrogen gas. The resulting suspension was allowed to cool overnight, and then it was filtered through a Whatman #1 paper filter to remove any large aggregates. The microgel solution was then distributed into centrifuge tubes and purified via centrifugation at ~8300 rcf to form a pellet, followed by removal of the supernatant and resuspension with deionized water; this process was completed 6 times. pNIPAm-co-APMAH microgels were

composed of NIPAm (90%), BIS (5%), and APMAH (5%) and synthesized in the same manner as the microgels above. After their synthesis, the microgels were lyophilized and redispersed in water to yield a concentration of 1 mg/mL.

Fabrication of Janus Microgels: In this investigation, two different modification approaches ("bottom" and "top" modification) were used to generate Janus microgels. For both approaches, glass microscope slides were previously cleaned by soaking in piranha solution (H_2SO_4/H_2O_2 7:3 V/V) for 4 h, to remove any impurities from the substrate surface. (***Caution****: piranha solutions react violently with organic materials and should not be stored in closed containers*). The substrates were then rinsed copiously with H_2O followed by 95% ethanol, and immediately used. Using the "bottom" modification approach, piranha-cleaned substrates were immersed in an ethanolic (absolute ethanol) solution containing 1% APTMS for at least 2 h. After 2 h, the substrates were removed from the APTMS solution and again rinsed copiously with 95% ethanol. Then, the substrates were rinsed with H_2O and dried under a stream of nitrogen gas and placed into a Petri dish. Next, 0.5 mL 15 nm Au NPs were added to the glass slides and the Petri dish was sealed to avoid solution evaporation for at least another 5 h and then the substrate was again rinsed copiously with DI water and dried under a stream of nitrogen gas. 20 mg of EDC was added to 1 mL of a 1 mg/mL pNIPAm-co-APMAH microgel solution, and after shaking, the mixture was added to the top of the Au NP-functionalized glass slide and left overnight. The excess microgels were subsequently rinsed off the surface with DI water, 95% ethanol and dried with

nitrogen gas. The glass slides were then immersed in DI water and sonication was used to release the microgels from the surface, yielding microgels in solution with Au NPs attached to one side of the microgels. For the 30 nm Au NPs, all the procedures above were the same except that the volume of Au NPs added onto the glass side was 1 mL.

For the "top" modification method, piranha-cleaned glass slides were soaked in 1 mL 1 mg/mL (pNIPAm-co-APMAH) microgel solution for 5 min. After 5 min, the slides were rinsed with H_2O and 95% ethanol and dried under a stream of nitrogen gas. 0.5 mL of a solution of 70 nm Au NPs were added to the top of the glass slides and the glass slides were placed inside a sealed Petri dish for 5 h. Then 1 mL 20 mg/mL EDC solution was added onto the gold modified glass slides and left overnight. The slides were then rinsed with H_2O and 95% ethanol and dried under a stream of nitrogen gas. The glass slides were subsequently immersed in DI water and sonication was used to release the microgels from the surface, yielding microgels in solution with Au NPs attached to one side of the microgels. Modification with the 50 nm Au NPs was done in the same way, although exposure to the Au NPs solution was reduced to 1 h.

Both the "bottom" and "top" modification approaches were used in conjunction to yield microgels with AuNPs immobilized on two different sides of their surface. To accomplish this, piranha-cleaned glass slides were immersed in an ethanolic (absolute ethanol) solution containing 1% APTMS for at least 2 h. The substrates were removed from the APTMS solution and rinsed copiously with 95% ethanol and H_2O and dried under a stream of nitrogen gas. Next, 1 mL of a solution of 30 nm Au NPs was added on top of the glass slides for at least another 5 h. 20 mg of EDC was added to 1 mL of

the 1 mg/mL pNIPAm-co-APMAH microgel solution, and after shaking, the mixture was added to the top of the Au NP-functionalized glass slide and left overnight. The glass slide was then washed by rinsing copiously with DI water and 95% ethanol and dried with nitrogen gas. 0.5 mL of a solution of 70 nm Au NPs was added to the top of the glass slides for at least 5 h. The slides were subsequently rinsed with H_2O and 95% ethanol and dried under a stream of nitrogen gas. 20 mg EDC was added to 1 mL of MES buffer and was added to the glass slides and allowed to react overnight. The slide was again rinsed copiously with DI water and 95% ethanol and dried with nitrogen gas.

In above case, the pNIPAm-co-APMAH microgels were positively charged, while the Au NPs were negatively charged, therefore all Janus microgels mentioned above are referred to as being "bipolar". "Monopolar" Janus microgels have the same charge on both sides of their surface, and are made in a similar manner as above, except for the use of negatively charged pNIPAm-co-AAc microgels and the use of cysteamine for the microgel modification. For example, consider JM 50’ in Table 1; 1 mL of 1 mg/mL pNIPAm-co-AAc microgel solution was added onto APTMS modified glass slides for 5 min (chosen because it yielded the desired surface coverage). After 5 min, the glass slides were rinsed copiously with DI water and 95% ethanol and dried with nitrogen gas. Then the microgel modified glass slides were soaked in 20 mL 30 mg/mL cysteamine solution and left overnight. The slides were then rinsed copiously with DI water and 95% ethanol and dried with nitrogen gas. 1 mL of a 20 mg/mL EDC solution was added on top of the slide and allowed to react overnight. The slides were again rinsed copiously with DI water and 95% ethanol and dried with nitrogen gas. Finally,

0.5 mL of a solution of 50 nm Au NPs solution (citrate surface or PVP surface) was added on top of the glass slides and allowed to react for 1 h.

All the above Janus particles were removed from glass slides by sonication in DI water for further experiments. The concentration of the Janus microgels in DI water was ~ 0.03 nM (by calculation). This calculation was done by imaging a 3 μm × 3 μm area via atomic force microscopy (AFM) and the number of particles in this area was counted. This number was then used to calculate the approximate number of particles on the whole 1 inch × 1 inch glass slide area. This calculation yielded ~ 2.58×10^{9} particles • $inch^{-2}$. For each Janus microgel solution, the particles were collected from eight 1-$inch^2$ slides via sonication in a total of 1 mL DI water.

DNA Guided Self-Assembly: The DNA functionalization process used here was slightly modified from a previous publication[17b]. In detail, 3 μL of 600 μM thiolated DNA solution was first exposed to 1 μL of 10 mM TCEP solution for 1 h. This was done to reduce the DNA disulfide groups to thiols. The thiolated DNA solution was then mixed with 1 mL of the resultant 0.28 nM Janus microgel solution (from above) and incubated for 12 h. 500 mM PBS buffer (pH=7.4) and 1 % SDS were added to the mixture solution to bring the final concentration to 10 mM PBS and 0.01 % SDS, respectively. To this mixture, 20 μL of 2 M NaCl was added, followed by sonication for 10 s. The salt addition was repeated five times every 20 min and the solution allowed to incubate for 24 h. The sequences of the DNA used here were complementary, and are: 5'-/5ThioMC6-D/ TTT TTT TTT TTT TTT GGT TTG AGT TCT GCT -3' and 5'-

/5ThioMC6-D/ TTT TTT TTT TTT TTT AGC AGA ACT CAA ACC-3'. The microgels in solution were then isolated by centrifuging at 8000 rpm for 10 min. The microgels were then resuspended in PBS buffer (10 mM, pH=7.4, NaCl=100 mM, SDS=0.01 %) and the entire centrifugation/resuspension process was repeated a total of 3 times. This was done to separate the DNA modified Janus microgels from the free DNA. The two sets of DNA-modified Janus microgels were then mixed together and allowed to incubate for 24 h for hybridization.

Characterization : UV-Vis spectra were obtained using an Agilent 8453 UV−Vis spectrophotometer equipped with an 89090A temperature controller and Peltier heating device (Agilent Technologies Canada Inc., ON, Canada). Transmission electron microscope (TEM) images were acquired using a JEOL, JEM 2100 (JEOL USA, Inc., MA, USA) with an accelerating voltage of 200 kV. The specimens were prepared by drying 5 μL solutions of highly diluted samples on carbon coated copper grids. Non-contact mode atomic force microscopy was used to image surfaces (Digital Instrument, Dimension 3100, Veeco Instruments Inc. NY, USA). The microgel diameter and zeta potential was measured using a Malvern Zetasizer Nano Series (Malvern Instruments Ltd, Malvern, UK).

6.3 Results and Discussion

We developed both a "top" and "bottom" modification protocol such that monopolar and bipolar Janus particles could be generated in a simple and

straightforward manner, which has not been reported extensively in previous publications.[186] The approach presented here is simple, template-free and requires no extra treatments, e.g., creating/removing sacrificial layers. Initial experiments focused on demonstrating that AuNPs can be immobilized on a single side of pNIPAm-based microgels. To accomplish this, we used pNIPAm-co-APMAH microgels and the "top" modification approach, as shown schematically in Figure 6-1(a). In this case, positively charged microgels were first immobilized onto the surface of glass slides, allowing the negatively charged Au NPs to attach to the exposed microgel surface via electrostatic interactions.

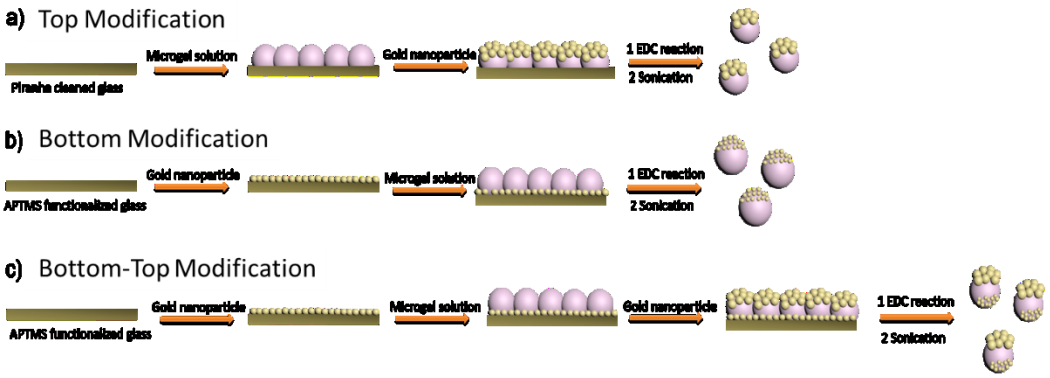

Figure 6-1 Schematic depiction of the three different Janus microgel synthesis approaches used in this investigation. Reproduced with permission from ref. 186, Copyright 2017, WILEY-VCH Verlag GmbH & Co. KGaA, Weinheim

For example, 1 mL of a 1 mg/mL pNIPAm-co-APMAH microgel solution (pH~5.5) was exposed to a piranha cleaned glass slide for 5 min followed by the addition of 70 nm citrate capped Au NPs. Exposure to EDC solution was then used to

covalently link the Au NPs to the microgels. After rinsing and sonication, the modified microgels could be isolated via centrifugation. The "bottom" modification approach is similar to the "top" modification, except for the fact that Au NPs are first attached to the surfaces before microgel addition (Figure 6-1(b)). As can be seen from the TEM images in Figure 6-2 (a-d), Au NPs of different diameters can be immobilized on a single side of the microgels.

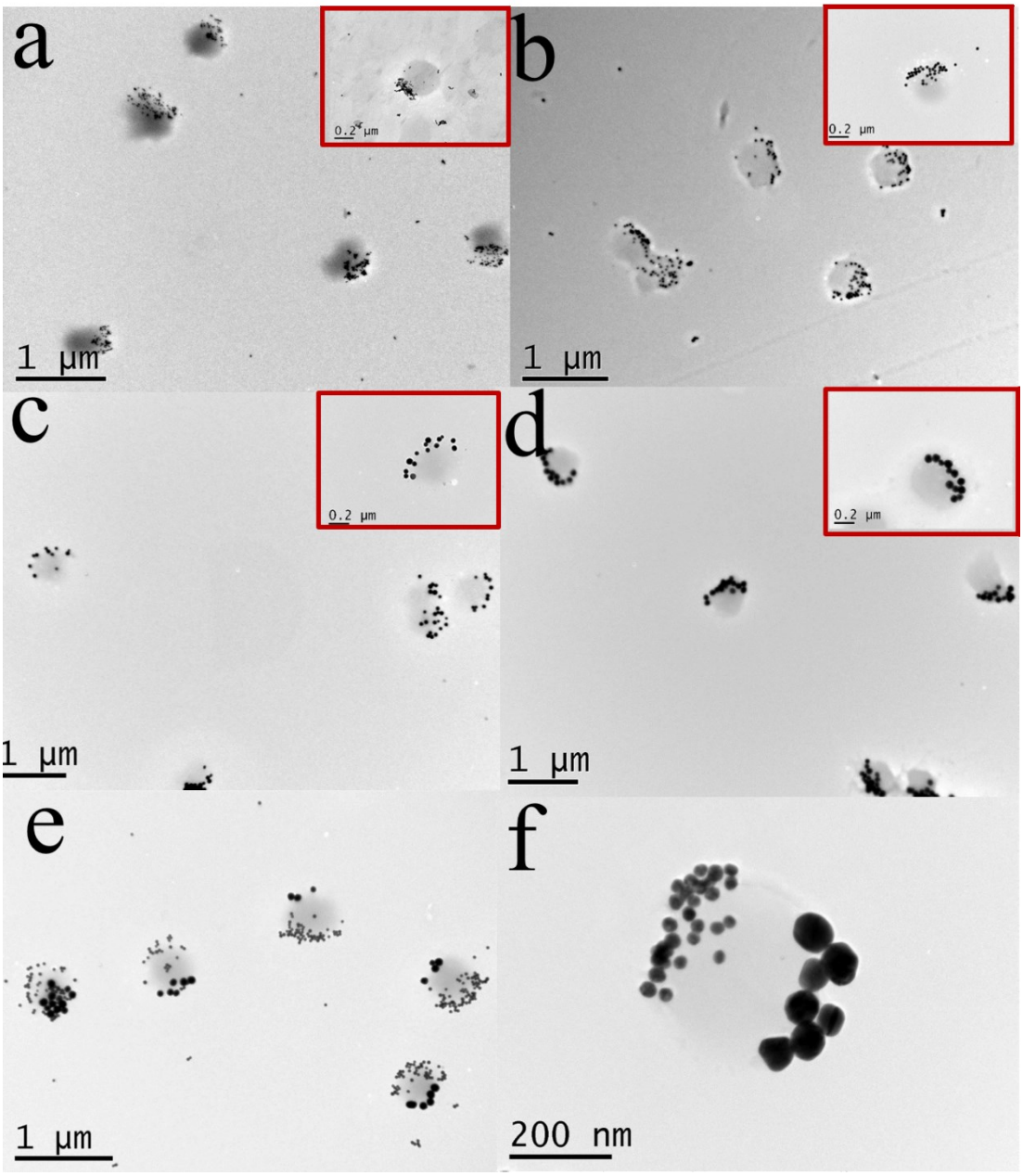

Figure 6-2 TEM images of a) JM 15; b) JM 30; c) JM 50; d) JM 70; e) and f) JM 30/70. Insets show zoomed in images of specific Janus microgels. Reproduced with permission from ref. 186, Copyright 2017, WILEY-VCH Verlag GmbH & Co. KGaA, Weinheim

We also pointed out that the larger the Au NPs' size, the smaller amount of Au NPs deposited onto the microgel surface, shown in Figure 6-3. From our analysis we found

a yield of ~85% percent for single sided Janus microgels and 78% for double sided Janus microgels. That is, 85% of the resultant microgels were coated on one side with Au NPs, while ~78% were coated on both sides.

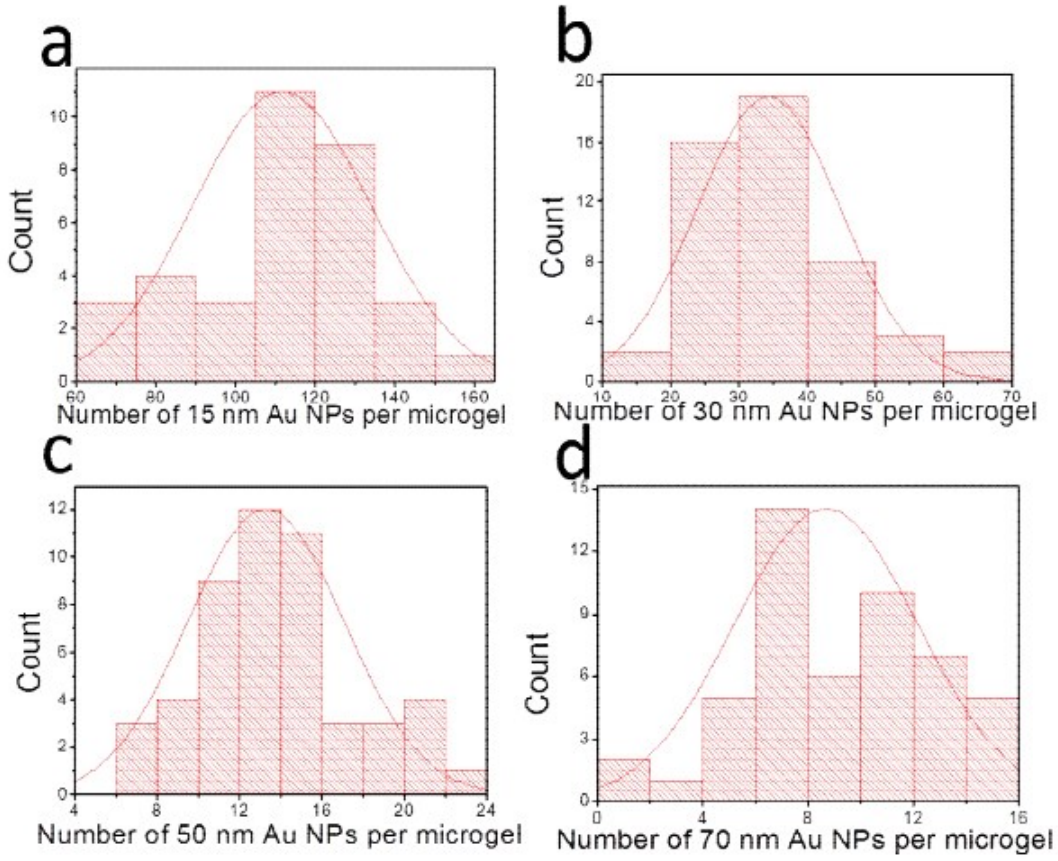

Figure 6-3 Histograms of the number of different size Au NPs found on each pNIPAm microgel. For each histogram, at least 50 Janus microgels were analyzed from representative images. Reproduced with permission from ref. 186, Copyright 2017, WILEY-VCH Verlag GmbH & Co. KGaA, Weinheim

UV-Vis of the resultant Janus microgels (Figure 6-4) also revealed the characteristic LSPR absorption peak that is observed for Au NPs dispersed in solution, which provided further proof that the Janus microgels are indeed modified with Au NPs.

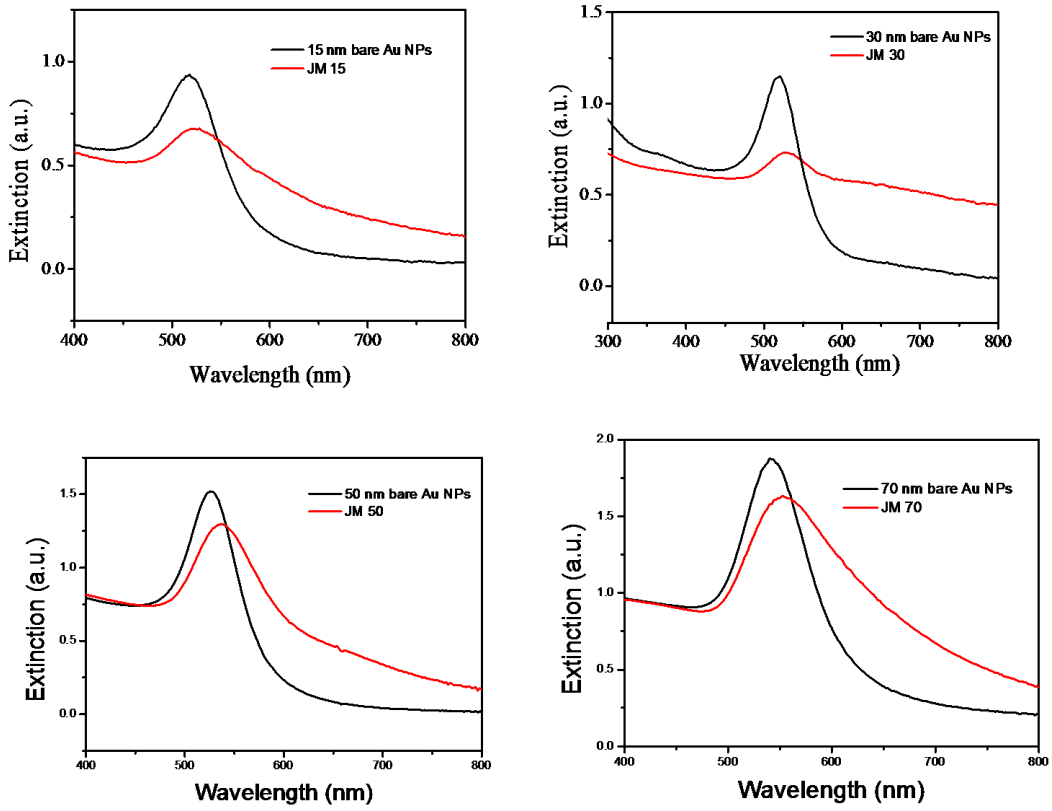

Figure 6-4 UV-Vis spectra of the Janus microgels and the corresponding bare Au NPs. Reproduced with permission from ref. 186, Copyright 2017, WILEY-VCH Verlag GmbH & Co. KGaA, Weinheim

Furthermore, as can be seen in the TEM images in Figure 6-2 (e,f), Janus microgels with two different diameter Au NPs immobilized on two different sides of the microgels can be generated using a combination of both "top" and "bottom" modification (Figure 1(c)). This is particularly important when the microgels are modified with "small" Au NPs (15 nm and 30 nm), which are more prone to penetrate the microgels if the "top" modification approach is used as shown in Figure 6-5.

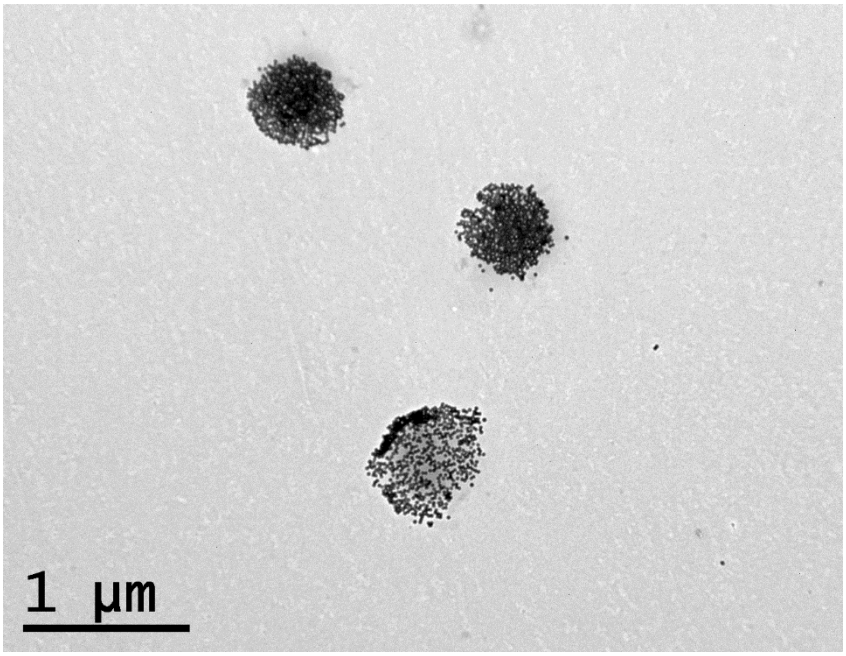

Figure 6-5 Small Au NPs used to modify microgels using the top modification procedure. Reproduced with permission from ref. 186, Copyright 2017, WILEY-VCH Verlag GmbH & Co. KGaA, Weinheim

For all above experiments, the resultant microgels are referred to as being "bipolar", since the microgels were positively charged, while the Au NPs were negatively charged. In subsequent experiments, we generated Janus microgels by modifying negatively charged pNIPAm-co-AAc microgels with negatively charged Au NPs; these are referred to as "monopolar" microgels (Figure 6-6).

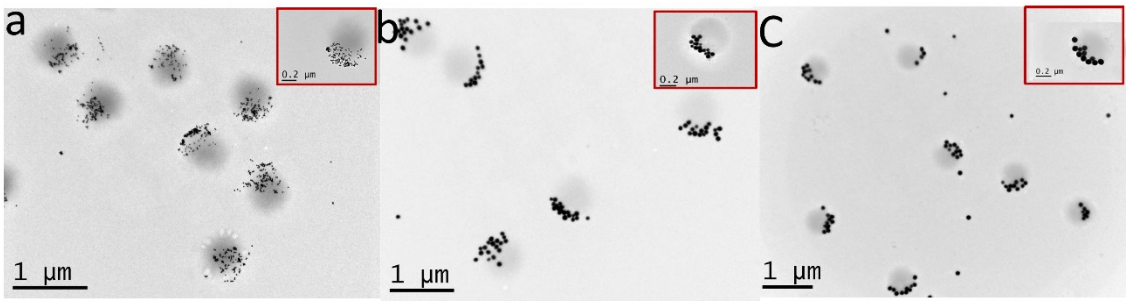

Figure 6-6 TEM images of monopolar Janus microgels a) JM 15'; b) JM 50'; c)JM 70'. Insets show zoomed in images of specific Janus microgels. Reproduced with

permission from ref. 186, Copyright 2017, WILEY-VCH Verlag GmbH & Co. KGaA, Weinheim

When generating monopolar microgels, cysteamine must be used as a crosslinker since the like charges prevent the electrostatic immobilization of the Au NPs on the surface. To accomplish this, the primary amine group of cysteamine was coupled with the microgel's carboxylic acid group via EDC coupling,[187] leaving the thiol group available to attach to the Au NPs.[188] It should be mentioned here that by exploiting the thiol-Au bond, Au NPs with various chemistries could also potentially be immobilized on the microgel surface. Here, we show that polyvinylpyrrolidone (PVP)-modified Au NPs could also be attached to the surface of microgels. Table 6-1 shows the various Janus microgels we generated as part of this study, and the appropriate synthetic route.

Sample	Modification Approach	Microgel Functionality	Au NP size	Au NP surface
JM 15	Bottom	APMAH	15 nm	Citrate
JM 30	Bottom	APMAH	30 nm	Citrate
JM 50	Top	APMAH	50 nm	Citrate
JM 70	Top	APMAH	70 nm	Citrate

JM 30/70	Bottom-top	APMAH	Bottom:30 nm Top: 70 nm	Both citrate
JM 15'	Bottom	AAc	15 nm	Citrate
JM 50'	Top	AAc	50 nm	Citrate
JM 70'	Top	AAc	70 nm	PVP

Table 6-1 Janus microgel details. Reproduced with permission from ref. 186, Copyright 2017, WILEY-VCH Verlag GmbH & Co. KGaA, Weinheim

Next, we go on to show that the temperature-dependent solvation state of pNIPAm-based microgels can influence the LSPR absorbance of the Au NPs attached to the microgel surface. We hypothesize that the change in refractive index of the microgels could have an influence on these properties.[70, 189] Perhaps more importantly, the microgel solvation state should be able to modulate the distance between the Au NPs, which is well known to change the LSPR absorbance of the Au NPs.[190] For example, in the collapsed state, the distance between Au NPs is much smaller than in the swollen state, resulting in relatively strong plasmon coupling between the Au NPs.[76] In this investigation, we showed that temperature and/or pH could be used to modulate the LSPR of the Au NPs attached to the microgels and use JM 50 to demonstrate this. First, we used DLS to measure the diameter of JM 50 and how it depended on solution temperature and pH. As can be seen in Table 6-2, the diameter of the Janus microgels

was 643±13 nm at pH=6, T=25 ºC, while the diameter decreased to 414±2 nm at pH=6, T=55 ºC. This decrease in diameter was attributed to the thermoresponsivity of the pNIPAm-based microgels. We point out that the Janus microgels were not stable at high pH (pH=12) and high temperature, and large aggregates formed, and therefore the microgel diameter could not be accurately measured at these conditions. We also show that the diameter of JM 50 depended on pH, exhibiting a diameter of 546±6 nm at pH=12, T=25 ºC, compared to 643±13 nm at pH=6, T=25 ºC. The observed increase in diameter was attributed to the protonation of the microgels, and their resultant swelling.

pH	**Temperature /°C**	**Zeta potential/mV**	**Hydrodynamic diameter/nm**
3	25	13.5±0.9	652±17
6	25	0.9±0.2	643±13
6	55	-1.3±0.7	414±2
12	25	-7.3±0.3	546±6

Table 6-2 DLS and zeta potential data for JM50 at various pH and temperature. Reproduced with permission from ref. 186, Copyright 2017, WILEY-VCH Verlag GmbH & Co. KGaA, Weinheim

Furthermore, DLS was used to determine the microgel diameter as a function of temperature to determine the LCST for the Janus microgels. The results show that JM 50 has a well-defined volume transition at ~35 °C, pH=6, which is comparable to that of pure pNIPAm-co-APMAH microgels (Figure 6-7(a)). In Figure 6-7(b), the heating-

cooling cycles of JM 50 show the reversibility of the microgel diameter as the solution temperature is varied above and below the transition temperature.

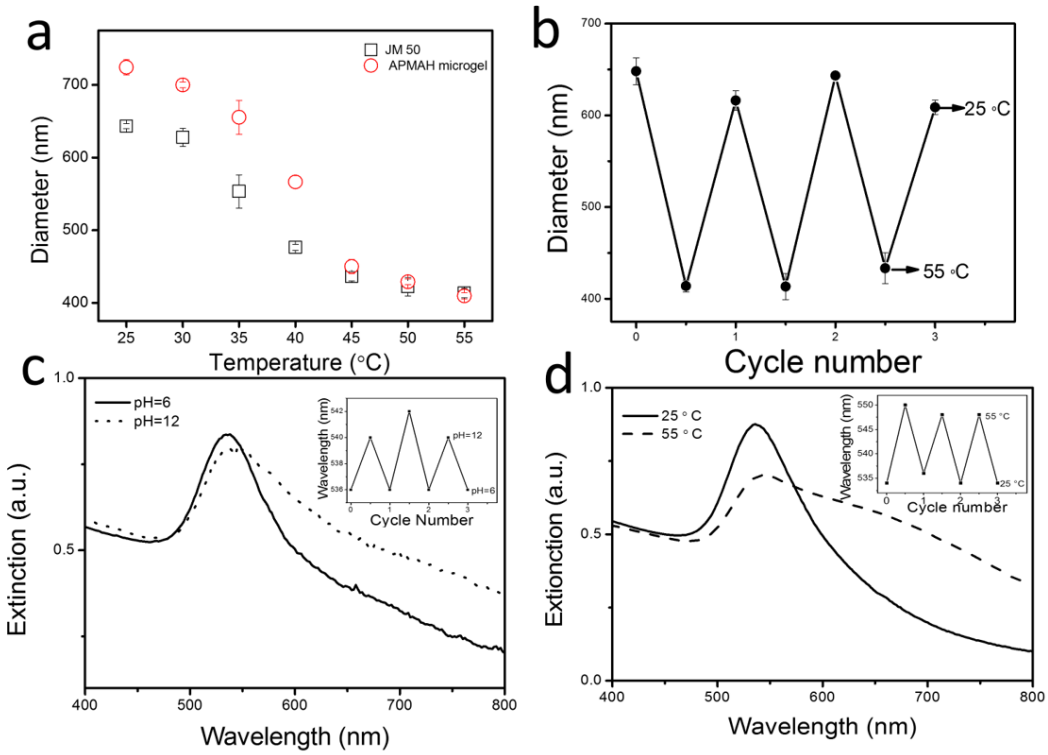

Figure 6-7 a) DLS measured diameter of JM 50 and APMAH microgels as a function of temperature at pH=6; b) The reversibility of the swelling/deswelling of JM 50 at pH 6.0; c) UV-Vis spectra for JM 50 at different pH; and d) UV-Vis spectra for JM 50 at different temperature. The insets show the reversibility of the response. Reproduced with permission from ref. 186, Copyright 2017, WILEY-VCH Verlag GmbH & Co. KGaA, Weinheim

The corresponding optical properties of JM 50 were subsequently monitored at the same conditions as above to show that the Au NP LSPR absorbance could be influenced by microgel solvation state. As can be seen in in Figure 6-7 (c, d), a red shift

and broadening of the LSPR peak at high pH (pH=12) and high temperature (T=55 ºC) was observed. This is consistent with our hypothesis that the change in refractive index and diameter of the microgels could influence the LSPR absorbance of the Au NPs. We also show in the figure insets that the optical properties were reversible over a number of cycles. We point out that since the microgels have a larger response to temperature (from 643±13 nm to 414±2 nm) than pH (from 643±13 nm to 546±6 nm), the response in more pronounced with (and dominated by) temperature.

Next, we investigated the ability of the generated Janus microgels to adsorb to surfaces. Our results revealed that compared to monopolar microgels, bipolar microgels had enhanced ability to adsorb to surfaces, which can be seen by comparing panels 1 and 2 in Figure 6-8(a). Specifically, when we add JM 50 (bipolar particles, pH=6) to the inside of a glass vial, the vial's surface turns visually red, which indicates that the Janus microgels were adsorbed to the glass surface. Alternatively, when the same concentration of JM 50' (monopolar particles) were exposed to the inside of a glass vial for the same amount of time as JM 50 above, there is minimal adsorption, as indicated by the minimal/no change in the color of the glass.

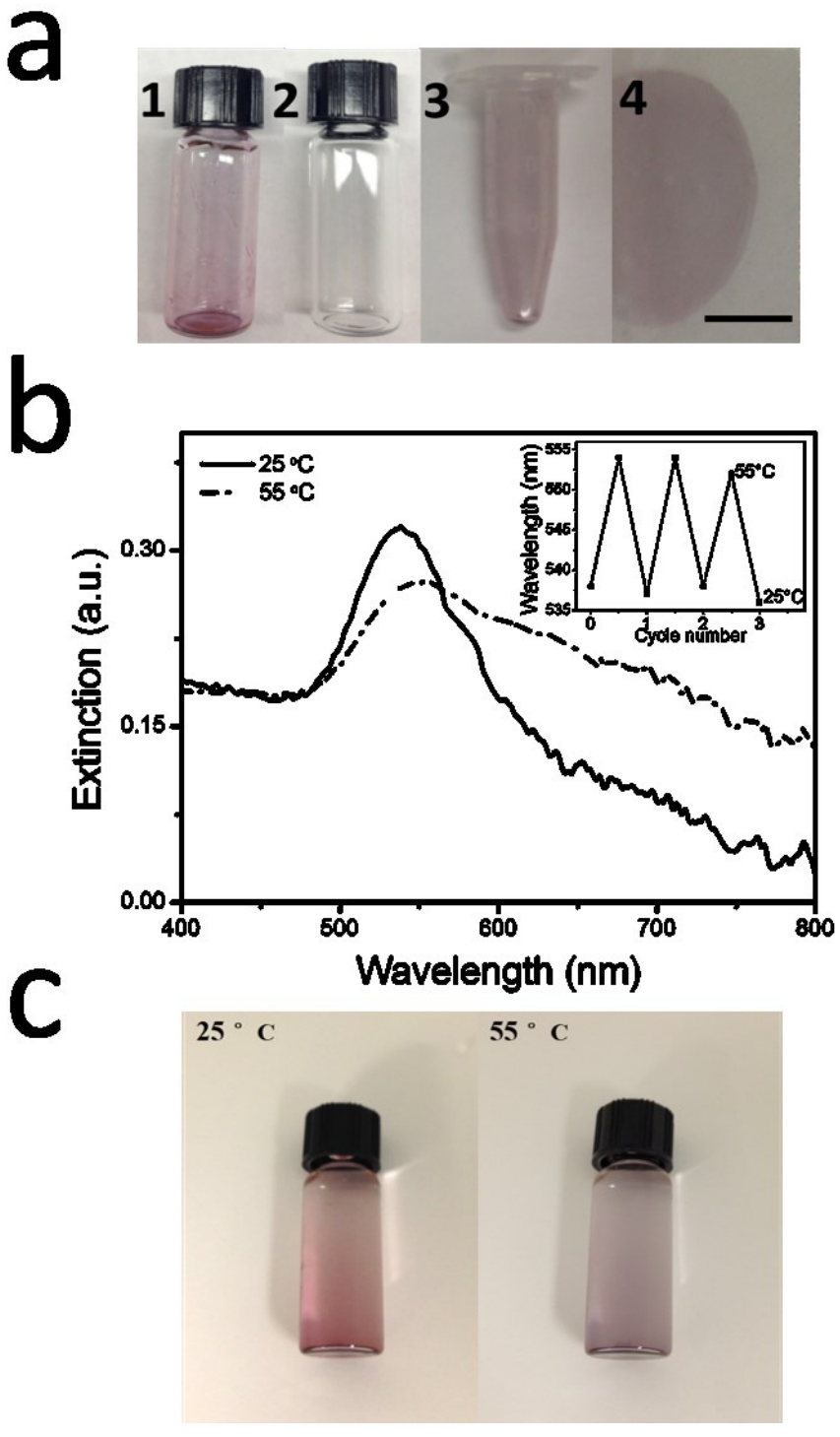

Figure 6-8 a) Panel 1 shows a photograph of a vial exposed to JM 50, which clearly shows a red color due to Janus particle adsorption to the vial surface. Panel 2 shows a similar vial exposed to JM 50', which does not effectively coat the vial surface. Panels

3-4 photographs of a polystyrene Eppendorf tube and a PDMS film, respectively, after exposure to JM 50. The scale bar is 0.5 mm; b) UV-Vis spectra of the surface coating at different temperature (pH 6.0), inset show the reversibility of the response; and c) the visual color of surface coated with JM 50 at the indicated temperatures. Reproduced with permission from ref. 186, Copyright 2017, WILEY-VCH Verlag GmbH & Co. KGaA, Weinheim

To investigate this further, we collected AFM images of the respective surfaces. The images in Figure 6-9 revealed that JM 50 formed large clusters on the glass surface, which was distinctly different than the resultant surfaces that were exposed to JM 50'.

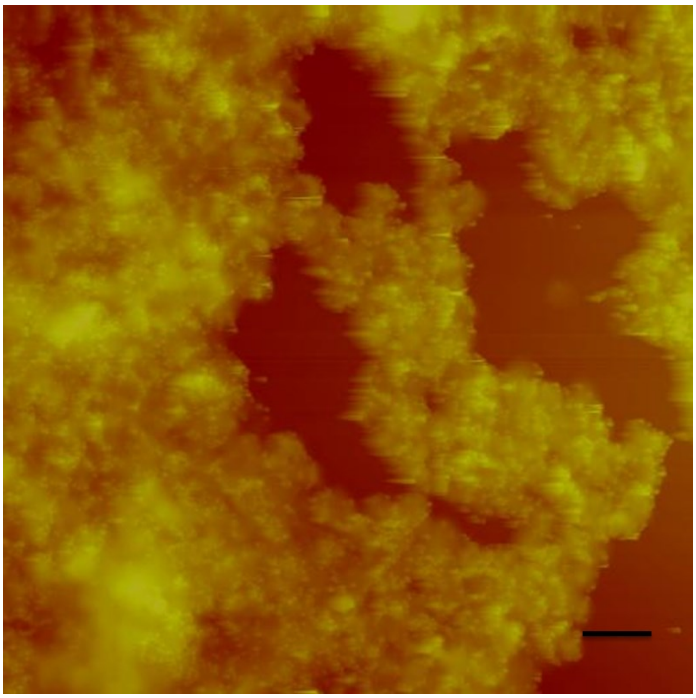

Figure 6-9 AFM image of the bipolar microgel coating on glass, scale bar is 1 μm. Reproduced with permission from ref. 186, Copyright 2017, WILEY-VCH Verlag GmbH & Co. KGaA, Weinheim

We went on to show that this phenomenon could be used to coat a polystyrene Eppendorf tube (Figure 6-8(a), panel 3) and a PDMS substrate (Figure 6-8(a), panel 4). We also showed that other bipolar microgels generated as part of this study could also adsorb to surfaces, in a manner similar to JM 50. We point out that the ability of the Janus microgels to adsorb to surfaces was greatly influenced by deposition pH, which modulates the Janus microgel charge. As a result, films at pH=12 or pH=3 were not stable.

In order to explain the observed phenomenon, we measured the zeta potential of JM 50 at pH=3, pH=6, and pH=12, and the results are shown in Table 6-2. The results revealed that at pH 6, the whole Janus microgel was neutral, even though both sides of the microgels should be highly charged at this pH. This is a result of the charges on the two halves of the microgel surface cancelling one another out, which can lead to strong electrostatic attraction between the highly charged halves, with minimal repulsive forces between the microgels as a whole. Although, at pH=3/pH=12 this is not the case, as one side of the Janus microgel has excess charge relative to the other rendering the microgel as a whole charged. This adds more repulsion between the microgels, which we hypothesize greatly influences the surface adsorption ability. Granick's group also showed that Janus particles could form large clusters at their electroneutral state, which supports our hypothesis and observations here.[191]

This ability of these Janus microgels to adsorb to surfaces makes them perfect for generating surface coatings with switchable optical properties in a manner that doesn't

require any surface pre-treatment. To demonstrate this potential, we added water (pH 6) to glass vials coated with Janus microgels and evaluated the optical properties via UV-Vis as a function of temperature. As can be seen in Figure 6-8 (b, c), the optical properties of the films/vial change as the solution temperature is varied from below to above the microgel transition temperature. Specifically, the color of the vial changes from red (T=25 ºC) to purple (T=55 ºC).

Finally, we demonstrated that the Janus microgels generated here could be used as building blocks for self-assembled structures. In this case, thiolated DNA was coupled with the Au NPs on JM 70' microgels; one set of microgels was modified with a sequence of DNA that was fully complementary to DNA that was attached to another set of JM 70' microgels. The full sequences are shown in the experimental section. Figure 6-10(a) shows the process schematically, while Figure 6-10(b) shows the TEM images of the mixed microgels, and reveals that dimer structures could be achieved.

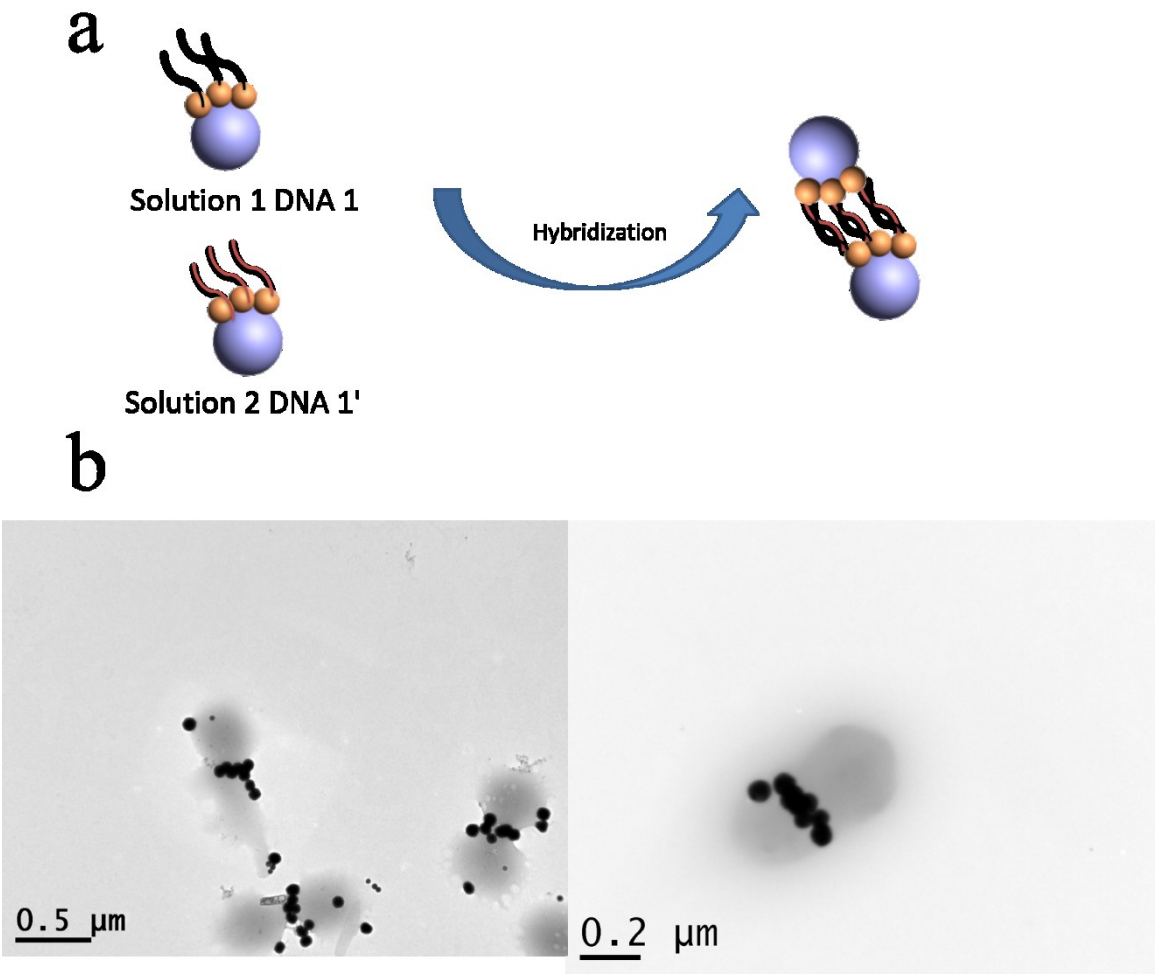

Figure 6-10 a) Schematic depiction of the dimerization of DNA-modified Janus microgels; and b) Representative dimers observed in TEM images. Reproduced with permission from ref. 186, Copyright 2017, WILEY-VCH Verlag GmbH & Co. KGaA, Weinheim

6.4 Conclusion

In this investigation, we demonstrated that a simple self-assembly method can be used to modify one or both sides of pNIPAm-based microgels with Au NPs. The Au

NPs are extremely versatile, as their surface chemistry can be easily changed by attachment of functional thiols to their surfaces. In this chapter, we showed that Janus microgels with the same (monopolar) or different (bipolar) charge on their surface could be generated, and that the optical properties of the Janus microgels could be modulated with temperature and pH, which was related to the solvation state of the microgels. We went on to show that bipolar microgels have enhanced surface adsorption capacity compared to monopolar Janus microgels. Interestingly, the resultant films exhibited tunable optical properties, which could be used for a variety of applications. Finally, we modified the Janus particles with DNA and showed that this property could be used to direct particle self-assembly. Due to the versatility of this system, we feel that these materials could find their way into sensors, and adaptive/responsive optical thin films.

Chapter 7 Preparation, Characterization of Thiolated Janus Microgels

In this chapter, we proposed a new method to prepare thiolated anisotropic pNIPAm-co-AAc microgels. Microgels can be deposited onto a thiol-functionalized slide and only the part contacted with the thiol-functionalized slide can be modified with thiol groups. XPS demonstrated that thiol groups have been successfully coupled with microgels. The thiol modified hemisphere can provide binding site with Au NPs in our case which can be used for further application.

7.1 Introduction

As mentioned in Chapter 1, microgels, which are colloidal hydrogel particles, have generated lots of research interest due to their intriguing applications in drug delivery[192], photonic crystals[193-194], biosensors[195-196] and water remediation[197-198]. One of the most extensively studied microgel is pNIPAm-based particles.[199] The thermoresponsibility of pNIPAm has been proved to be useful in the biomedical field such as cell culture[15, 200] and tissue engineering[201]. In addition, AAc as the popular comonomer can bring carboxylic group into polymer network which can be used as chemical handle for further bioconjugation. Through EDC carbodiimide chemistry, Lyon's group successfully modified pNIPAm-co-AAc microgels with biotin and prepared biotinylated microgel microlenses to detect protein[202].

In the meanwhile, thiol-modified hydrogels received the intense research interest in biomedical field. Previous investigations show that disulfide bonds can form between thiolated hydrogel particles and mucus glycoproteins, thus enhancing drug absorption

capacity. Furthermore, thiol groups on the surface can attach a wide range of molecules through metal–thiol bond[203] or be used for thiol-ene click chemistry[204], which can find various applications such as fabricating macromolecules with sophisticated architectures[205-206], or for bio-imaging[207].

For the majority of the previous publications, people modified the pNIPAm microgels homogeneously. Recent research shows that it is also desired to make particles with distinct regions which have unique properties compared to their homogenous counterparts. For example, by selectively coating particles' each hemisphere with different color, these anisotropic particles can be used in display[208]. In another example, by making half of the particle hydrophilic and the other half hydrophobic, the amphiphilic particle can behave like surfactant molecules[209]. Therefore, it is also interesting to investigate the anisotropically modified pNIPAm microgels.

For a traditional method to synthesize anisotropic particles, one side of the particle is shielded by substrates[88] or Pickering emulsions[210], only the exposed part is available for chemical modification. In this Chapter, we developed a new method to prove that the anisotropicity of particles can be obtained from its contact part with the thiol functionalized glass slides.

7.2 Experimental Section

Materials: N-isopropylacrylamide (NIPAm) was purchased from TCI (Portland, Oregon) and purified by recrystallization from hexanes (ACS reagent grade, EMD, Gibbstown, NJ) prior to use. *N,N'*-methylenebisacrylamide (BIS) (99%), acrylic acid

(AAc) (99%) , ammonium persufate (APS) (98%) cyesteamine and 1,9-nonanedithol were obtained from Aldrich (St. Louis, MO) and were used as received. Deionized (DI) water with a resistivity of 18.2 MΩ·cm was used. All different sizes of gold nanoparticles used in the Chapter were purchased from Nanocomposix (San Diego, CA). Microscope glass slides were cut into three pieces (25 × 25 mm) and obtained from Fisher Scientific (Ottawa, Ontario). All DNA was purchased from Integrated DNA Technologies (Coralville, IA). Tris(2-carboxyethyl) phosphine hydrochloride (TCEP•HCl) and 1-Ethyl-3-[3-dimethylaminopropyl] carbodiimide hydrochloride (EDC) were purchased from thermofisher scientific (Rockford, IL).

Thiolated Janus microgels fabrication: Microgels were synthesized following previous publications. Generally speaking, a 3-neck flask was fitted with a reflux condenser, nitrogen inlet, and temperature probe (as above), and charged with a solution of NIPAm (11.9 mmol) and BIS (0.703 mmol) in 99 mL deionized water, previously filtered through a 0.2 μm filter. The solution was purged with N_2 and allowed to heat to 70 °C, over ~1 hour. AAc (1.43 mmol) was added to the heated reaction mixture in one aliquot. The reaction was then initiated with a solution of APS (0.2 mmol) in 1 mL of deionized water. The reaction was and allowed to proceed at 70 °C for 4 hours under a blanket of nitrogen. The resulting suspension was allowed to cool overnight, and then it was filtered through a Whatman #1 paper filter to remove any large aggregates. The microgel solution was then distributed into centrifuge tubes and purified via centrifugation at ~8300 rcf to form a pellet, followed by removal of the supernatant and resuspension with deionized water, 6x. After synthesis, microgels were lyophilized and

redispered into water in pre-determined concentration (80 mg/mL). 2 nm Cr and 50 nm Au was evaporated onto the glass slides through thermal evaporation system (Torr International Inc., New Windsor, NY). Gold covered glass slides were then soaked into 1,9-nonanedithiol solution (10 % v/v in absolute ethanol) for 2 h. Afterwards, thiol functionalized slides were washed several times by ethanol, dried by nitrogen gas and then soaked into cysteamine solution (1 M in absolute ethanol). 1 mL 1 M NaI and 1mL 0.1 M $FeCl_3$ were quickly added into the cysteamine solution. The mixtures were under stirring for overnight. After overnight, glass slides were washing thoroughly by copious DI water and 95% ethanol and then dried under nitrogen gas. Next, microgel was painted onto the slides following the 'paint-on protocol' in previous publication.[115] Then, the microgel coated glass slides were soaked into 20 mg/mL EDC-MES buffer for overnight. After overnight, the slides were washed several times by DI water and dried under nitrogen gas. Then the glass slides were soaked into 10 mL 10 mM TCEP solution for 1 h. The Janus microgels were collected through sonication for 1 min.

All the above Janus particles were removed from glass slides by sonication in DI water for further experiments. The concentration of the Janus microgels in DI water was ~ 0.04 nM (by calculation). This calculation was done by imaging a 5 μm × 5 μm area via atomic force microscopy (AFM) and the number of particles in this area was counted. This number was then used to calculate the approximate number of particles on the whole 1 inch × 1 inch glass slide area. This calculation yielded ~ 6.5×10^9 particles $inch^{-2}$. For each Janus microgel solution, the particles were collected from four 1-$inch^2$ slides via sonication in a total of 1 mL DI water.

To prove only half of the microgels is modified with thiol, we mix the Au NP solutions with Janus microgel solution. Specifically, 40 μL 15 nm Au NPs and 80 μL 70 nm Au NPs were separately added into 1 mL thiolated Janus microgel solution. After shaking overnight, the solution was centrifuged at 8000 rpm in 10 min to get rid of extra Au NPs. The precipitate were redispersed in 1 mL DI water for further characterization.

Characterization: UV-Vis spectra were taking by an Agilent 8453 UV−Vis spectrophotometer equipped with an 89090A temperature controller and Peltier heating device (Agilent Technologies Canada Inc., ON, Canada). Transmission electron microscope (TEM) images were acquired using a JEOL, JEM 2100 (JEOL USA, Inc., MA, USA) with an accelerating voltage of 200 kV. The specimens were prepared by drying 5 μL solutions of highly diluted samples on carbon coated copper grids. Non-contact mode atomic force microscopy was used to image surfaces (Digital Instrument, Dimension 3100, Veeco Instruments Inc. NY, USA). The microgel diameter was measured using a Malvern Zetasizer Nano Series (Malvern Instruments Ltd, Malvern, UK). Contact angle was measured using an automated goniometer with drop image Advanced V2.4 software from rame-hart Instrument Co. (NJ, USA).

7.3 Results and Discussion

Figure 7-1 shows the process to make partially thiolated pNIPAm-co-AAc microgels. In detail, 50 nm Au was evaporated onto a pre-cleaned glass slide fist. Next, the Au coated slide was immersed in a 0.05 M ethanolic solution of 1,9-nonanedithiol

for 2 h. Formation of alkanedithiol self-assembled monolayers (SAMs) on Au surface has been reported intensively.[203, 211-212] People have already shown that for double-ended alkanedithiols, only one end can attach to gold surface while the other thiol group end is available for further modification as shown in Figure 7-1.[213-214]

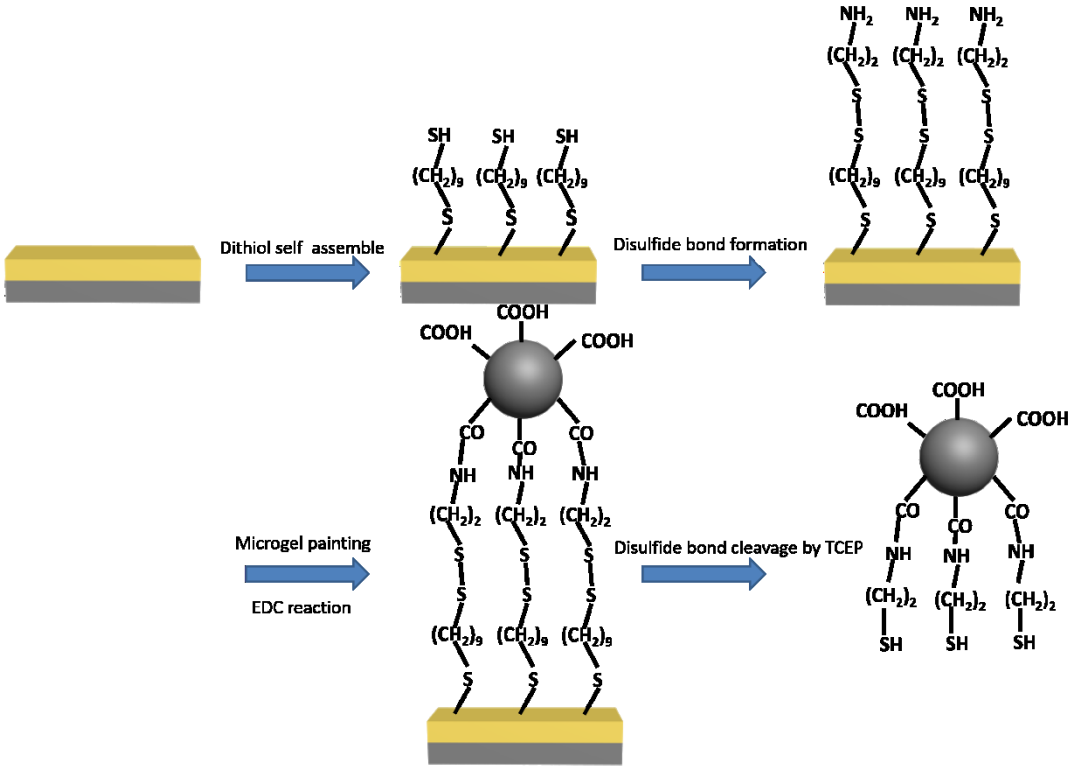

Figure 7-1 Schematic depiction of thiolated Janus microgel fabrication process

We measured the contact angle of the Au slide after 1,9-nonanedithiol modification since the long carbon chain from 1,9-nonanedithiol can make the surface more hydrophobic. While the contact angle of water on the blank Au slide is around 54±2°, the contact angle of water on the SAM of 1,9-nonanedithiol changed to 73±3° (Figure 7-2 from a to b) which is very close to the previous published data, demonstrating the successfulness of dithiol modification.[214]

Figure 7-2 Contact angles for water on a) Blank gold slide, 54±2° b) 1,9-nonanedithiol modified Au slide, 73±3°; c) 1,9-nonanedithiol modified Au slide after coupling with cysteamine, 45±2°

Next, we coupled cysteamine with the monolayer through disulfide bond formation. Iodine has been widely utilized as the oxidant for the synthesis of disulfide bond.[215] In our design, we soaked 1,9-nonanedithiol functionalized Au slides into 10 mL 1 M cysteamine solution first. Then 1 mL 1 M NaI and 1mL 0.1 M $FeCl_3$ were quickly added into the cysteamine solution. NaI is quickly oxidized by $FeCl_3$. Iodine was immediately formed and yellow-brown color was observed. The mixtures were under stirring for overnight incubation. Then the slide was washed three times by DI water to remove any impurities on surface. After cysteamine modification, the slide's contact angle changed to 45±2° (Figure 7-2(c)), which indirectly proves the successfulness of the reaction. XPS was conducted in order to further prove cysteamine has been coupled with the 1,9-nonanedithiol monolayer. After cysteamine modification, the N 1s peak appears around 400 eV (Figure 7-3(a)), which demonstrated primary amine groups from cysteamine were introduced to the surface.

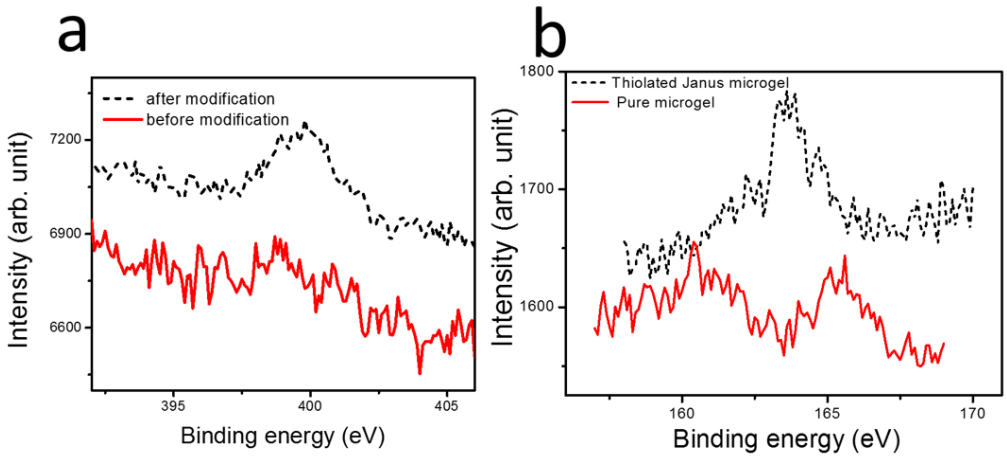

Figure 7-3 XPS data for a) After cysteamine modification; N 1s peak clearly shows up at around 400 eV; b) Compared to pure microgel, thiolated microgel clearly shows S 2p peak at 164 eV

Next, we followed a "paint-on" protocol published previously to paint a 40 µL aliquot of concentrated microgel solution on top of the slide to form a monolithic microgel layer[115]. The AFM image of the slide after microgel layer deposition is shown in Figure 7-4. The amount of microgels on a slide was done by imaging a 5 µm × 5 µm area via AFM and the number of particles in this area was counted. This number was then used to calculate the approximate number of particles on the whole 1 inch × 1 inch glass slide area. This calculation yielded $\sim 6.5\times10^{9}$ particles inch^{-2}.

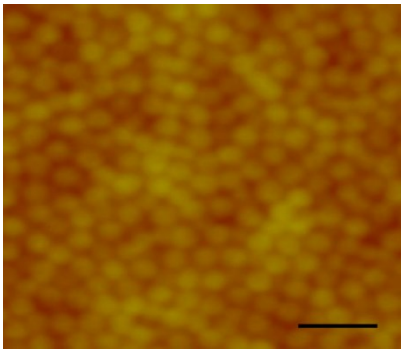

Figure 7-4 AFM images of pNIPAm microgels deposited onto a slide. The scale bar is

1 μm

Afterwards, we soaked the slide into 10 mL 1mg/mL EDC solution to covalently couple carboxylic group from microgel layer with amine group from slides. Last, disulfide bond was cleaved by tris(2-carboxyethyl) phosphine hydrochloride (TECP). After soaking the slide in DI water, sonication was applied for 1 min to remove the thiol-functionalized particle from the surface. Centrifuge was conducted three times to purify these thiolated microgels. The resultant particles were kept at pH=6.5 solution for further characterization. To prove thiol groups have already been successfully introduced to the microgel particles, XPS was used. Compared to pure microgel, modified microgel showed clearly SH peak at 164 eV (Figure 7-3(b)).

Such thiolated microgels' TEM image is shown in figure 7-5(a). They preserved pNIPAm-co-AAc microgels' spherical shape and good monodispersity. In addition, the resultant thiolated microgels retain the thermoresponsibility of pNIPAm-co-AAc microgels. DLS was used to monitor the temperature-dependent diameter for thiolated particles to determine their LCST. As shown in figure 7-5(b), in pH=6.5 solution, thiolated microgel shows the volume transition temperature around 50 ºC. The diameter is decreased from 695 ± 12 nm at 25 ºC to 294 ± 11 nm at 70 ºC. And DLS data from heating-cooling cycles show the reversibility of the thiolated microgels' phase transition as the solution temperature is switched above and below the transition temperature.

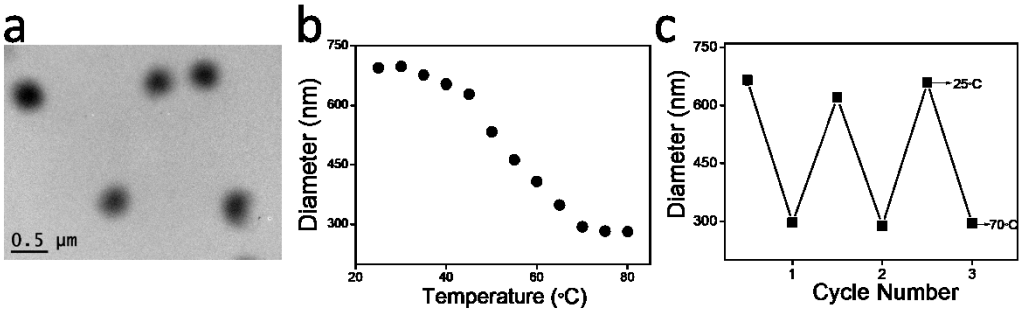

Figure 7-5 a) TEM image for thiolated Janus microgel; b) DLS data for thiolated Janus microgel under different temperature, c) Reversibility of the diameter change under 3 heating-cooling cycles

To further prove sulfhydryl groups only covered one hemisphere of the microgels, next we mixed different sizes of Au NPs with thiol-modified microgels. Au NPs is supposed to bind only with sulfhydryl groups on the microgels' surface through Au-thiol bond. TEM images in figure 7-6 shows that despite of different size, 70 nm Au NPs and 15 nm Au NPs will preferentially bind with only one hemisphere of the thiol-modified microgels which proves thiol groups only exist on one hemisphere. Next, the Au NPs functionalized Janus microgels are investigated for further application.

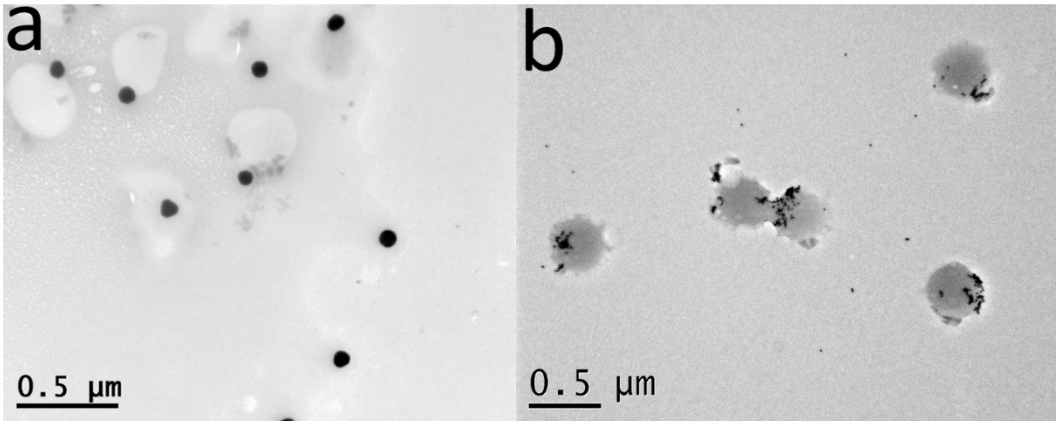

Figure 7-6 Thiolated microgel coupled with a) 70 nm Au NPs; b) 15 nm Au NPs

Previous publications demonstrated that the temperature-dependent solvation state of pNIPAm-based polymer can influence the LSPR absorbance of the Au NPs due to the change of polymer's refractive index.[70, 216] Since thiolated microgel shows thermoresponsibility, we expected that the Au NPs modified Janus microgel can have the optical responsibility under different temperatures. Here, we used 70 nm Au NPs modified Janus microgel as an example. As shown in figure 7-7 (a), at pH=6.5 solution, the absorption peak shifts from 556 nm at 25 ºC to 570 nm at 70 ºC and obviously increasing in peak intensity is also observed. Since, peak intensity change is more obvious than peak shift, in figure 7-7(b), we monitor the intensity change at 550 nm at low (25 ºC) and high (70 ºC) temperature, which proves optical change is also reversible under multiple heating-cooling cycles.

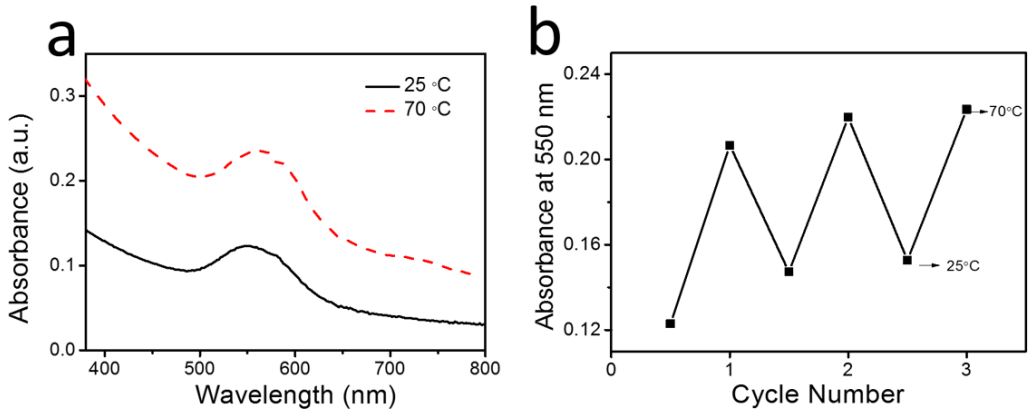

Figure 7-7 a) UV-Vis spectra for 70 nm Au NPs modified thiolated Janus microgel at different temperature; b) The reversibility of the optical response

7.4 Conclusion

In this Chapter, we proposed a novel method to prepare thiolated Janus microgels. The anisotropicity is from the contact area of microgels with substrates. XPS and TEM images prove the successfulness of this approach. And the thiolated Janus microgel preserve the thermoresponsibility of pNIPAm microgel which is shown by DLS data under different temperatures. We also demonstrated that Au NPs can only preferentially bind with the thiolated hemisphere which proved the Janus structure of these resultant particles. After Au NPs modification, we proved that the resultant particles can tune their optical property under heating-cooling cycles.

Chapter 8 Conclusion and Future Outlook

8.1 Conclusions and Future Outlooks of the Electroresponsive Devices

The first part of this dissertation describes the pNIPAm microgel-based devices with electroresponsivities. As the active part of the device, pNIPAm microgel's electroresponsive behavior controls the whole devices' properties. We concluded that there are two possible mechanisms explored in this dissertation to realize the microgel layer's electroresponsivity.

First, upon the application of a suitable potential, water electrolysis at the electrode surface is able to change the pH of the surrounding solution enough to make the microgels change their ionization degree and size. In Chapter 3, one layer of pNIPAm-co-AAc microgels was painted onto an Au electrode. Through strong electrostatic interactions, the negatively charged microgel layer can trap positively charged small molecule (CV) inside the polymer network which can be used as a drug delivery system. The pH change due to water electrolysis can neutralize the microgel layer and trigger CV release. In Chapter 4, another Au overlayer was evaporated onto the pNIPAm microgel layer to make the etalon devices discovered by our group previously. Similarly, one etalon device as a working electrode can be assembled into an electrochemical cell with one ITO glass slide as a counter electrode. Electrically-induced pH change can modulate the pNIPAm-co-AAc microgel layer's solvation state which can tune the distance between the two Au layers and result in optical change of the etalon devices. However, the drawbacks for the work in Chapter 4 is that ITO glass has been shown to

react with water electrolysis products, leading to a decrease in its conductivity and transparency.

In order to make durable devices, in Chapter 5, we proposed the second electroresponsive mechanism and utilized the interaction between the charged Au plates and the middle microgel layer to modulate the microgel layer's actuation in non-short circuits. We showed that even below water electrolysis potential, the above mentioned strong interactions can compress and elongate the elastic microgel layer.

For the future work of this part, first, we are interested to investigate the relationship between the amount of drug loaded and the microgels' composition. The release amount of loaded drugs are also needed to investigate. We will continue to explore the relationship between applied voltage and drug release. For example, in this dissertation, we only apply the pulsed voltage every 1 min. We would be interest to investigate the influence of voltage frequency on triggering the drug release from microgel layer. In addition, we pointed out that pH change induced by water electrolysis and charged drug electrophoresis both could be the reasons for controlled drug release. We only tested and proved that pH indeed change near the electrode. Further experiments are needed to explore the impact of drug electrophoresis.

In addition, we will try to understand more aboutthe interactions of the microgel dielectric layer and the two Au layers. For example, we can apply the constant voltage ($\leq$ 1 V) across the etalon device and make sure there is no other interferences from water electrolysis. Upon pressing the top Au layer, the elastic microgel layer can be compressed. The current of the system will be dramatically increased since the two Au

layers come closer, which can be utilized as pressure sensor. Similarly, metal NPs/carbon nanotubes can be incorporated into the microgel layers. The microgel layer's contraction under external stimuli can have the influence on its conductivity.

Furthermore, the whole etalon structure can be build up on an elastomer surface. The electrically-induced microgels' contraction/elongation can generate large forces and be used as actuators. The big advantage for such an electroresponsive system is that the actuation speed will be fast and accurate.

8.2 Conclusions and Future Outlooks of the Anisotropic Particles

The second part of this thesis investigated the approaches to make asymmetric pNIPAm-based microgels. We concluded that a self-assembly method can selectively coat one pole or both sides (poles) of microgels with Au NPs in Chapter 6. In addition, Chapter 7 describes that such asymmetric structures can also be obtained by selectively modifying only one hemisphere with thiol groups.

Combining pNIPAm-based microgels and metal NPs can generate lots of novel properties. In this dissertation, we already proved that such anisotropic particles' optical properties can be tuned by temperature or pH which can be used as optical sensors. Furthermore, such anisotropic features can make Janus microgels as building blocks to realize specific self-assembled structures.

For the future work, we will try to incorporate different metal NPs with microgels to generate Janus microgels with different properties. For example, Ag NPs can be coated on the surface of microgels to make antibacterial materials. One side of the microgels can be modified to selectively anchor onto certain contaminated surfaces

while the Ag side can kill bacterial. Furthermore, the structure of microgels with Au NPs modified on both poles resembles the etalon structure. It is possible that reassemble these particles onto a glass slide could generate certain tunable optical properties. The properties of such anisotropic microgels are also interesting to be explored.

References

[1] I. Tokarev, S. Minko, *Soft Matter* **2009**, 5, 511.

[2] M. A. C. Stuart, W. T. Huck, J. Genzer, M. Müller, C. Ober, M. Stamm, G. B. Sukhorukov, I. Szleifer, V. V. Tsukruk, M. Urban, *Nature Materials* **2010**, 9, 101.

[3] D. Roy, J. N. Cambre, B. S. Sumerlin, *Progress in Polymer Science* **2010**, 35, 278.

[4] A. S. Hoffman, *Advanced Drug Delivery Reviews* **2012**, 64, 18.

[5] T. R. Hoare, D. S. Kohane, *Polymer* **2008**, 49, 1993.

[6] N. Bhattarai, J. Gunn, M. Zhang, *Advanced Drug Delivery Reviews* **2010**, 62, 83.

[7] M. Hamidi, A. Azadi, P. Rafiei, *Advanced Drug Delivery Reviews* **2008**, 60, 1638.

[8] K. Haraguchi, H. J. Li, *Angewandte Chemie International Edition* **2005**, 44, 6500.

[9] O. Jeon, K. H. Bouhadir, J. M. Mansour, E. Alsberg, *Biomaterials* **2009**, 30, 2724.

[10] B. W. Garner, T. Cai, S. Ghosh, Z. Hu, A. Neogi, *Applied Physics Express* **2009**, 2, 057001.

[11] J. H. Kim, S. B. Lee, S. J. Kim, Y. M. Lee, *Polymer* **2002**, 43, 7549.

[12] Y. Huang, W. Leobandung, A. Foss, N. A. Peppas, *Journal of Controlled Release* **2000**, 65, 63.

[13] L. Chen, M. Liu, L. Lin, T. Zhang, J. Ma, Y. Song, L. Jiang, *Soft Matter* **2010**,

6, 2708.

[14] A. M. Kloxin, C. J. Kloxin, C. N. Bowman, K. S. Anseth, *Advanced Materials* **2010**, 22, 3484.

[15] S. Schmidt, M. Zeiser, T. Hellweg, C. Duschl, A. Fery, H. Möhwald, *Advanced Functional Materials* **2010**, 20, 3235.

[16] J. Kim, J. Yoon, R. C. Hayward, *Nature Materials* **2010**, 9, 159.

[17] J. H. Holtz, S. A. Asher, *Nature* **1997**, 389, 829.

[18] I. Tokarev, S. Minko, *Advanced Materials* **2010**, 22, 3446.

[19] T. Tanaka, D. J. Fillmore, *The Journal of Chemical Physics* **1979**, 70, 1214.

[20] B. R. Saunders, B. Vincent, *Advances in Colloid and Interface Science* **1999**, 80, 1.

[21] S. Saxena, C. E. Hansen, L. A. Lyon, *Accounts of Chemical Research* **2014**, 47, 2426.

[22] M. Karg, T. Hellweg, *Current Opinion in Colloid & Interface Science* **2009**, 14, 438.

[23] J. Gao, Z. Hu, *Langmuir* **2002**, 18, 1360.

[24] C. Echeverria, D. López, C. Mijangos, *Macromolecules* **2009**, 42, 9118.

[25] B. A. Pineda-Contreras, H. Schmalz, S. Agarwal, *Polymer Chemistry* **2016**, 7, 1979.

[26] C. Echeverria, N. A. Peppas, C. Mijangos, *Soft Matter* **2012**, 8, 337.

[27] S. H. Li, E. M. Woo, *Journal of Polymer Science Part B: Polymer Physics* **2008**, 46, 2355.

[28] H. G. Schild, *Progress in Polymer Science* **1992**, 17, 163.

[29] H. Vihola, A. Laukkanen, L. Valtola, H. Tenhu, J. Hirvonen, *Biomaterials* **2005**, 26, 3055.

[30] Y. Maeda, T. Nakamura, I. Ikeda, *Macromolecules* **2002**, 35, 217.

[31] H.-N. Lee, T. P. Lodge, *The Journal of Physical Chemistry Letters* **2010**, 1, 1962.

[32] I. Idziak, D. Avoce, D. Lessard, D. Gravel, X. Zhu, *Macromolecules* **1999**, 32, 1260.

[33] E. C. Cho, J. Lee, K. Cho, *Macromolecules* **2003**, 36, 9929.

[34] H. Feil, Y. H. Bae, J. Feijen, S. W. Kim, *Macromolecules* **1993**, 26, 2496.

[35] H. Liu, X. Zhu, *Polymer* **1999**, 40, 6985.

[36] S. Furyk, Y. Zhang, D. Ortiz‐Acosta, P. S. Cremer, D. E. Bergbreiter, *Journal of Polymer Science Part A: Polymer Chemistry* **2006**, 44, 1492.

[37] G. Dalkas, K. Pagonis, G. Bokias, *Polymer* **2006**, 47, 243.

[38] R. O. Costa, R. F. Freitas, *Polymer* **2002**, 43, 5879.

[39] H. Senff, W. Richtering, *Colloid & Polymer Science* **2000**, 278, 830.

[40] G. Huang, J. Gao, Z. Hu, J. V. S. John, B. C. Ponder, D. Moro, *Journal of Controlled Release* **2004**, 94, 303.

[41] C. Wang, N. T. Flynn, R. Langer, *Advanced Materials* **2004**, 16, 1074.

[42] J. Amalvy, E. Wanless, Y. Li, V. Michailidou, S. Armes, Y. Duccini, *Langmuir* **2004**, 20, 8992.

[43] J. C. Cuggino, M. C. Strumia, P. Welker, K. Licha, D. Steinhilber, R.-C. Mutihac, M. Calderón, *Soft Matter* **2011**, 7, 11259.

[44] S. Zhou, B. Chu, *The Journal of Physical Chemistry B* **1998**, 102, 1364.

[45] L. A. Lyon, Z. Meng, N. Singh, C. D. Sorrell, A. S. John, *Chemical Society Reviews* **2009**, 38, 865.

[46] Q. Sun, Y. Deng, *Journal of the American Chemical Society* **2005**, 127, 8274.

[47] S. Nayak, D. Gan, M. J. Serpe, L. A. Lyon, *Small* **2005**, 1, 416.

[48] I. Berndt, W. Richtering, *Macromolecules* **2003**, 36, 8780.

[49] I. Berndt, J. S. Pedersen, W. Richtering, *Angewandte Chemie International Edition* **2006**, 118, 1769.

[50] M. J. Serpe, C. D. Jones, L. A. Lyon, *Langmuir* **2003**, 19, 8759.

[51] Y. Guan, Y. Zhang, *Soft Matter* **2011**, 7, 6375.

[52] R. K. Shah, J.-W. Kim, J. J. Agresti, D. A. Weitz, L.-Y. Chu, *Soft Matter* **2008**, 4, 2303.

[53] R. Pelton, T. Hoare, *Microgel Suspensions: Fundamentals and Applications* **2011**, 1, 1.

[54] M. Destribats, M. Eyharts, V. R. Lapeyre, E. Sellier, I. Varga, V. R. Ravaine, V. R. Schmitt, *Langmuir* **2014**, 30, 1768.

[55] T. Gilányi, I. Varga, R. Mészáros, G. Filipcsei, M. Zrínyi, *Physical Chemistry Chemical Physics* **2000**, 2, 1973.

[56] K. Kratz, T. Hellweg, W. Eimer, *Colloids and Surfaces A: Physicochemical and Engineering Aspects* **2000**, 170, 137.

[57] I. Varga, T. Gilányi, R. Meszaros, G. Filipcsei, M. Zrinyi, *The Journal of Physical Chemistry B* **2001**, 105, 9071.

[58] M. J. Snowden, B. Z. Chowdhry, B. Vincent, G. E. Morris, *Journal of the Chemical Society, Faraday Transactions* **1996**, 92, 5013.

[59] G. Chen, A. S. Hoffman, *Nature* **1995**, 373, 49.

[60] M. Sauer, D. Streich, W. Meier, *Advanced Materials* **2001**, 13, 1649.

[61] S. Murdan, *Journal of Controlled Release* **2003**, 92, 1.

[62] T. Tanaka, I. Nishio, S.-T. Sun, S. Ueno-Nishio, *Science* **1982**, 218, 467.

[63] V. Thomas, M. Namdeo, Y. Murali Mohan, S. Bajpai, M. Bajpai, *Journal of Macromolecular Science, Part A: Pure and Applied Chemistry* **2007**, 45, 107.

[64] P. Thoniyot, M. J. Tan, A. A. Karim, D. J. Young, X. J. Loh, *Advanced Science* **2015**, 2.

[65] V. Pardo-Yissar, R. Gabai, A. Shipway, T. Bourenko, I. Willner, *Advanced Materials* **2001**, 13, 1320.

[66] X. Zhao, X. Ding, Z. Deng, Z. Zheng, Y. Peng, X. Long, *Macromolecular Rapid Communications* **2005**, 26, 1784.

[67] D. N. Heo, W.-K. Ko, M. S. Bae, J. B. Lee, D.-W. Lee, W. Byun, C. H. Lee, E.-C. Kim, B.-Y. Jung, I. K. Kwon, *Journal of Materials Chemistry B* **2014**, 2, 1584.

[68] Y. Xiang, D. Chen, *European Polymer Journal* **2007**, 43, 4178.

[69] J. Zhang, S. Xu, E. Kumacheva, *Journal of the American Chemical Society* **2004**, 126, 7908.

[70] R. Contreras-Cáceres, A. Sánchez-Iglesias, M. Karg, I. Pastoriza-Santos, J. Pérez-Juste, J. Pacifico, T. Hellweg, A. Fernández-Barbero, L. M. Liz-Marzán,

Advanced Materials **2008**, 20, 1666.

[71] T. Kawano, Y. Niidome, T. Mori, Y. Katayama, T. Niidome, *Bioconjugate Chemistry* **2009**, 20, 209.

[72] B. M. Budhlall, M. Marquez, O. D. Velev, *Langmuir* **2008**, 24, 11959.

[73] A. Shiotani, T. Mori, T. Niidome, Y. Niidome, Y. Katayama, *Langmuir* **2007**, 23, 4012.

[74] C. D. Jones, L. A. Lyon, *Journal of the American Chemical Society* **2003**, 125, 460.

[75] M.-Q. Zhu, L.-Q. Wang, G. J. Exarhos, A. D. Li, *Journal of the American Chemical Society* **2004**, 126, 2656.

[76] D. Suzuki, H. Kawaguchi, *Langmuir* **2005**, 21, 8175.

[77] J. Li, X. Hong, Y. Liu, D. Li, Y. W. Wang, J. H. Li, Y. B. Bai, T. J. Li, *Advanced Materials* **2005**, 17, 163.

[78] T. Miyata, N. Asami, T. Uragami, *Nature* **1999**, 399, 766.

[79] T. Miyata, T. Uragami, K. Nakamae, *Advanced Drug Delivery Reviews* **2002**, 54, 79.

[80] M. Lutolf, J. Lauer-Fields, H. Schmoekel, A. Metters, F. Weber, G. Fields, J. Hubbell, *Proceedings of the National Academy of Sciences* **2003**, 100, 5413.

[81] Y.-L. Zhao, J. F. Stoddart, *Langmuir* **2009**, 25, 8442.

[82] I. Tomatsu, A. Hashidzume, A. Harada, *Macromolecules* **2005**, 38, 5223.

[83] R. A. Barry, P. Wiltzius, *Langmuir* **2006**, 22, 1369.

[84] B. Comiskey, J. Albert, H. Yoshizawa, J. Jacobson, *Nature* **1998**, 394, 253.

[85] T. Nisisako, T. Torii, T. Takahashi, Y. Takizawa, *Advanced Materials* **2006**, 18, 1152.

[86] W. F. Paxton, K. C. Kistler, C. C. Olmeda, A. Sen, S. K. St. Angelo, Y. Cao, T. E. Mallouk, P. E. Lammert, V. H. Crespi, *Journal of the American Chemical Society* **2004**, 126, 13424.

[87] A. Perro, S. Reculusa, S. Ravaine, E. Bourgeat-Lami, E. Duguet, *Journal of Materials Chemistry* **2005**, 15, 3745.

[88] H. Takei, N. Shimizu, *Langmuir* **1997**, 13, 1865.

[89] L. Hong, S. Jiang, S. Granick, *Langmuir* **2006**, 22, 9495.

[90] Z. Nie, W. Li, M. Seo, S. Xu, E. Kumacheva, *Journal of the American Chemical Society* **2006**, 128, 9408.

[91] K.-H. Roh, D. C. Martin, J. Lahann, *Nature Materials* **2005**, 4, 759.

[92] M. Enayati, M.-W. Chang, F. Bragman, M. Edirisinghe, E. Stride, *Colloids and Surfaces A: Physicochemical and Engineering Aspects* **2011**, 382, 154.

[93] S. Jiang, S. Granick, *Langmuir* **2009**, 25, 8915.

[94] G. Zhang, D. Wang, H. Möhwald, *Nano Letters* **2005**, 5, 143.

[95] G. Zhang, D. Wang, H. Möhwald, *Angewandte Chemie International Edition* **2005**, 44, 7767.

[96] X. Y. Ling, I. Y. Phang, C. Acikgoz, M. D. Yilmaz, M. A. Hempenius, G. J. Vancso, J. Huskens, *Angewandte Chemie International Edition* **2009**, 121, 7813.

[97] W. Xu, Y. Yao, J. S. Klassen, M. J. Serpe, *Soft Matter* **2015**, 11, 7151.

[98] A. C. Edrington, A. M. Urbas, P. DeRege, C. X. Chen, T. M. Swager, N.

Hadjichristidis, M. Xenidou, L. J. Fetters, J. D. Joannopoulos, Y. Fink, *Advanced Materials* **2001**, 13, 421.

[99] C. López, *Advanced Materials* **2003**, 15, 1679.

[100] A. C. Arsenault, D. P. Puzzo, I. Manners, G. A. Ozin, *Nature Photonics* **2007**, 1, 468.

[101] H. Shen, Z. Wang, Y. Wu, B. Yang, *RSC Advances* **2016**, 6, 4505.

[102] C. M. Anderson, K. P. Giapis, *Physical Review Letters* **1996**, 77, 2949.

[103] P. R. Villeneuve, M. Piche, *Physical Review B* **1992**, 46, 4969.

[104] O. Rogach, A. Kornowski, A. Kapitonov, N. Gaponenko, S. Gaponenko, A. Eychmüller, A. Rogach, *Materials Science and Engineering: B* **1999**, 64, 64.

[105] A. Blanco, E. Chomski, S. Grabtchak, M. Ibisate, S. John, S. W. Leonard, C. Lopez, F. Meseguer, H. Miguez, J. P. Mondia, *Nature* **2000**, 405, 437.

[106] J. Ge, Y. Yin, *Angewandte Chemie International Edition* **2011**, 50, 1492.

[107] S. Ye, J. Ge, *Journal of Materials Chemistry C* **2015**, 3, 8097.

[108] K. Lee, S. A. Asher, *Journal of the American Chemical Society* **2000**, 122, 9534.

[109] C. Fenzl, T. Hirsch, O. S. Wolfbeis, *Angewandte Chemie International Edition* **2014**, 53, 3318.

[110] Y. Xia, B. Gates, Z. Y. Li, *Advanced Materials* **2001**, 13, 409.

[111] C. I. Aguirre, E. Reguera, A. Stein, *Advanced Functional Materials* **2010**, 20, 2565.

[112] R. C. Schroden, M. Al-Daous, C. F. Blanford, A. Stein, *Chemistry of Materials* **2002**, 14, 3305.

[113] Y. Kang, J. J. Walish, T. Gorishnyy, E. L. Thomas, *Nature Materials* **2007**, 6, 957.

[114] O. Toader, T. Y. Chan, S. John, *Physical Review Letters* **2004**, 92, 043905.

[115] C. D. Sorrell, M. C. Carter, M. J. Serpe, *ACS Applied Materials & Interfaces* **2011**, 3, 1140.

[116] C. D. Sorrell, M. J. Serpe, *Advanced Materials* **2011**, 23, 4088.

[117] K. C. Johnson, F. Mendez, M. J. Serpe, *Analytical Chimica Acta* **2012**, 739, 83.

[118] C. D. Sorrell, M. J. Serpe, *Analytical and Bioanalytical Chemistry* **2012**, 402, 2385.

[119] M. C. Carter, C. D. Sorrell, M. J. Serpe, *The Journal of Physical Chemistry B* **2011**, 115, 14359.

[120] M. R. Islam, M. J. Serpe, *Chemical Communications* **2013**, 49, 2646.

[121] D. Patra, S. Sengupta, W. Duan, H. Zhang, R. Pavlick, A. Sen, *Nanoscale* **2013**, 5, 1273.

[122] Y.-K. Oh, P. D. Senter, S.-C. Song, *Bioconjugate Chemistry* **2009**, 20, 1813.

[123] A. Vashist, A. Vashist, Y. Gupta, S. Ahmad, *Journal of Materials Chemistry B* **2014**, 2, 147.

[124] S. Goenka, V. Sant, S. Sant, *Journal of Controlled Release* **2014**, 173, 75.

[125] A. Servant, V. Leon, D. Jasim, L. Methven, P. Limousin, E. V. Fernandez‐Pacheco, M. Prato, K. Kostarelos, *Advanced Healthcare Materials* **2014**, 3, 1334.

[126] W. Miao, G. Shim, C. M. Kang, S. Lee, Y. S. Choe, H.-G. Choi, Y.-K. Oh,

Biomaterials **2013**, 34, 9638.

[127] S. Mura, J. Nicolas, P. Couvreur, *Nature Materials* **2013**, 12, 991.

[128] B. Koppolu, Z. Bhavsar, A. S. Wadajkar, S. Nattama, M. Rahimi, F. Nwariaku, K. T. Nguyen, *Journal of Biomedical Nanotechnology* **2012**, 8, 983.

[129] T. M. Allen, P. R. Cullis, *Advanced Drug Delivery Reviews* **2013**, 65, 36.

[130] F. Ye, Å. Barrefelt, H. Asem, M. Abedi-Valugerdi, I. El-Serafi, M. Saghafian, K. Abu-Salah, S. Alrokayan, M. Muhammed, M. Hassan, *Biomaterials* **2014**, 35, 3885.

[131] Y. Jiang, J. Chen, C. Deng, E. J. Suuronen, Z. Zhong, *Biomaterials* **2014**, 35, 4969.

[132] M. C. Darnell, J.-Y. Sun, M. Mehta, C. Johnson, P. R. Arany, Z. Suo, D. J. Mooney, *Biomaterials* **2013**, 34, 8042.

[133] T. N. Vo, A. K. Ekenseair, P. P. Spicer, B. M. Watson, S. N. Tzouanas, T. T. Roh, A. G. Mikos, *Journal of Controlled Release* **2015**, 205, 25.

[134] N. K. Singh, D. S. Lee, *Journal of Controlled Release* **2014**, 193, 214.

[135] Y. Li, J. Rodrigues, H. Tomas, *Chemical Society Reviews* **2012**, 41, 2193.

[136] T. Sun, Y. S. Zhang, B. Pang, D. C. Hyun, M. Yang, Y. Xia, *Angewandte Chemie International Edition* **2014**, 53, 12320.

[137] A. Servant, L. Methven, R. P. Williams, K. Kostarelos, *Advanced Healthcare Materials* **2013**, 2, 806.

[138] G. Cirillo, S. Hampel, U. G. Spizzirri, O. I. Parisi, N. Picci, F. Iemma, *BioMed Research International* **2014**, 2014.

[139] S. Maya, B. Sarmento, A. Nair, N. S. Rejinold, S. V. Nair, R. Jayakumar, *Current Pharmaceutical Design* **2013**, 19, 7203.

[140] G. Orive, R. M. Hernandez, A. R. g. Gascón, A. Domínguez-Gil, J. L. Pedraz, *Current Opinion in Biotechnology* **2003**, 14, 659.

[141] Z. M. Shakhsher, I. Odeh, S. Jabr, W. R. Seitz, *Microchimica Acta* **2004**, 144, 147.

[142] M. R. Islam, Z. Lu, X. Li, A. K. Sarker, L. Hu, P. Choi, X. Li, N. Hakobyan, M. J. Serpe, *Analytica Chimica Acta* **2013**, 789, 17.

[143] X. Li, Y. Gao, M. J. Serpe, *Macromolecular Rapid Communications* **2015**, 36, 1382.

[144] Y. Gao, G. P. Zago, Z. Jia, M. J. Serpe, *ACS Applied Materials & Interfaces* **2013**, 5, 9803.

[145] S. Guo, Y. Gao, M. Wei, Q. M. Zhang, M. J. Serpe, *Journal of Materials Chemistry B* **2015**, 3, 2516.

[146] S. H. Yuk, S. H. Cho, H. B. Lee, *Pharmaceutical Research* **1992**, 9, 955.

[147] S. G. Bratsch, *Journal of Physical and Chemical Reference Data* **1989**, 18, 1.

[148] A. Tikhonov, R. D. Coalson, S. A. Asher, *Physical Review B* **2008**, 77, 235404.

[149] M. Honda, T. Seki, Y. Takeoka, *Advanced Materials* **2009**, 21, 1801.

[150] Z. Wang, J. Zhang, J. Xie, Z. Wang, Y. Yin, J. Li, Y. Li, S. Liang, L. Zhang, L. Cui, *Journal of Materials Chemistry* **2012**, 22, 7887.

[151] J. J. Walish, Y. Kang, R. A. Mickiewicz, E. L. Thomas, *Advanced Materials* **2009**, 21, 3078.

[152] H. Fudouzi, Y. Xia, *Langmuir* **2003**, 19, 9653.

[153] K. Hwang, D. Kwak, C. Kang, D. Kim, Y. Ahn, Y. Kang, *Angewandte Chemie International Edition* **2011**, 50, 6311.

[154] J. Ge, J. Goebl, L. He, Z. Lu, Y. Yin, *Advanced Materials* **2009**, 21, 4259.

[155] W. Xu, Y. Gao, M. J. Serpe, *Journal of Materials Chemistry C* **2014**, 2, 3873.

[156] I. N. Heppner, M. J. Serpe, *Colloid and Polymer Science* **2013**, 1.

[157] S. G. Bratsch, *Standard electrode potentials and temperature coefficients in water at 298.15 K*, American Chemical Society and the American Institute of Physics for the National Institute of Standards and Technology, **1989**.

[158] L. Hu, M. J. Serpe, *Chemical Communication* **2013**, 49, 2649.

[159] K. Sierros, N. Morris, S. Kukureka, D. Cairns, *Wear* **2009**, 267, 625.

[160] M. Raes, M. Smeets, presented at *Advanced Packaging Materials: Processes, Properties and Interfaces, International Symposium* on **2005**.

[161] K. Ueno, K. Matsubara, M. Watanabe, Y. Takeoka, *Advanced Materials* **2007**, 19, 2807.

[162] J. Gong, T. Nitta, Y. Osada, *The Journal of Physical Chemistry* **1994**, 98, 9583.

[163] P. Grimshaw, J. Nussbaum, A. Grodzinsky, M. Yarmush, *The Journal of Chemical Physics* **1990**, 93, 4462.

[164] E. Kim, C. Kang, H. Baek, K. Hwang, D. Kwak, E. Lee, Y. Kang, E. L. Thomas, *Advanced Functional Materials* **2010**, 20, 1728.

[165] L. Hu, M. J. Serpe, *Chemical Communications* **2013**, 49, 2649.

[166] T. Billiet, M. Vandenhaute, J. Schelfhout, S. Van Vlierberghe, P. Dubruel,

Biomaterials **2012**, 33, 6020.

[167] A. S. Hoffman, *Advanced Drug Delivery Reviews* **2013**, 65, 10.

[168] J. Y. Sun, C. Keplinger, G. M. Whitesides, Z. Suo, *Advanced Materials* **2014**, 26, 7608.

[169] L. Ionov, *Materials Today* **2014**, 17, 494.

[170] B. Xu, R. C. Hayward, *Advanced Materials* **2013**, 25, 5555.

[171] R. Liu, M. Fraylich, B. R. Saunders, *Colloid and Polymer Science* **2009**, 287, 627.

[172] Y. Gao, W. Xu, M. J. Serpe, *Journal of Materials Chemistry C* **2014,** 2, .6961.

[173] Q. M. Zhang, W. Xu, M. J. Serpe, *Angewandte Chemie International Edition* **2014**, 53, 4827.

[174] Q. M. Zhang, A. Ahiabu, Y. Gao, M. J. Serpe, *Journal of Materials Chemistry C* **2015**, 3, 495.

[175] S. Schmidt, H. Motschmann, T. Hellweg, R. von Klitzing, *Polymer* **2008**, 49, 749.

[176] V. Nerapusri, J. L. Keddie, B. Vincent, I. A. Bushnak, *Langmuir* **2006**, 22, 5036.

[177] C. D. Sorrell, L. A. Lyon, *The Journal of Physical Chemistry B* **2007**, 111, 4060.

[178] S. Schmidt, T. Hellweg, R. Von Klitzing, *Langmuir* **2008**, 24, 12595.

[179] O. Kim, T. J. Shin, M. J. Park, *Nature Communications* **2013**, 4, 2208.

[180] K. Mukai, K. Asaka, K. Hata, H. Oike, *Smart Materials and Structures* **2011**, 20, 124008.

[181] E. C. Dreaden, A. M. Alkilany, X. Huang, C. J. Murphy, M. A. El-Sayed,

Chemical Society Reviews **2012**, 41, 2740.

[182] M. D. McConnell, M. J. Kraeutler, S. Yang, R. J. Composto, *Nano Letters* **2010**, 10, 603.

[183] D. Suzuki, H. Kawaguchi, *Colloid and Polymer Science* **2006**, 284, 1471.

[184] D. Kohler, N. Madaboosi, M. Delcea, S. Schmidt, B. De Geest, D. Volodkin, H. Möhwald, A. Skirtach, *Advanced Materials* **2012**, 24, 1095.

[185] H. Xing, Z. Wang, Z. Xu, N. Y. Wong, Y. Xiang, G. L. Liu, Y. Lu, *ACS Nano* **2011**, 6, 802.

[186] W. Xu, M. Wei, M. J. Serpe, *Advanced Optical Materials* **2017**, 2, 2195.

[187] N. Nakajima, Y. Ikada, *Bioconjugate Chemistry* **1995**, 6, 123.

[188] M.-C. Daniel, D. Astruc, *Chemical Reviews* **2004**, 104, 293.

[189] J. N. Anker, W. P. Hall, O. Lyandres, N. C. Shah, J. Zhao, R. P. Van Duyne, *Nature Materials* **2008**, 7, 442.

[190] J. J. Storhoff, A. A. Lazarides, R. C. Mucic, C. A. Mirkin, R. L. Letsinger, G. C. Schatz, *Journal of the American Chemical Society* **2000**, 122, 4640.

[191] L. Hong, A. Cacciuto, E. Luijten, S. Granick, *Nano Letters* **2006**, 6, 2510.

[192] Y. Gao, A. Ahiabu, M. J. Serpe, *ACS Applied Materials & Interfaces* **2014**, 6, 13749.

[193] C. E. Reese, A. V. Mikhonin, M. Kamenjicki, A. Tikhonov, S. A. Asher, *Journal of the American Chemical Society* **2004**, 126, 1493.

[194] M. Chen, L. Zhou, Y. Guan, Y. Zhang, *Angewandte Chemie International Edition* **2013**, 52, 9961.

[195] Q. Wu, X. Wang, C. Liao, Q. Wei, Q. Wang, *Nanoscale* **2015**, 7, 16578.

[196] M. R. Islam, M. J. Serpe, *Macromolecules* **2013**, 46, 1599.

[197] D. Parasuraman, A. K. Sarker, M. J. Serpe, *Colloid and Polymer Science* **2013**, 291, 1795.

[198] D. Parasuraman, M. J. Serpe, *ACS Applied Materials & Interfaces* **2011**, 3, 2732.

[199] J. Wu, B. Zhou, Z. Hu, *Physical Review Letters* **2003**, 90, 048304.

[200] M. E. Nash, W. M. Carroll, N. Nikoloskya, R. Yang, C. O. Connell, A. V. Gorelov, P. Dockery, C. Liptrot, F. M. Lyng, A. Garcia, *ACS Applied Materials & Interfaces* **2011**, 3, 1980.

[201] S. Ohya, Y. Nakayama, T. Matsuda, *Biomacromolecules* **2001**, 2, 856.

[202] J. Kim, S. Nayak, L. A. Lyon, *Journal of the American Chemical Society* **2005**, 127, 9588.

[203] C. D. Bain, E. B. Troughton, Y. T. Tao, J. Evall, G. M. Whitesides, R. G. Nuzzo, *Journal of the American Chemical Society* **1989**, 111, 321.

[204] C. E. Hoyle, C. N. Bowman, *Angewandte Chemie International Edition* **2010**, 49, 1540.

[205] K. L. Killops, L. M. Campos, C. J. Hawker, *Journal of the American Chemical Society* **2008**, 130, 5062.

[206] L. A. Connal, C. R. Kinnane, A. N. Zelikin, F. Caruso, *Chemistry of materials* **2009**, 21, 576.

[207] S. T. Selvan, T. T. Y. Tan, D. K. Yi, N. R. Jana, *Langmuir* **2009**, 26, 11631.

[208] S. N. Yin, C. F. Wang, Z. Y. Yu, J. Wang, S. S. Liu, S. Chen, *Advanced materials*

2011, 23, 2915.

[209] S. Jiang, Q. Chen, M. Tripathy, E. Luijten, K. S. Schweizer, S. Granick, *Advanced Materials* **2010**, 22, 1060.

[210] D. Suzuki, S. Tsuji, H. Kawaguchi, *Journal of the American Chemical Society* **2007**, 129, 8088.

[211] C. D. Bain, J. Evall, G. M. Whitesides, *Journal of the American Chemical Society* **1989**, 111, 7155.

[212] C. D. Bain, H. A. Biebuyck, G. M. Whitesides, *Langmuir* **1989**, 5, 723.

[213] R. P. Andres, T. Bein, M. Dorogi, S. Feng, *Science* **1996**, 272, 1323.

[214] W. Deng, L. Yang, D. Fujita, H. Nejoh, C. Bai, *Applied Physics A* **2000**, 71, 639.

[215] B. Mandal, B. Basu, *RSC Advances* **2014**, 4, 13854.

[216] R. Contreras-Cáceres, J. Pacifico, I. Pastoriza-Santos, J. Pérez-Juste, A. Fernández-Barbero, L. M. Liz-Marzán, *Advanced Functional Materials* **2009**, 19, 3070.

Appendix A: Magnetic Field Assisted Programming of Particle Shapes and Patterns[3]

Anisotropic particles have generated an enormous amount of research interest due to their applications for drug delivery, electronic displays and as micromotors. However, up till now, there is no single protocol capable of generating particles of "patchy" composition with a variety of well-defined and predictable shapes. To address this, in this section we dispersed magnetic nanoparticles (MNPs) in a non-magnetic fluid containing monomer and crosslinker. This solution was added to the surface of Teflon, which was submerged in the solvent 2,2,4-trimethylpentane. Under these conditions a round, stable droplet was formed on the Teflon. Upon exposure to a permanent magnet, the MNPs self-assembled into clusters with a variety shapes and sizes. The shape and size of the clusters depended on the magnetic field strength, which we controlled by systematically varying the distance between the magnet and the droplet. Interestingly, the shape of the liquid droplet was also influenced by the magnetic field. Upon polymerization, the MNP patterns and the droplet shape was preserved. We also show that very complex MNP patterns and particle shapes could be generated by controlling the distance between the drop and both a magnet above and below the droplet. In this case, the resulting patterns depended on whether the magnets were attracting or repelling each other, which was capable of changing the field lines that the MNPs align with. Overall, this approach is capable of generating particles with predictable MNP patterns and particle shapes without the use of any templates or complex synthetic steps.

[3] This Chapter has been adapted from a previously published paper. Wenwen Xu, Yuyu Yao, John S. Klassen and Michael J. Serpe, Soft Matter, 2015, 11, 7151-7158.

Furthermore, by using a sprayer (or similar approaches, e.g., ink jet printing) this technique can be easily scaled up to produce many complex anisotropic particles in a short amount of time. However, the detailed mechanism for these strips formation and how we could predict the pattern formation are subject to future study.

A.1 Introduction

The fabrication of particles with various and controllable shapes, and/or localized chemistry differences is of extreme interest for a variety of applications.[1-2] This has been driven by their ability to be used for drug delivery,[3] electronic paper,[4] micromotors,[5] and bar coding technology.[6] There are several methods proposed for anisotropic particle synthesis; the use of Pickering emulsions is one example.[7] Specifically, Granick and coworkers,[8] adsorbed particles at the interface of wax and water, one half of the particle was shielded from the water (due to its attachment to the wax) while the other half remained exposed to the water, which allows for its easy chemical modification independent of the other half. One downfall of this approach is the fact that particles can be detached from the wax during the functionalization, leading to homogenous particle modification, lowering the yield of the asymmetrically modified (Janus) particles. Another approach that is widely used for generating Janus particles is to use microfluidic devices. However, this method is not universal, and can be cumbersome to optimize to yield the desired particles. For example, flow rate, microchannel chemistry, and microchannel shape have to be carefully tuned and optimized to make specific particles. Yet another way to make Janus particles is via

block copolymer self-assembly.[9] However, solvent selection for phase separation, the requirement for precisely defined molecular composition, and very carefully controlled environments (temperature, humidity, etc.) makes this method tedious to implement.[10] While generating basic Janus particles can be cumbersome, the complexity is increased if patches of controlled and defined sizes are required (Janus balance). Controlling these parameters is very important for directing the assembly and attachment of anisotropic particles.[11-12]

The generation of non-spherical Janus particles is another very interesting area because it can yield self-assembled structures with much more complex architectures not available with spheres.[13] This is especially challenging due to the fact that most cases obtained spherical Janus particles which offer the lowest surface-to-volume ratio and minimizes the interfacial energy. While this is the case, such particles have been realized. For example, Müller's group synthesized triblock copolymer to yield disc/sheet like Janus particles.[14] By asymmetric wet-etching at the Pickering emulsion interface, Yang's group also fabricated non-spherical silica Janus particles.[15] However, generally speaking, those methods above are complicated. Therefore, simpler and more efficient methods are highly desirable to generate non-spherical Janus particles.

To address the above needs, in this section, we developed a new method for anisotropic particle fabrication, which is simple, effective and versatile. This approach utilizes interfacial polymerization of a monomer/crosslinker solution that has magnetic nanoparticles (MNPs) dissolved. By using magnetic fields, and modulation

of their strength and the magnetic field line directions, we were able to generate very complex anisotropic particles with well-defined shapes and conformations. These particles not only offer a diverse range of flexibility when it comes to structural and compositional diversity, but they can find utility as building blocks for microactuators in the pharmaceutical industry for cellular manipulation.[16-17] We point out that this approach can be used to synthesize complex particles much smaller than what is presented here by simply depositing smaller volumes of liquid on the teflon. Furthermore, the same techniques that can be used to make smaller particles can also be used to make multiple particles in very short amounts of time; e.g., nebulization or ink jet printing.

A.2 Experimental Section

Materials: 2-Hydroxylethylmethacrylate (HEMA) (≥ 97%), poly(ethylene glycol) diacrylate (PEGDA) (M_n = 700), 2,2,4-trimethylpentane (TMP) (≥ 99%), ammonium persulfate (APS) (≥ 98%) , N,N,N',N' – Tetramethylethylenediamine (TEMED) (≥ 99%) as well as Fe (II, III) oxide nanoparticles (50 nm - 100 nm diameter) with no surface modification was purchased from Sigma Aldrich (Oakville, Ontario). Ultra high-pull Neodymium-Iron-Boron (NdFeB) magnets (5×5×1 cm) were purchased from McMaster-Carr Company (Elmhurst, IL). Deionized water (DI water) with a resistivity of 18.2 MΩ cm was used and obtained from a Milli-Q Plus system (Millipore Co., Billerica, MA). Polyetrafluoroethylene (PTFE) was provided by Johnston Industrial Plastics (Edmonton, Alberta).

Preparation of anisotropic particles: Fe (II, III) oxide MNPs (0.37 M), 2-hydroxylethylmethacrylate (HEMA) (3.52 M), and poly(ethylene glycol) diacrylate (PEGDA) (0.23 M)) aqueous solution was used as the "pre-gel" solution. Aqueous solutions of the initiator ammonium persulfate (APS) (0.44 M) and accelerator N,N,N',N' –tetramethylethylenediamine (TEMED) (0.67 M) were also used. 10 μL of the APS solution and 10 μL of the TEMED solution were added to 0.1 mL of the pre-gel solution and mixed, and 5 μL aliquots (in most cases) manually added to the PTFE-TMP interface. The external magnetic field was applied by custom-build magnetic stage where two NdFeB magnets were fixed above and below the Petri dish, with positioning screws to accurately and precisely control the distance between the Petri dish and the magnets. The polymerization was allowed to proceed for 1 h before the particles were collected. The mechanism of the polymerization accelerated by TEMED has been studied in detail previously.[18] Breifly, the initiation of the polymerization is proposed as follows. TEMED reacted with APS through redox reaction and produced free radicals 1 and 2 to initiate the whole polymerization.

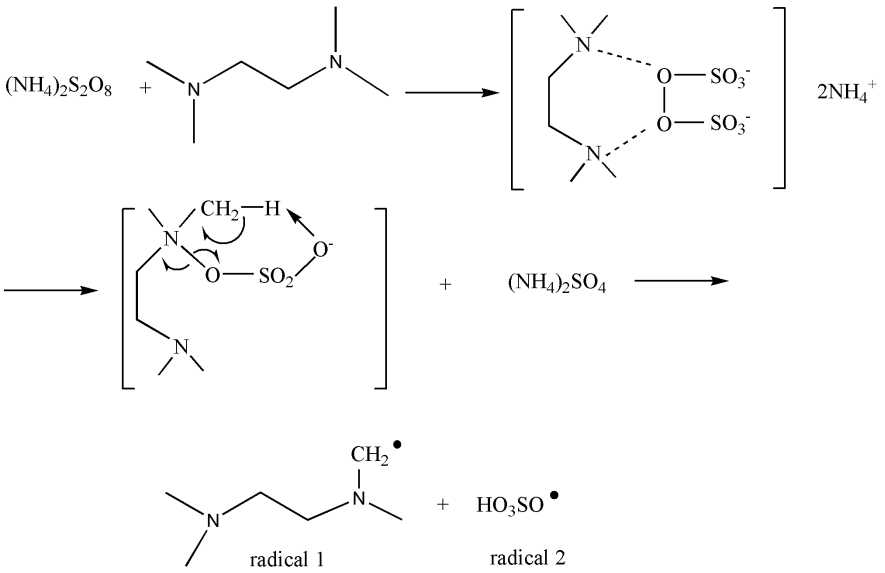

To analyze the final concentration of iron oxide inside the particles, thermal gravimetric analysis (TGA) was performed and the results (supporting information) shows that the MNPs is about 6 % (w/w) of the particle.

Instrumentation: Photographs of the particles were obtained using a Nikon camera equipped with a 105 mm Nikon macrolens (Nikon, Ontario, Canada). Optical microscopy (Olympus IX-70 Melville, New York, USA)) was used to image smaller particle. Contact angle was measured using an automated goniometer with drop image Advanced V2.4 software from rame-hart Instrument Co. (New Jersey, USA). Magnetic measurements of the purchased MNPs were performed using a Quantum Design 9T-PPMS magnetometer with fields up to 1 T at room temperature. TGA was performed using a Perkin Elmer Pyris TGA1 under a nitrogen atmosphere, heating from 25.00 ºC to 600.00 ºC at scan rate 10.00 ºC /min

A.3 Results and Discussion

Our whole system is based on MNPs suspending in pre-gel solution (non-magnetic liquid carrier). Specifically, we used Fe (II, III) oxide magnetic nanoparticles MNPs (0.37 M), 2-hydroxylethylmethacrylate (HEMA) (3.52 M), and poly (ethylene glycol) diacrylate (PEGDA) (0.23 M)) mixture solution as the "pre-gel" solution. Aqueous solutions of ammonium persulfate (APS) (0.44 M) as initiator and *N,N,N',N'*–tetramethylethylenediamine (TEMED) (0.67 M) as accelerator were made, and were mixed with the pre-gel solution to make particles. In one case, 100 µL of the pre-gel solution was mixed with 10 µL of the APS solution and 10 µL of the TEMED solution.

After this solution was shaken for ~ 5 s, 5 µL droplets were dispensed via digital pipet onto a piece of Teflon that was submerged in 2,2,4-trimethylpentane (TMP) all in a Petri dish. Under these conditions, the drops formed nearly perfect spheres on the Teflon surface. This was expected from previously published results.[19] In this case, in the absence of a magnetic field, the MNPs were randomly distributed in the droplet (and polymerized particle) due to Brownian motion; the resultant particle shape was spherical. However, when there is external magnetic field, chain structures (clusters) are observed within 1 s and polymerization can fully lock the whole pattern of the particles. (Figure A-1 (d)).

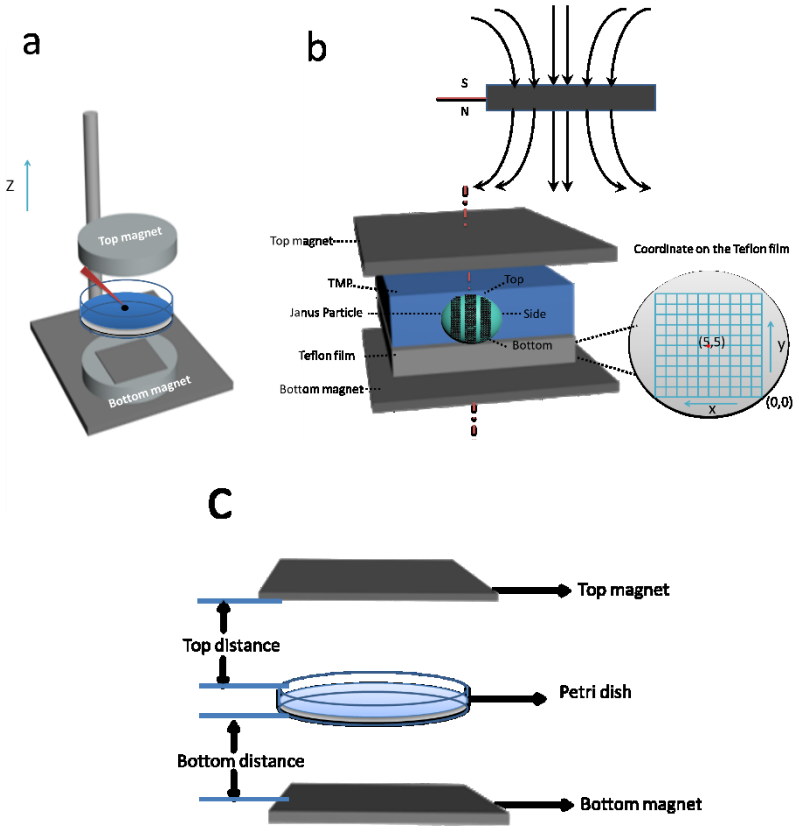

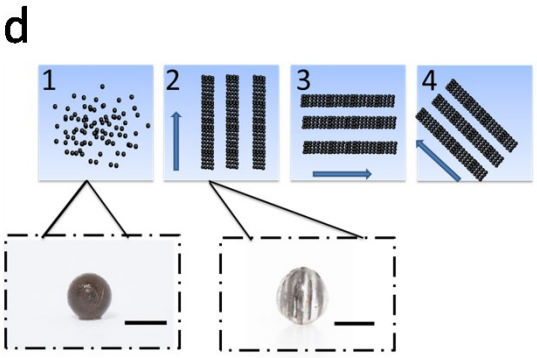

Figure A-1 a) Schematic of the setup used for the anisotropic particle synthesis. The polymerization solution was manually dispensed onto the Teflon, which was submerged in TMP. The distance between the magnets and the Petri dish could be very carefully controlled using positioning screws on the magnets. b) Side view of the setup, with "top", "side", and "bottom" defined. Furthermore, the coordinates on the Teflon are defined -- each square is 5 mm2. c) The relative distance between the magnets and the Petri dish; d) Schematic illustrating how (1) the MNPs are randomly dispersed at zero field, with corresponding photograph of the resulting particle. (2, 3, 4) Schematic of the MNP chain configuration in the presence of a magnetic field of different directions, with a corresponding photograph of a representative particle. All scale bars in the pictures are 1 mm. Reproduced with permission from ref. 99, Copyright 2015, Royal Society of Chemistry

Similarly cluster formation is also observed and well reported in the area of magnetorheological fluids.[20] The huge difference between magnetorheological fluids and our system is that the magnetic particles suspended in the carrier is much larger, usually in micron-size range. Previous paper also proves that MNPs can respond to the

external field in the similar time scale.[20]

Figure A-1(a) shows a schematic of the setup we used to fabricate anisotropic particles with complex structures and shapes. The setup is composed of a stand capable of holding the Petri dish assembly used above, but also allows for control of the distance between the two magnets and the Petri dish. We point out that the holders for two magnets were made of aluminum, which made it extremely strong and stable. Figure A-1(b) shows the simplified side view of our system. It is important to note that the magnetic field is not uniform over the whole magnet area, so for these experiment, it was important to record the position of every drop relative to the magnet. In order to do this, a coordinate system was used as defined in Figure A-1(b). For our experiments, we always made sure to fix the position of the magnets and the coordinate system, such that it was the same from experiment to experiment. For these studies, it was important to consistently define and measure the proximity of the magnets to the particles. This is detailed in Figure A-1(c), which shows the top distance as the distance between the bottom of the top magnet and the top edge of the Petri dish, while the bottom distance is the distance between top of the bottom magnet and the bottom face of the Petri dish. The same Petri dish and Teflon was used for all experiments -- the wall thickness of the Petri dish was 2 mm with a depth of 1 cm and diameter is 8.5 cm; the Teflon was 3 mm thick and had a diameter is 8.2 cm. This way of measuring distance was chosen due to its ease and reproducibility; it was also beneficial because it didn't disturb the system. For demonstration purposes, Figure A-1(d) shows how an external magnetic field could be used to manipulate magnetic particles in the droplet. If polymerization of the drops

composed of MNPs proceeded in the presence of a magnetic field, by properly positioning the magnet near the Petri dish used for polymerization, the MNPs could align themselves with the magnetic field lines. Furthermore, when there is applied magnetic field, MNPs obtain an induced dipole moment which causes them to self-assemble into chain structures parallel to the external field lines to minimize the free energy of the system.[21] To explain how the magnetic field can be used to assemble the MNPs in the pre-gel solution prior to polymerization, the ratio of the magnetic energy to thermal energy as is shown in equation A-1 needs to be considered, which can be expressed as[21-22]

$$\lambda = \frac{W_m}{K_B T} = \frac{\mu_0 \vec{m}^2}{16\pi r^3 K_B T} \qquad (A-1)$$

$$\vec{m} = \frac{4}{3}\pi r^3 \chi_{eff} \vec{H} \qquad (A-2)$$

$$\chi_{eff} = 3\frac{\mu_p - \mu_s}{\mu_p + 2\mu_s} \qquad (A-3)$$

$$\chi_p = \mu_p - 1 \qquad (A-4)$$

where W_m: magnetic inter-particle interaction energy; μ_0: magnetic permeability of vacuum; K_B: Boltzmann constant; T: temperature in Kelvin; r: the radius of the particle; $\vec{m}$: induced magnetic moment; $\vec{H}$: external field strength; χ_{eff}: effective susceptibility; μ_p: relative permeability of MNPs; μ_s: relative permeability of solvent and it is equal to the vacuum permeability which is a universal constant; χ_p is the MNPs' susceptibility. In our case, χ_p for MNPs is 0.38, their diameter is about 50 nm and the maximum field strength for the permanent magnet is 1777 G. Specificly, λ is the ratio of magnetic energy between MNPs to MNPs' thermal energy (Brownian movement). When λ is high, magnetic energy can suppress thermal energy (Brownian random movement) and

the chain structure can be formed. According to the above equations, using the above parameters, λ in our system is ~31, indicating that magnetic forces play a dominant role over thermal fluctuation which can make the particles self- assemble into stable chain clusters. Therefore, the role of the external field is to align MNP chains with the external field, assisting stacking of chains along the axis of the field and then draw them towards the ends of the permanent magnets where the magnetic field gradient is the steepest. The magnet movement and relative positions, and the dipole forces between MNPs can allow the formation of different patterns and even change the shape of the droplet, which we will talk about in detail later.

We first investigated the case of a single magnet located below the Petri dish and droplet. The influence of the magnetic field on the droplet shape is shown in Figure A-2(a). As can be seen, well-known magnetowetting phenomena are observed.[23] That is, the applied field forces the droplet to flatten (relative to no applied magnetic field) and the contact angle decreases. Furthermore, the magnetic field can cause the MNPs to form patterns, which are easily visible after the particles polymerize, which locks in the MNP structure in the particle. This behavior is clearly shown in the photographs in Figure A-2(b), which shows MNP chains being formed. The alignment of the MNPs in the magnetic field appear similar to what was observed by the Pyun group.[24]

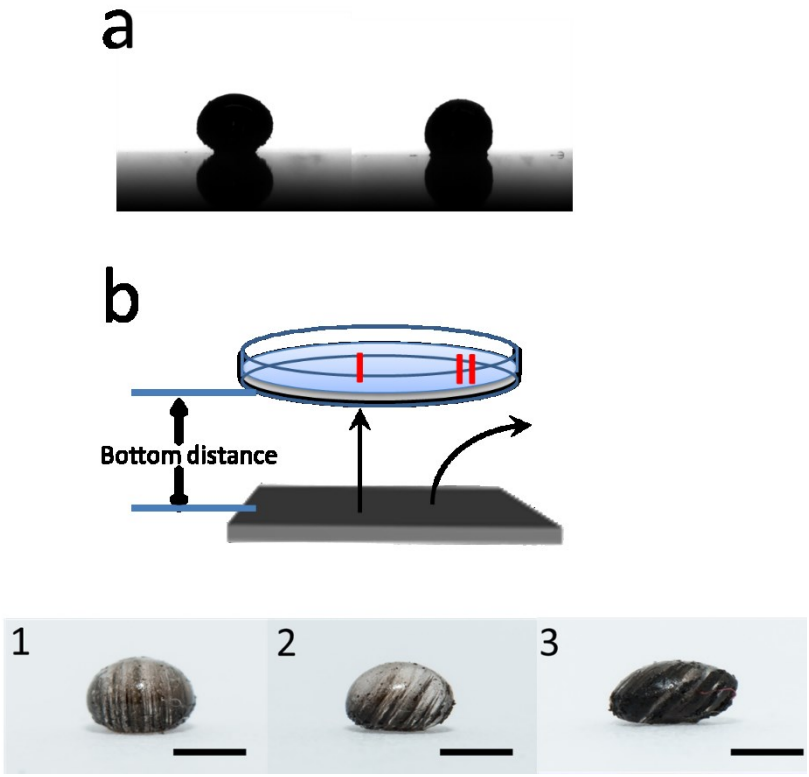

Figure A-2 a) Photograph of a pregel droplet deposited at the (5,5) position, with a magnet below the droplet. (Left) when the magnet is 4 cm away the contact angle is 165.45 ±0.07, while it is 146 ±1 when the magnet is 0.3 cm away. b) Photographs of the resulting particles polymerized with the magnet below the droplet all synthesized at a distance of 0.3 cm, for 1 at position (5,5) which is the center of the Teflon film (place I), for 2 at position (1,2) which is at the edge of the Teflon film (place II), 3 is also synthesized at position (1,2) with the concentration of MNPs increased to 0.55 M. All scale bars in the pictures are 1 mm. Reproduced with permission from ref. 99, Copyright 2015, Royal Society of Chemistry

The reason for the parallel MNP chain structure formation is due to the angular

dependence of the dipolar interaction. The external field can cause particles to generate a preferred head-to-tail alignment. Closer examination revealed that the uniform dipole orientation causes a second possibility: side-by-side particles with aligned dipoles resulting in dipole repulsion. This angular dependence of the dipolar interaction effectively eliminates half of the possible particle binding events by making it impossible for particles to bind with each other when they approach from a direction that is orthogonal to the applied field. Regardless of the field direction, the patterns on the particles we obtained are always chains parallel to each other as in Figure A-2(b). The direction of the magnetic field also has an influence on the pattern of the particle. When the MNP-containing droplet is added to a different coordinates on the Teflon (i.e., different parts of the magnet), it is exposed to a different magnetic field and magnetic field line directions.

In all the upcoming examples, we show the relative position between the Petri dish and magnets and the magnetic field line is indicated as a black arrow. As can be seen in Figure A-2 (b, 1), when the droplet was placed at the position (5,5), which is the center of the magnet, the vertical field lines will force the MNPs to self-assemble into vertical chains. We point out that "vertical" is parallel to the "z-axis" in Figure A-1(a), while horizontal is perpendicular to the "z-axis". On the other hand, when the droplet was placed at position (1,2) where the field line is "diagonal", there will be diagonal chains formed and obvious deformation of the droplet shape, see Figure A-2 (b, 2). Photographs were taken of each resulting particle, one showing a side view of the particle as it was positioned on the Teflon, the other two are of the top (near the top

magnet) and bottom (near the bottom magnet) of the particle.

Under an external magnetic field, the droplets are subject to two opposing forces: the TMP/water (pre gel solution) droplet interfacial tension and interaction between the induced magnetic field on the MNPs.[25-26] The former tends to minimize the interface between the TMP/water, while the latter favors an extended interface to minimize the dipole-dipole interactions. In our system, the dipole-dipole interaction is so strong that MNPs form the chainlike structures and the droplet shape is deformed in order to increase the interfacial area to attenuate the dipole interactions. Therefore, when we increased the concentration of MNPs, we also observed much more pronounced particle shape distortion, e.g., see Figure A-2 (b, 3).

Figure A-3 shows particles synthesized when a single magnet is located above the Petri dish instead of below. When the distance between top magnet and Petri-dish is 5 cm, MNPs tend to migrate to the top side which has the strongest field strength and as a result, a teardrop shape particle is formed, Figure A-3 (1). When the magnetic field is strong enough, rods can be formed that protrude out of the main droplet. After polymerization, the structure is locked in; see Figure A-3 (2). The key characteristics of the ferromagnetic MNPs used in our experiment, that distinguishes them from their paramagnetic counterparts, is the quasi-irreversibility of the MNP chain formation process. When the external magnetic field is partially removed, the MNPs partially demagnetize very quickly, and gravity plays an important role in this case and draws the MNPs rod back into the droplet. However, MNPs still have magnetic attraction, which hold them together and dominate over Brownian motion, which would force the

MNPs to redisperse. Therefore, as can be seen in Figure A-3 (3 and 4), we can change the length of the rod that is formed on the particles.

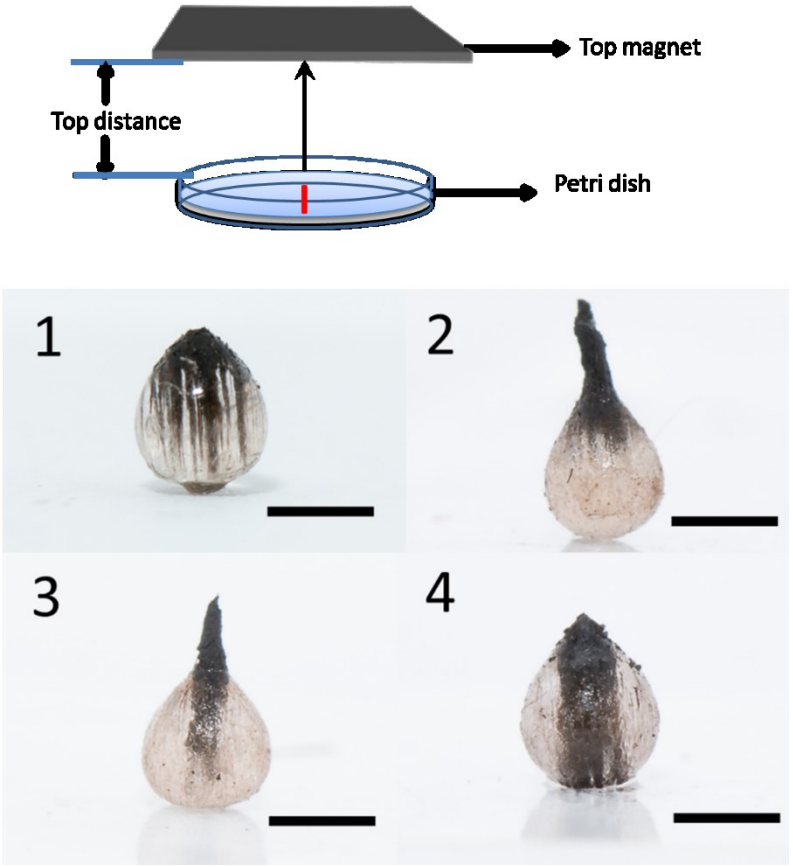

Figure A-3 Photographs of the resulting particles polymerized with the magnet above the droplet at a distance of (1) 5 cm, and (2) 4.5 cm. For (3), first the magnet was <4.5 cm to make the rod structure as shown in 2, then moved to a distance of 5 cm. As can be seen, the gravitational force pulls the rod back into the particle. 4 is the same as 3, but the final distance of the magnet is 6 cm, which allows even more of the rod to enter the particle to make a stripe. All particles were synthesized at the (5,5) position, which is the center position (I). All scale bars in the pictures are 1mm. Reproduced with permission from ref. 99, Copyright 2015, Royal Society of Chemistry

We also synthesized particles in the presence of two of the same permanent magnets, one above and below the Petri dish. These magnets can either be attracting or repelling one another. This is shown in Figure A-1. Depending on the configuration, we can generate different particle shapes and MNP patterns formed. In this case, we make the assumption that the magnet material's coercivity is sufficiently high that the magnetic field from the first magnet cannot substantially alter the magnetization of the second magnet.

Figure A-4 shows that when the two magnets generate attractive forces, vertical MNP chains will again be generated. As is shown, they are parallel to the external field line. Although, in this case, the MNP chain formation can be controlled. For example, when the distance between the bottom magnet and Petri dish is fixed at 2 cm, decreasing the distance between the top magnet and Petri dish will increase the magnetic field flux density. As a result, the number of formed chains will decrease and the chains will become thicker.

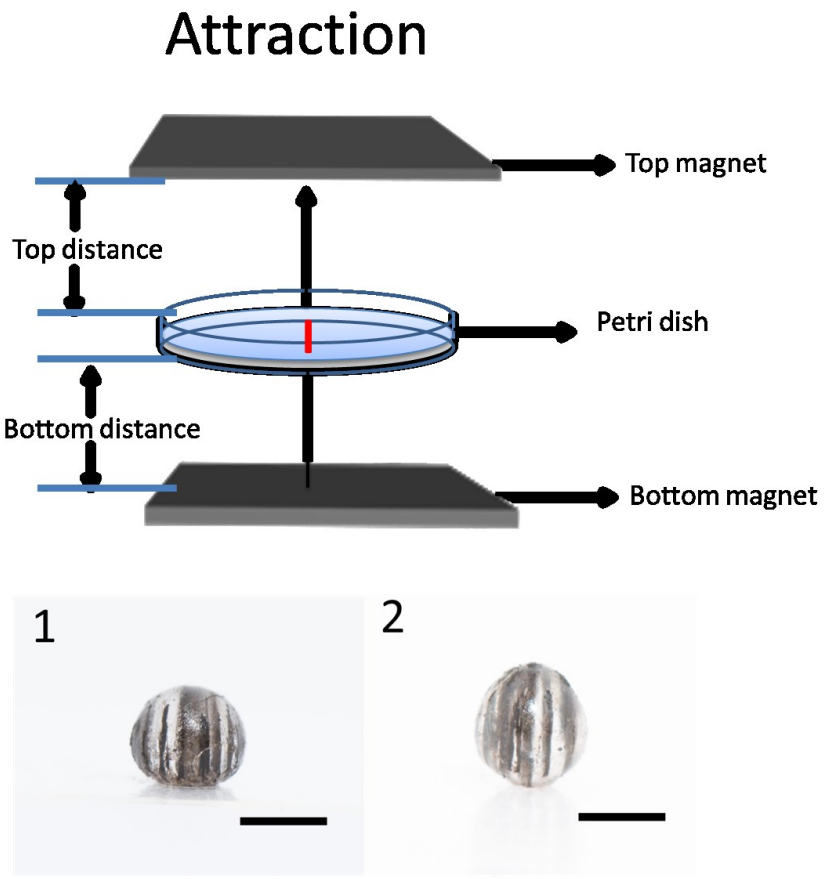

Figure A-4 Photographs of the resulting particles polymerized with a magnet above and below the droplet in the attractive regime. The bottom distance is fixed as 2 cm and both particles are synthesized at center (place I) (5,5). Top distance for (1) is 5 cm and for (2) is 3.5 cm. All scale bars in the pictures are 1mm. Reproduced with permission from ref. 99, Copyright 2015, Royal Society of Chemistry

When the two magnets are generating repulsive forces, the results shown in Figure A-5 are obtained; this is completely different than the attractive case. For example, at certain distances, opposing fields cancel each other out, leading to localized magnetic field minima. As a result, particles will experience forces that go outwards to the surrounding region of higher magnetic field.[27] By controlling the local magnetic field

strength, we can control the number and coverage of MNP chains on the particles. The coverage of horizontal chains can be controlled through adjustment of the relative distance between the top magnet and the Petri dish. In Figure A-5(a), we fix the distance between the bottom magnet and Petri dish at 2 cm, and the distance between the top magnet and the Petri dish is varied. When the top magnet is 5 cm from the Petri dish, the bottom magnetic field is stronger than the top one, and the chains mainly formed at the bottom of the particle (Figure A-5 (1)). When the distance between the top magnet and the Petri dish is decreased to 4 cm, the chains are observed throughout the particle, Figure A-5 (2) . When the distance between the top magnet and the Petri dish is decreased to 3.5 cm, the chains mainly occupy at the top half of the particle, Figure A-5 (3). Finally, when the distance between the top magnet and the Petri dish is decreased to 3 cm, the MNP chains are mainly at the top side of the particle Figure A-5 (4). When the repulsive magnetic field direction is horizontal (at certain magnet-magnet distances), the shape of the particle becomes ellipsoidal, as seen in Figure A-5 (1-3). When the top magnet is close enough to the Petri dish (<3 cm), the drop will pull off the Teflon and float on the TMP/air interface to generate a particle with a flat surface. Additionally, by comparing Figure A-5(5) with Figure A-5(2), it can be seen that the number of MNP chains in the particles can be controlled by controlling the magnet-magnet distance. When the distance between the bottom magnet and Petri dish is 0.3 cm, and the top magnet is "far away" from the Petri dish (5 cm), we observed a hemispherical particle with off the MNP chains on the bottom Figure A-5(6). However, when both magnets are very close to the Petri dish (bottom is 0.3 cm and top is 2.4 cm), the particle became

a semi-cuboid (Figure A-5 (7)).

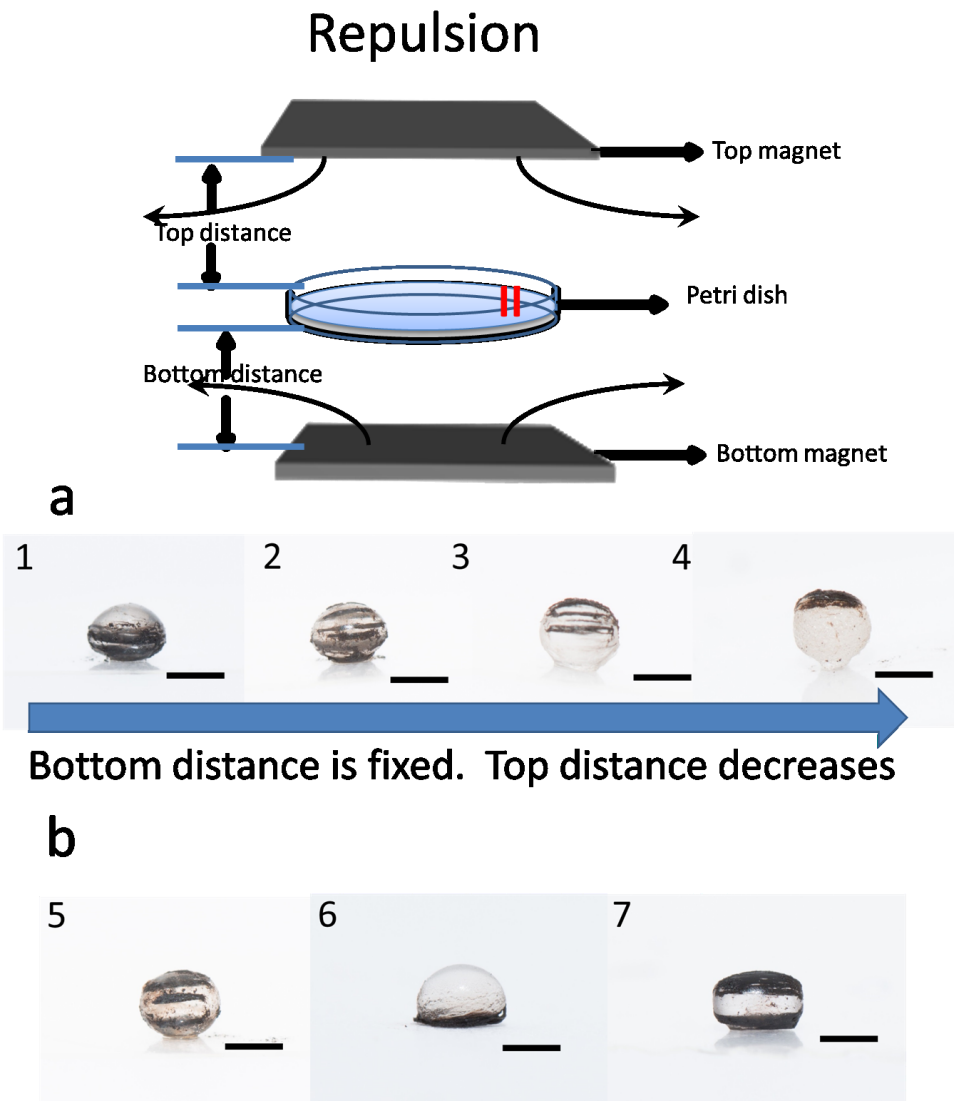

Figure A-5 Photographs of the resulting particles polymerized with a magnet above and below the droplet in the repulsive regime. All the particles are synthezed at the edge area (place II) of the Teflon film due to the influence of the external magnetic field. For (a), the bottom magnet distance is fixed at 2 cm and they are all synthezised at place (1,1); the top distance gradually decreased: for (1) is 5 cm, for (2) is 4 cm, for (3) is 3.5 cm, for (4) is 3 cm. As the top magnet distance decreases, it gradually changes the

coverage of the horizontal stripes on the particle. In part b, we can control the number of the stripes on the particle (compare (5) with (2)). (5) was synthesized at position (1,1) on the Teflon, the top distance is 3 cm, the bottom distance is 1 cm. For (6) and (7), they were both synthesized at position (2,3) on the Teflon and bottom distance is 0.3 cm. The top distance for (6) is 5 cm, for (7) is 2.4 cm. All scale bars in the pictures are 1mm. Reproduced with permission from ref. 99, Copyright 2015, Royal Society of Chemistry

Next, we showed that the anisotropic particles generated from these experiments could be differentially manipulated depending on the MNP patterns in the particles and the magnetic field. As is shown in Figure A-6, the MNP chains in the particles are oriented parallel to the magnet's field line. We show that the same particle in Figure A-6 can be precisely controlled by an external magnet. Specifically, the anisotropic particle rotates and moves in a fashion that is synchronized with the external field, using a single rotation axis. It is also very easy to control the translational movement of the anisotropic particle under external magnetic field. Finally, we showed that our particles are very sensitive to external fields, and are capable of assembling into unique anisotropic patterns shown in Figure A-6. To accomplish this, synthesized anisotropic particles were added to a capillary tube with a diameter of ~ 2 mm and filled with DI water. External magnets were placed near the tube, which resulted in particle orientation, which could be easily switched by changing the relative distances between the magnets and the tube.

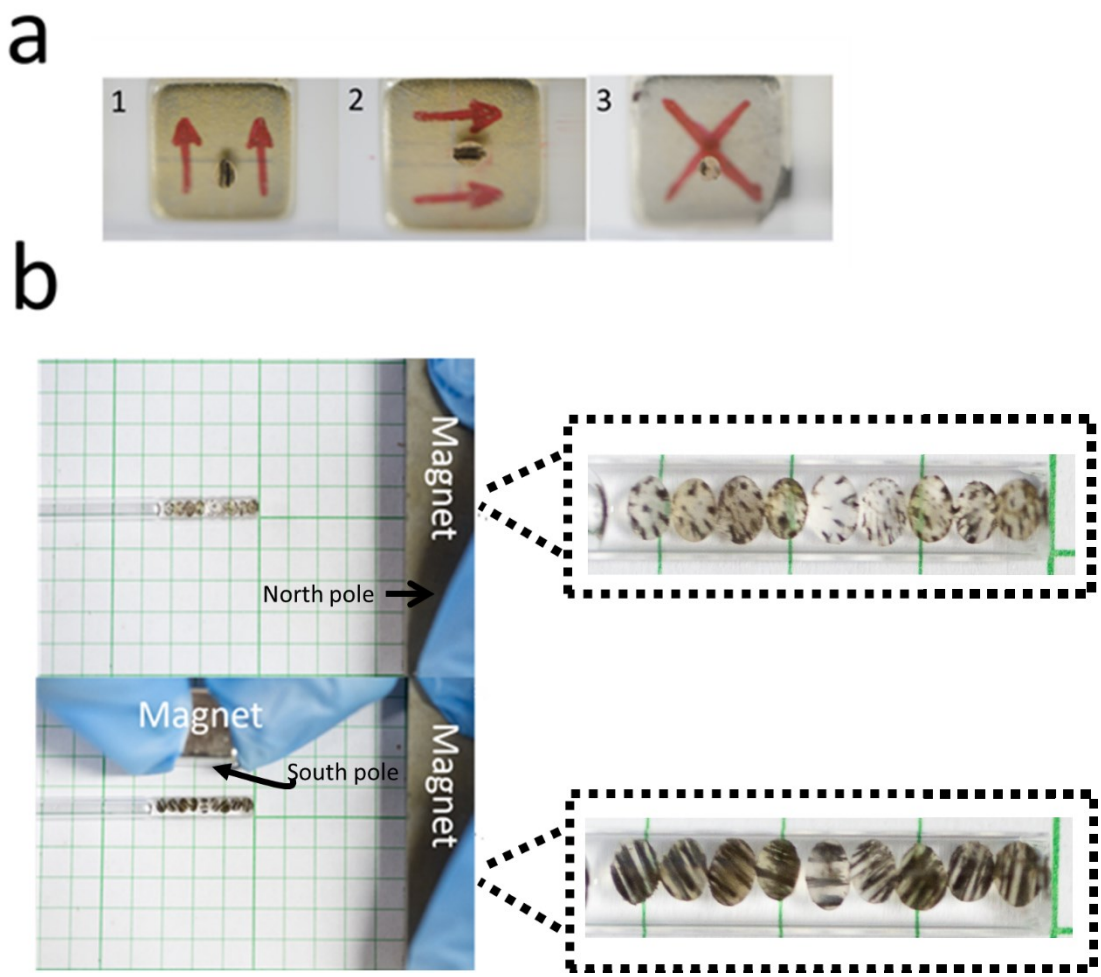

Figure A-6 a) A representative Janus particle is aligned with the magnet's field lines and moves in response to its changes. -- the field lines are indicated by the red marks on the magnet. b) Representative anisotropic particles can orient themselves according to the field line orientations, which can be influenced by changing the distance between the magnets and the particles. Reproduced with permission from ref. 99, Copyright 2015, Royal Society of Chemistry

Finally, we showed that the synthesis of anisotropic particles could be scaled up,

such that many particles could be synthesized in a simple manner and in a short time. In one example, we added the monomer solution to a spray bottle, and simply sprayed the monomer solution into the Petri dish assembly; the generated aerosol particles form the droplets that polymerize on the Teflon. This is illustrated in Figure A-7(a). An even more efficient approach to synthesize many particles simply and quickly, while allowing for the particle size to be easily tuned, is shown in Figure A-7(b). This approach simply uses a high pressure nitrogen gas stream directed at the tip of a tube, out of which a monomer solution could be pumped. The gas stream is capable of generating a fine mist, and the mist droplets (containing in this example monomer and photoinitiator) settle onto the Teflon surface. The drops on the Teflon could be polymerized by simple exposure to UV light. For this experiment, we used a pre-gel solution composed of poly(ethylene glycol) diacrylate (PEGDA (95% v/v)), photointiator 2,2-dimethoxy-2-phenylacetophenone (5% v/v) and MNPs (amount could be varied). The gas stream pressure and angle relative to the tip of the monomer solution delivery tube can be easily tuned to adjust the particle size. Microscope images (obtained with an Olympus optical microscope) of representative particles that were generated in this manner are shown in Figure A-7 (c-f). As can be seen from the representative microscope images, particles with diameters in the range of 5 μm - 400 μm could be readily generated. Furthermore, Figure A-7 (c) shows that the structure of the magnetic particles could be retained after polymerization.

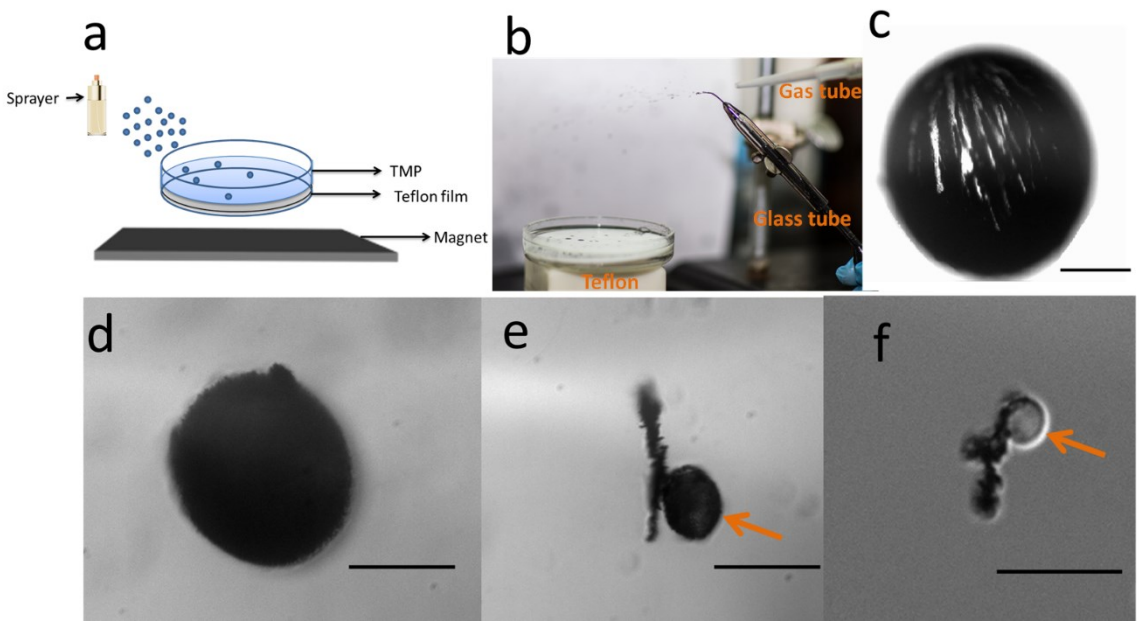

Figure A-7 a) Schematic illustration of the system used to prepare anisotropic particles via a spray bottle; b) a tube used to supply nitrogen gas is directed onto a glass tube, out of which monomer/photoinitiator is being pumped; the gas dispersed the solution into a fine mist, which settled on the Teflon film, which underwent photopolymerization to generate particles; c) microscope image of a representative anisotropic particle with a diameter of ~ 400 μm -- the scale bar is 100 μm. d-f) microscope images of various particles that can be produced using the procedure in (b), (d, e) the scale bar is 50 μm; (f) the scale bar is 20 μm. Reproduced with permission from ref. 99, Copyright 2015, Royal Society of Chemistry

A.4 Conclusion

Using a simple setup composed of magnets interacting with MNPs, very complex particle structures, with very intricate MNP patterns inside each particle could be synthesized. The exact particle shape and arrangement of the MNP chains in the particles depended on if one or two magnets were used, and their distance away from the synthesis vessel. We showed that the synthetic conditions and setup are extremely robust, and can be used to synthesize many particles with predefined shape/configuration in a very reliable and reproducible manner. We also showed that the particles could be manipulated by external magnetic fields. Finally, the synthetic approach was shown to be scalable, such that many particles could be synthesized in parallel and the diameter can be reduced to hundreds of microns with easy system modification. These systems have many interesting potential applications for patterning, actuation, and for memory storage and encryption applications, which will be the topic of future studies.

Appendix B: Supramolecular Hydrogels Fabricated from Supramonomers: A Novel Wound Dressing Material[4]

Severe burn patients frequently suffer from daily repeated wound dressing changes, leading to additional trauma to newly formed tissue and prolonging the healing process. Therefore, wound dressings that are easily removable can have many positive impacts by allowing wounds to heal faster. In this Chapter, we designed and fabricated a novel wound dressing material, which is capable of easy removal by chemical irrigation. Furthermore, the supramolecular hydrogels are able to load and release therapeutic agents to a system and they are transparent, non-toxic, self-repairable, making it a promising candidate for the new generation of wound dressing.

B.1 Introduction

Wound dressings serve a very important purpose in promoting healthy and timely wound healing by protecting a wound from the environment.[28] Traditional cotton-based wound dressings (bandages, gauzes, etc.) are most commonly employed for covering clean and dry wounds or used as secondary dressing to absorb exudates and protect the wound. Recently, new dressings have been developed that are capable of keeping the wound site moist, since it has been shown that moisture can lead to more rapid and successful wound healing.[29] Classified by the materials from which they are fabricated, these modern wound dressings can be composed of hydrocolloids, alginates,

[4] This Chapter has been adapted from a previously published paper. Wenwen Xu**,** Qiao Song, Jiang-fei Xu, Michael J. Serpe, and Xi Zhang, ACS Appl. Mater. Interfaces, 2017, 9, 11368-11372.

and hydrogels, among which hydrogels possess most of the desirable properties of an "ideal dressing".[30-33] However, most of the hydrogel wound dressings are chemically crosslinked, which usually adhere to the wounds in some degree. Mechanical debridement accompanied with anesthesia is required to remove such dressings, which is time-consuming, has the high risk of damaging newly formed tissue and can cause additional pain to patients physically and emotionally.[34] Gentler and less invasive approaches to remove wound dressing materials are therefore desperately needed for clinical applications.[35]

Supramolecular materials are generated by exploiting noncovalent interactions between components.[36-37] The dynamic nature of noncovalent interactions endows supramolecular materials with reversible, adaptive, stimuli-responsive, self-healing and degradable properties.[38-43] Supramonomers are bifunctional monomers that are fabricated by noncovalent synthesis, but can undergo traditional covalent polymerization.[44] Recently, supramolecular polymers have been generated from different types of supramonomers using a variety of polymerization methods.[45-50] Furthermore, supramonomers have been used as supramolecular cross-linkers to generate supramolecular microgels with stimuli-responsive and degradable properties.[51] In this Chapter, we show that supramonomers can be used to construct dynamic and degradable supramolecular hydrogels for use as wound dressings that will be capable of dissolution upon the application of a stimulus; this can therefore lead to wound dressings that are capable of promoting fast wound healing.

B.2 Experimental Section

Methods: ^{1}H NMR spectra were recorded on a JOEL JNM-ECA400 apparatus (400 MHz). UV-vis spectra were obtained using a HITACHI UH-4150. The UV irradiation process was performed by CEAULIGHT CEL-M500/350 UV irradiator with a high-pressure mercury lamp. SEM images were collected using a JEOL JSM-7401F apparatus. The rheological measurements were performed on a Malvern Kinexus ultra+ apparatus. Four types of rheological experiments were performed in 6 mm parallel-plate geometry with gap size of 0.5 mm: (i) Time sweep test was carried out at a fixed strain of 1% and frequency of 1 Hz at 25 °C for 5 min; (ii) Strain sweep test was carried out from 0.01% to 1000% with a fixed frequency of 1 Hz at 25 °C; (iii) Frequency sweep was carried out from 0.001 Hz to 10 Hz with a fixed strain of 1%; (iv) Temperature ramp test was carried out from 25 °C to 80 °C at a fix strain of 1% and frequency of 1 Hz with rate of 2 °C/min.

Materials preparation: FGG-EA: The synthesis of FGG-EA was reported previously.[51] Supramolecular hydrogel preparation: Supramolecular hydrogels were prepared by copolymerization of AAm and supramonomers. For a typical experiment, AAm (100 mg, 1.4 mmol), FGG-EA (2.46 mg, 0.005 mmol), CB[8] (4.51 mg, 0.0025 mmol) were dissolved in 1 mL deionized water, with 2-hydroxy-1-[4-(2-hydroxyethoxy)phenyl]-2-methyl-1-propanone (0.2 mg) as photo-initiator. N_2 gas was bubbled through the pre-gel solutions for 10 min. The pre-gel solution was then irradiated under UV light for 30 min to give transparent hydrogel. For all the

preparation process, the amount of FGG-EA, CB[8], photo-initiator as well as DI water were kept constant while ranging the AAm amount from 50 mg to 200 mg.

Swelling Behavior: To investigate the swelling behavior of the supramolecular hydrogel, the as-prepared hydrogel was immersed into PBS buffer (20 mM, pH=7.4). Hydrogel was removed from the buffer and weighted after wiping out the surface water at different time intervals. The swelling ratio is defined as the mass at time t divided by original mass.

Cytotoxicity: HaCaT cells were cultured in Dulbecco's Modified Eagle Medium (DMEM) supplemented with 10% fetal bovine serum (FBS). HaCaT cells were seeded in 96-well U-bottom plated at a density of 5×10^3 cells/well and incubated at 37 °C for 24 h. And the cells were incubated with the different concentrations of supramolecular hydrogel solutions at 37 °C for 24 h. After discarding the supernatant, MTT (1 $mg \cdot mL^{-1}$ in medium, 100 μL/well) was added to the wells followed by incubation at 37 °C for 4 h. The supernatant was removed and 100 μL DMSO per well was added to dissolve the produced formazan. After shaking the plates for 10 min, absorbance values of the wells were read with a microplate reader at 520 nm. The cell viability rate (VR) was calculated according to the following equation: $VR = A/A_0 \times 100\%$. Where A is the absorbance of the experimental group treated by drugs and A_0 is the absorbance of the control group without any treatment.

B.3 Results and Discussion

To generate these materials, the host-guest noncovalent interactions between the tripeptide Phe-Gly-Gly ester derivative (FGG-EA) and cucurbit[8]uril (CB[8]) were exploited to yield supramonomers with one acrylate moiety at each end. This is shown in Scheme 1. Then supramolecular hydrogels were synthesized via copolymerization of acrylamide (AAm) with the supramolecular cross-linkers. Like traditional chemically crosslinked polyacrylamide (PAAm) hydrogels, the supramolecular hydrogels were capable of absorbing water. Furthermore, the materials are biocompatible, soft, elastic, and capable of being loaded with therapeutic agents that can be delivered to a system. Due to the fact that these hydrogels are composed of dynamic and reversible supramolecular crosslinks, we propose that the supramolecular hydrogels will be capable of quickly dissolving upon exposure to crosslink disrupting molecules.[52-61] As a result, the stimuli-dissolving supramolecular hydrogel fabricated from supramonomers will present a new generation of wound dressing materials.

Supramolecular hydrogels were prepared by copolymerizing the supramonomers and AAm in aqueous solution under UV irradiation, with 2-hydroxy-1-[4-(2-hydroxyethoxy)phenyl]-2-methyl-1-propanone added as a photo-initiator.

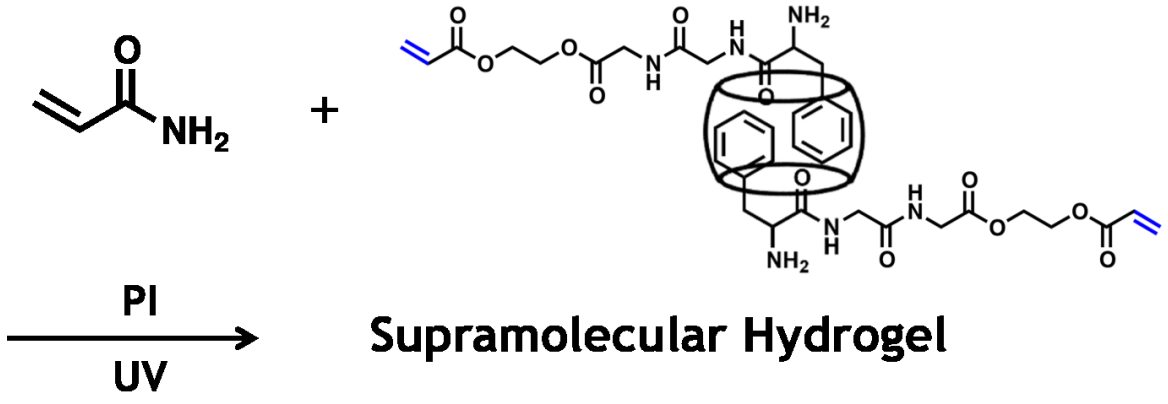

Scheme 1 Schematic depiction of supramolecular hydrogel synthesis. PI represents photoinitiator in this chapter. Reproduced with permission from ref. 257, Copyright 2017, American Chemical Society

A series of supramolecular hydrogels were generated with different monomer concentrations while keeping the supramonomer concentration constant. To simplify, we named each hydrogel according to the initial monomer concentration. The resultant hydrogels were transparent (Figure B-1(a)) while the scanning electron microscope (SEM) images showed that PAAm supramolecular hydrogels had the expected porous structure (Figure B-1(b)).

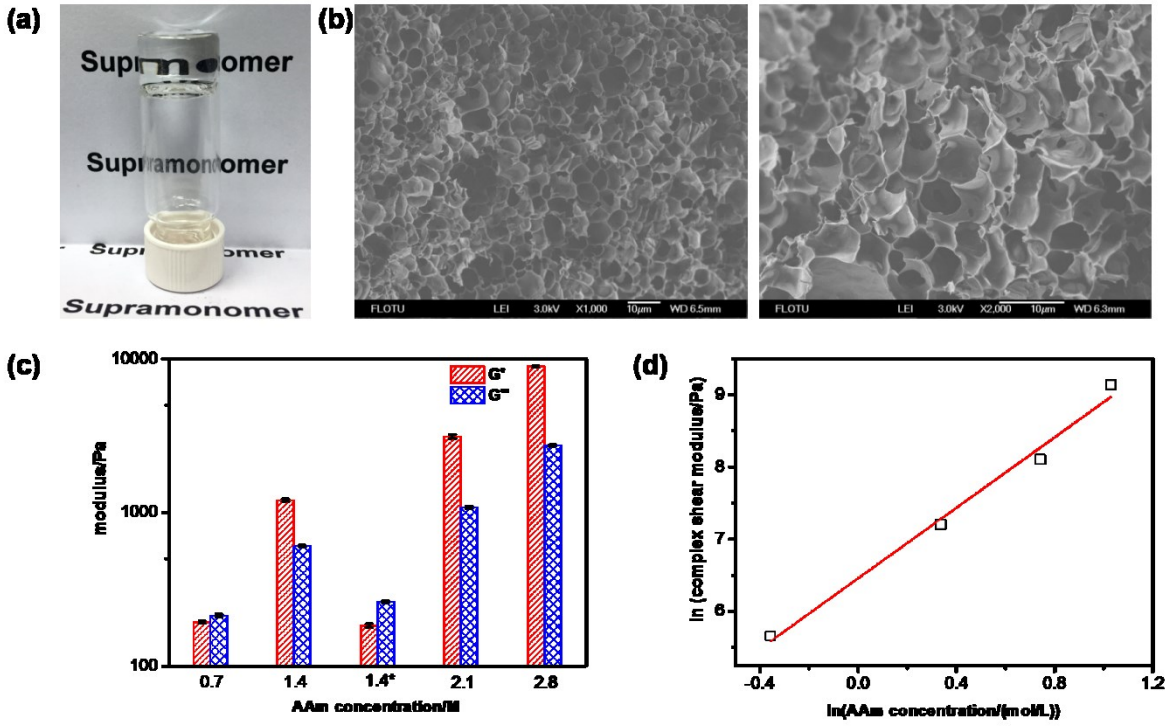

Figure B-1 a) Representative photo of the supramolecular hydrogel; b) SEM images for 1.4 M gel c) G' and G" for the supramolecular hydrogels with different monomer

concentration (1.4 M* gel was made from the complexation of the polymer with FGG moieties and CB[8]); d) Plot on a double logarithmic scale of G* versus AAm monomer concentration (coefficient of determination R^2=0.985). Reproduced with permission from ref. 257, Copyright 2017, American Chemical Society

Rheological measurements were employed to study the dynamic mechanical properties of the supramolecular hydrogels. Samples were subjected to strain sweep tests at 1 Hz to determine the storage modulus G' (describes elasticity) and the loss modulus G'' (describes viscosity), and the linear viscoelastic region (Figure B-2).

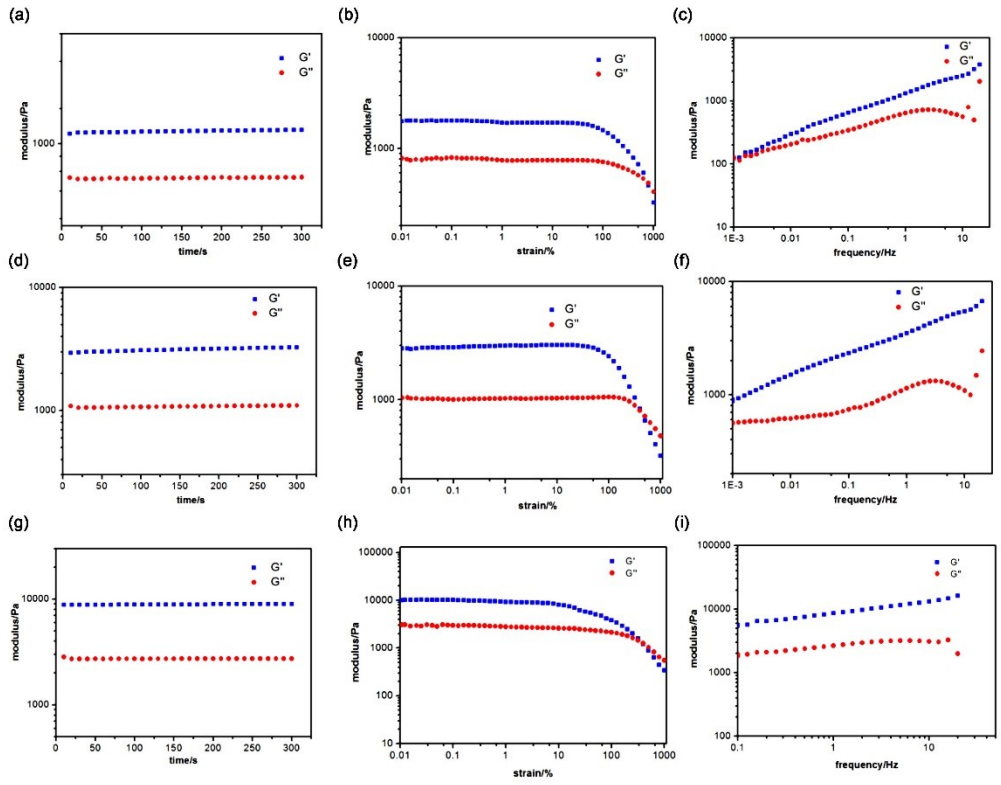

Figure B-2 Time, strain, frequency sweep for a-c) 1.4 M gel; d-f) 2.1 M gel; g-i) 2.8 M gel. Reproduced with permission from ref. 257, Copyright 2017, American Chemical Society

In our case, 1 Hz frequency and 1% strain were chosen to perform the experiments in Figure B-1(c), B-1(d). As shown in Figure B-1(c), all the hydrogels, except for the 0.7 M gel, exhibited properties characteristic of hydrogels, as the measured G' was significantly higher than G''. Both G' and G'' of the supramolecular hydrogels increased as the concentration of AAm increased. In other words, increasing the monomer concentration yielded tougher supramolecular hydrogels. As can be seen in the double log plot in Figure B-1(d), the complex modulus G* increased linearly as the AAm monomer concentration increased, over the range of 290 Pa to 9320 Pa. This shows that the mechanical properties of the supramolecular hydrogels are tunable over a large range. To further prove the advantage of using the supramonomer strategy to generate supramolecular hydrogels, we synthesized linear polymers with FGG moieties first and then added CB[8] to generate crosslinks, forming "traditional" supramolecular hydrogels. Figure B-1(d) shows that compared to the 1.4 M gel generated from the supramonomer strategy (G'=1200 Pa, G''=610 Pa), the 1.4 M gel generated via the traditional method was significantly less mechanically robust (G'=185 Pa, G''=260 Pa). This may be due to the viscous solution of the polymer with FGG moieties limiting the solubility and diffusion of CB[8] into the polymer to form extensive crosslinks, thus leading to heterogeneous crosslinking points. However, such a problem is successfully

avoided using the supramonomer strategy here, where the supramolecular hydrogel is formed by the polymerization between the AAm and supramonomers.

Next, we determined if the prepared supramolecular hydrogels could be dissolved under mild conditions. To answer this question, 3,5-dimethyl-1-adamantanamine hydrochloride (DMADA) was selected as a potential wound irrigant. We point out that the binding constant between FGG-EA and CB[8] is 2.0×10^{11} M^{-2} while DMADA has a much higher binding affinity of 4.33×10^{11} M^{-1} for CB[8].[62] Therefore, we predict that the supramonomer will be destroyed by the competitive replacement of FGG by DMADA, leading to the dissolution of the supramolecular hydrogel. Furthermore, DMADA is water soluble, odorless, and is an FDA-approved drug which is used to treat patients with Parkinson and Alzheimer's disease.[63-64] To investigate this property, the supramolecular hydrogels were exposed to the DMADA, and the initial mass of the hydrogel (W_0) was compared to the mass remaining after dissolution (W_t) and the mass percentage of remaining hydrogel calculated as a function of DMADA irrigation time. As can be seen in Figure B-3(a), exposure to DMADA resulted in the dissolution of the supramolecular hydrogel while exposure to deionized (DI) water, could not destroy the hydrogel network. Moreover, increasing DMADA concentration accelerated the degradation kinetics significantly. For the 1.4 M gel, the 100 mM DMADA solution dissolved the whole hydrogel in less than 2 min, while it took about 7 min upon exposure to 2 mM DMADA. We also observed the relationship between the mechanical strength of the hydrogels and their degradation time. As shown in Figure B-3(b), at the same concentration of DMADA, the increase of AAm

concentration in the supramolecular hydrogel resulted in a higher mechanical strength but much longer degradation times (25 min for 1.4 M gel versus 35 min for 2.1 M gel). To balance the mechanical properties and dissolution behavior of the supramolecular hydrogels, we chose 1.4 M gel which exhibited proper mechanical strength and short dissolution time as the optimized formula for the hydrogel wound dressing.

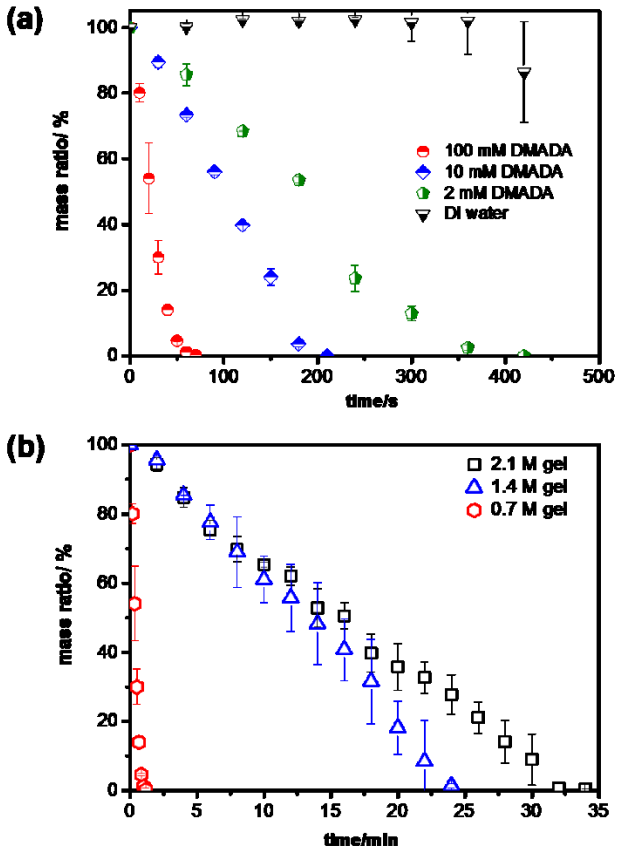

Figure B-3 a) 1.4 M gel's dissolution rate upon exposure to different DMADA concentration as well as DI water; b) Dissolution rate of hydrogel with different AAm concentration in 100 mM DMADA solution. Reproduced with permission from ref. 257, Copyright 2017, American Chemical Society

Figure B-4 shows the photographs of the 1.4 M gel degradation process. DMADA-soaked gauze was applied to half of the hydrogel dyed with Rhodamine B. After 1.5 min, the gauze was removed and only the half of the hydrogel covered with DMADA-soaked gauze was dissolved. To the best of our knowledge, this supramolecular hydrogel shows the fastest dissolution time in the wound dressing materials.

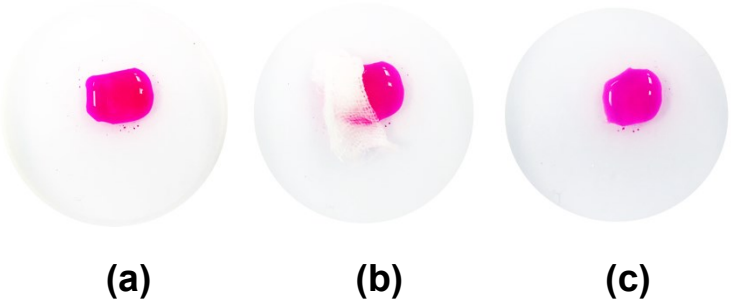

Figure B-4 Photographs of the 1.4 M gel degradation process. a) Original hydrogel dyed with Rhodamine B. b) DMADA-soaked gauze was applied to half of the hydrogel. c) After 1.5 min, gauze was removed and only half of the hydrogel remained. Reproduced with permission from ref. 257, Copyright 2017, American Chemical Society

The supramolecular hydrogel generated here also exhibits other properties that are ideal for wound dressing. First it has good water absorption behavior, guaranteeing its capacity to absorb wound exudate and preserve a moist environment around the wound. As shown in Figure B-5, the hydrogels were able to swell to 200% of its original mass within 1 h after immersion in PBS buffer (pH=7.4).

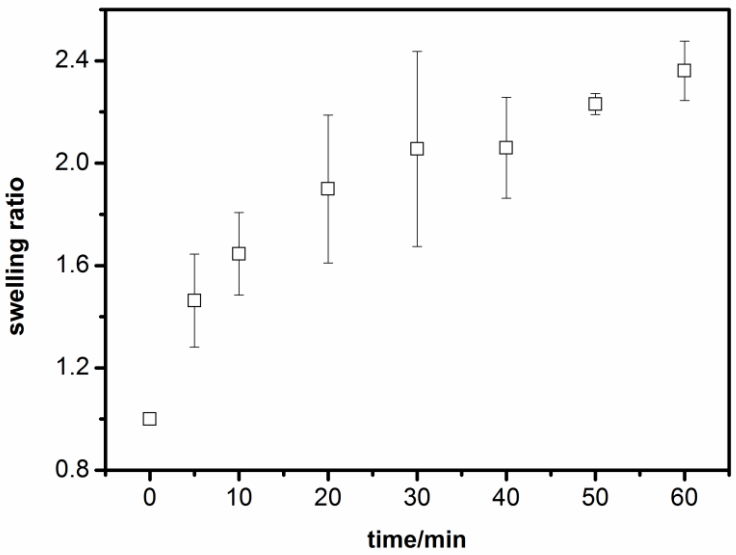

Figure B-5 Swelling behavior of the as-prepared 1.4 M gel in PBS buffer. Reproduced with permission from ref. 257, Copyright 2017, American Chemical Society

Secondly, we demonstrated that the supramolecular hydrogel was non-cytotoxicity. This was done by exposing human keratinocyte cells (HaCaT) to a wide concentration range of the hydrogel solution. As shown in Figure B-6, there was little-to-no cytotoxicity for any of the hydrogels, as examined by MTT assay. This is further evidence that these hydrogels could find practical clinical applications as wounding dressings.

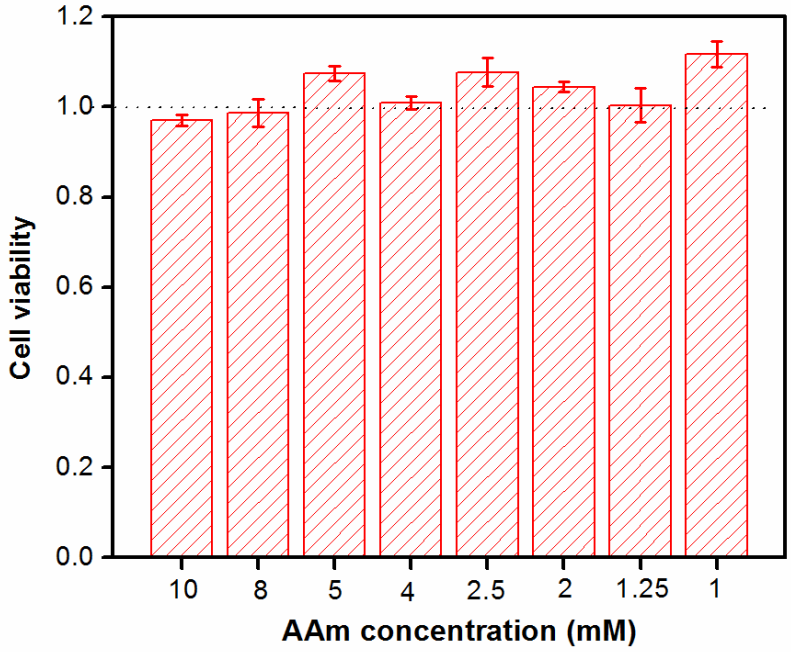

Figure B-6 Viability assay of HaCaT cells treated with different concentrations of the hydrogel solutions. Reproduced with permission from ref. 257, Copyright 2017, American Chemical Society

We also investigated if the supramolecular hydrogels could work as a stable and sterile wound dressing at various environmental conditions, which would minimize the need for frequent wound dressing changes. Figure B-7(a) shows that the supramolecular hydrogels preserved their mechanical properties at temperatures ranging from 20 to 80 ºC, even though the crosslinks are noncovalent. In addition, such a supramolecular hydrogel is capable of self-repairing. To demonstrate this, we measured the mechanical properties at an applied frequency of 1 Hz, and showed that the supramolecular hydrogel was stable at 1% strain, while it was destroyed at strain high than 800% (Figure B-7(b)). In the self-healing experiment, at 1 Hz frequency, 1000% strain was

applied to destroy the hydrogel network while 1% strain was applied to examine the recovery speed of the hydrogel. As shown in Figure B-7(c), the supramolecular hydrogel could recover to its original G'/G'' within 1 min. Therefore, the supramolecular hydrogels exhibit good thermal stability and fast self-repairability, which can meet the needs of a practical wound dressing for clinical application.

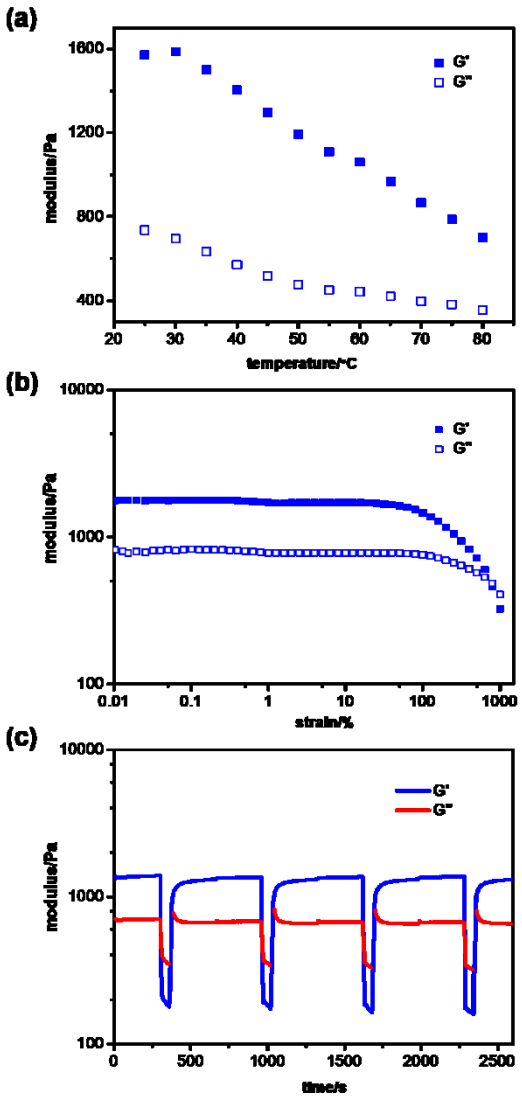

Figure B-7 a) G' and G'' of 1.4 M gel at different temperatures ranging from 25 °C to 80 °C; b) Strain-dependent oscillatory shear measurement of 1.4 M gel at 1 Hz frequency; c) Step-rate time-sweep measurements displaying the ability of the 1.4 M

hydrogel to self-repair (frequency constant at 1 Hz, 1.4 M gel was subjected to 1% strain for 300 s, then 1000% strain was applied to damage the hydrogel for 30 s and later strain went back to 1% for recovery for another 300 s. This continuous measurement was repeated 4 times). Reproduced with permission from ref. 257, Copyright 2017, American Chemical Society

Finally, we showed that the materials generated here could load and deliver therapeutic agents, such as antimicrobials, growth factors, vitamins and mineral supplements to wounds. Ofloxacin, a drug for the treatment of bacterial infections, was used to demonstrate that the supramolecular hydrogel could be utilized as a carrier for therapeutic agents. Ofloxacin was added into the pre-gel solution before UV irradiation. A small piece of ofloxacin-loaded hydrogel was immersed into PBS buffer and the release of ofloxacin monitored as a function of time by monitoring the increase in absorbance at 285 nm. As can be seen in Figure B-8, the drug was fully released from the hydrogel network within 1 h. Therefore, in addition to the above advantages, such a supramolecular hydrogel can load and release antimicrobials, which can prevent the infection and promote healing.

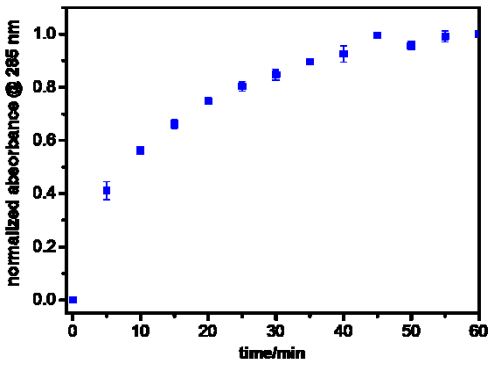

Figure B-8 Release profile of ofloxacin from 1.4 M gel when immersed into PBS buffer by monitoring the absorption band of ofloxacin peaked at 285 nm upon time. Reproduced with permission from ref. 257, Copyright 2017, American Chemical Society

B.4 Conclusion

In this Chapter, for the first time we have employed the concept of supramonomers for the fabrication of supramolecular hydrogels for wound dressings. We showed that the resultant hydrogels were transparent, non-toxic, self-repairable and exhibit desirable mechanical properties that can be tuned over a wide range. We also showed that exposure to the mild chemical irrigant DMADA led to hydrogel dissolution within 2 min, which would alleviate pain and shorten wound-healing time for patients. Considering that the above desired properties of the supramolecular hydrogel fabricated in this way can be tailor-made in a rational manner, we believe that this kind of supramolecular hydrogel represents a promising candidate for the new generation of hydrogel wound dressing.

References for appendices

[1] S. C. Glotzer, *Science* **2004**, 306, 419.

[2] A. Walther, A. H. Müller, *Chemical Reviews* **2013**, 113, 5194.

[3] S. Mitragotri, J. Lahann, *Nature Materials* **2009**, 8, 15.

[4] S. H. Kim, S. J. Jeon, W. C. Jeong, H. S. Park, S. M. Yang, *Advanced Materials* **2008**, 20, 4129.

[5] W. Gao, J. Wang, *ACS Nano* **2014**, 8, 3170.

[6] H. Lee, J. Kim, H. Kim, J. Kim, S. Kwon, *Nature Materials* **2010**, 9, 745.

[7] B. Liu, W. Wei, X. Qu, Z. Yang, *Angewandte Chemie International Edition* **2008**, 120, 4037.

[8] S. Jiang, M. J. Schultz, Q. Chen, J. S. Moore, S. Granick, *Langmuir* **2008**, 24, 10073.

[9] R. Erhardt, A. Böker, H. Zettl, H. Kaya, W. Pyckhout-Hintzen, G. Krausch, V. Abetz, A. H. Müller, *Macromolecules* **2001**, 34, 1069.

[10] R. Deng, S. Liu, F. Liang, K. Wang, J. Zhu, Z. Yang, *Macromolecules* **2014**, 47, 3701.

[11] A. H. Gröschel, A. Walther, T. I. Löbling, J. Schmelz, A. Hanisch, H. Schmalz, A. H. Müller, *Journal of the American Chemical Society* **2012**, 134, 13850.

[12] S. Jiang, S. Granick, *Langmuir* **2008**, 24, 2438.

[13] D. Zerrouki, J. Baudry, D. Pine, P. Chaikin, J. Bibette, *Nature* **2008**, 455, 380.

[14] A. Walther, X. André, M. Drechsler, V. Abetz, A. H. Müller, *Journal of the American Chemical Society* **2007**, 129, 6187.

[15] B. Liu, C. Zhang, J. Liu, X. Qu, Z. Yang, *Chemical Communications* **2009**, 3871.

[16] S. D. Kong, J. Lee, S. Ramachandran, B. P. Eliceiri, V. I. Shubayev, R. Lal, S. Jin, *Journal of Controlled Release* **2012**, 164, 49.

[17] L. O. Mair, B. Evans, A. R. Hall, J. Carpenter, A. Shields, K. Ford, M. Millard, R. Superfine, *Journal of Physics D: Applied Physics* **2011**, 44, 125001.

[18] X. D. Feng, X. Q. Guo, K. Y. Qiu, *Macromolecular Chemistry and Physics* **1988**, 189, 77.

[19] L. Hu, Z. Chen, M. J. Serpe, *Soft Matter* **2012**, 8, 10095.

[20] B. J. Park, F. F. Fang, H. J. Choi, *Soft Matter* **2010**, 6, 5246.

[21] A. K. Vuppu, A. A. Garcia, M. A. Hayes, *Langmuir* **2003**, 19, 8646.

[22] H. Singh, P. E. Laibinis, T. A. Hatton, *Langmuir* **2005**, 21, 11500.

[23] N.-T. Nguyen, G. Zhu, Y.-C. Chua, V.-N. Phan, S.-H. Tan, *Langmuir* **2010**, 26, 12553.

[24] J. J. Benkoski, S. E. Bowles, B. D. Korth, R. L. Jones, J. F. Douglas, A. Karim, J. Pyun, *Journal of the American Chemical Society* **2007**, 129, 6291.

[25] R. Rungsawang, J. da Silva, C.-P. Wu, E. Sivaniah, A. Ionescu, C. H. Barnes, N. J. Darton, *Physical review letters* **2010**, 104, 255703.

[26] J. Bacri, D. Salin, *Journal de Physique Lettres* **1982**, 43, 649.

[27] F. Xu, C. a. M. Wu, V. Rengarajan, T. D. Finley, H. O. Keles, Y. Sung, B. Li, U. A. Gurkan, U. Demirci, *Advanced Materials* **2011**, 23, 4254.

[28] L. G. Ovington, *Clinics in Dermatology* **2007**, 25, 33.

[29] C. K. Field, M. D. Kerstein, *The American journal of surgery* **1994**, 167, S2.

[30] K. Murakami, H. Aoki, S. Nakamura, S.-I. Nakamura, M. Takikawa, M. Hanzawa, S. Kishimoto, H. Hattori, Y. Tanaka, T. Kiyosawa, *Biomaterials* **2010**, 31, 83.

[31] S. Q. Liu, C. Yang, Y. Huang, X. Ding, Y. Li, W. M. Fan, J. L. Hedrick, Y. Y. Yang, *Advanced Materials* **2012**, 24, 6484.

[32] D. L. Taylor, *Advanced Materials* **2016**.

[33] I. Irwansyah, Y. Q. Li, W. Shi, D. Qi, W. R. Leow, M. B. Tang, S. Li, X. Chen, *Advanced Materials* **2015**, 27, 648.

[34] N. E. Atchison, P. F. Osgood, D. B. Carr, S. K. Szyfelbein, *Pain* **1991**, 47, 41.

[35] W. Xu, Q. Song, J.-F. Xu, M. J. Serpe, X. Zhang, *ACS Applied Materials & Interfaces* **2017**, 9, 11368.

[36] M. J. Webber, E. A. Appel, E. Meijer, R. Langer, *Nature Materials* **2016**, 15, 13.

[37] K. Liu, Y. Kang, Z. Wang, X. Zhang, *Advanced Materials* **2013**, 25, 5530.

[38] C. F. Faul, M. Antonietti, *Advanced Materials* **2003**, 15, 673.

[39] L. Yang, X. Tan, Z. Wang, X. Zhang, *Chemical Reviews* **2015**, 115, 7196.

[40] X. Yan, F. Wang, B. Zheng, F. Huang, *Chemical Society Reviews* **2012**, 41, 6042.

[41] F. Herbst, D. Döhler, P. Michael, W. H. Binder, *Macromolecular Rapid Communications* **2013**, 34, 203.

[42] M. Martina, D. W. Hutmacher, *Polymer International* **2007**, 56, 145.

[43] X. Ma, Y. Zhao, *Chemical Reviews* **2014**, 115, 7794.

[44] J.-f. Xu, X. Zhang, *Acta Polymerica Sinica* **2017**, 3.

[45] L. Yang, X. Liu, X. Tan, H. Yang, Z. Wang, X. Zhang, *Polymer Chemistry* **2014**,

5, 323.

[46] N. Roy, E. Buhler, J.-M. Lehn, *Polymer Chemistry* **2013**, 4, 2949.

[47] Q. Song, F. Li, X. Tan, L. Yang, Z. Wang, X. Zhang, *Polymer Chemistry* **2014**, 5, 5895.

[48] Q. Song, F. Li, L. Yang, Z. Wang, X. Zhang, *Polymer Chemistry* **2015**, 6, 369.

[49] Z. Huang, Y. Fang, Q. Luo, S. Liu, G. An, C. Hou, C. Lang, J. Xu, Z. Dong, J. Liu, *Chemical Communications* **2016**, 52, 2083.

[50] X. Liu, J.-F. Xu, Z. Wang, X. Zhang, *Polymer Chemistry* **2016**, 7, 2333.

[51] Q. Song, Y. Gao, J.-F. Xu, B. Qin, M. J. Serpe, X. Zhang, *ACS Macro Letters* **2016**, 5, 1084.

[52] E. A. Appel, J. del Barrio, X. J. Loh, O. A. Scherman, *Chemical Society Reviews* **2012**, 41, 6195.

[53] C. D. Jones, J. W. Steed, *Chemical Society Reviews* **2016**, 45, 6546.

[54] L. Voorhaar, R. Hoogenboom, *Chemical Society Reviews* **2016**, 45, 4013.

[55] E. A. Appel, F. Biedermann, U. Rauwald, S. T. Jones, J. M. Zayed, O. A. Scherman, *Journal of the American Chemical Society* **2010**, 132, 14251.

[56] C. Ghobril, K. Charoen, E. K. Rodriguez, A. Nazarian, M. W. Grinstaff, *Angewandte Chemie International Edition* **2013**, 52, 14070.

[57] M. D. Konieczynska, J. C. Villa‐Camacho, C. Ghobril, M. Perez‐Viloria, K. M. Tevis, W. A. Blessing, A. Nazarian, E. K. Rodriguez, M. W. Grinstaff, *Angewandte Chemie International Edition* **2016**, 55, 9984.

[58] V. Yesilyurt, M. J. Webber, E. A. Appel, C. Godwin, R. Langer, D. G. Anderson,

Advanced Materials **2016**, 28, 86.

[59] C. Li, M. J. Rowland, Y. Shao, T. Cao, C. Chen, H. Jia, X. Zhou, Z. Yang, O. A. Scherman, D. Liu, *Advanced Materials* **2015**, 27, 3298.

[60] H. Wang, S. C. Heilshorn, *Advanced Materials* **2015**, 27, 3717.

[61] J. Liu, C. S. Y. Tan, Z. Yu, Y. Lan, C. Abell, O. A. Scherman, *Advanced Materials* **2017**, 29.

[62] S. Liu, C. Ruspic, P. Mukhopadhyay, S. Chakrabarti, P. Y. Zavalij, L. Isaacs, *Journal of the American Chemical Society* **2005**, 127, 15959.

[63] C. Parsons, W. Danysz, G. Quack, *Neuropharmacology* **1999**, 38, 735.

[64] S. A. Lipton, *Nature Reviews Drug Discovery* **2006**, 5, 160.